

UNCLASSIFIED

AD NUMBER
AD893426
NEW LIMITATION CHANGE
TO Approved for public release, distribution unlimited
FROM Distribution authorized to U.S. Gov't. agencies only; Test and Evaluation; Dec 1977. Other requests shall be referred to Air Force Flight Dynamics Lab., Wright-Patterson AFB, OH 45433.
AUTHORITY
AFFDL ltr, 6 Nov 1973

THIS PAGE IS UNCLASSIFIED

AFFDL-TR-71-75

AD 893426

AD 113
DDC FILE COPY

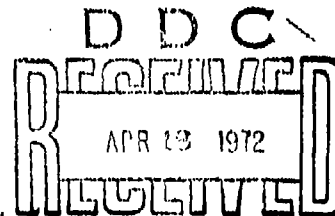
LOW SPEED AERODYNAMICS FOR ULTRA-QUIET FLIGHT

R. A. KROEGER, H. D. GRUSCHKA,
T. C. HELVEY, ET AL.

THE UNIVERSITY OF TENNESSEE SPACE INSTITUTE
TULLAHOMA, TENNESSEE

TECHNICAL REPORT AFFDL-TR-71-75

MARCH 1972



Distribution limited to U.S. Government agencies only; test and evaluation; statement applied December, 1971. Other requests for this document must be referred to AF Flight Dynamics Laboratory (FY), Wright-Patterson AFB, Ohio 45433.

AIR FORCE FLIGHT DYNAMICS LABORATORY
AIR FORCE SYSTEMS COMMAND
WRIGHT-PATTERSON AIR FORCE BASE, OHIO

169

WHITE SECTION ☐
BUFF SECTION ☒

UNANNOUNCED
JUSTIFICATION

BY
DISTRIBUTION/AVAILABILITY CODES

DIST.	AVAIL.	OR	SPECIAL
B			

LOW SPEED AERODYNAMICS FOR ULTRA-QUIET FLIGHT

*R. A. KROEGER, H. D. GRUSCHKA,
T. C. HELVEY, ET AL.*

Details of Illustrations in
this document may be better
studied on microfiche

Distribution limited to U.S. Government agencies only; test and evaluation; statement applied December, 1971. Other requests for this document must be referred to AF Flight Dynamics Laboratory (FY), Wright-Patterson AFB, Ohio 45433.

FOREWORD

This report was prepared by The University of Tennessee Space Institute, Tullahoma, Tennessee, for the Aero-Acoustics Branch, Vehicle Dynamics Division, Air Force Flight Dynamics Laboratory, Wright-Patterson Air Force Base, Ohio, under Contract F33615-70-C-1762. The work described herein is a part of the Air Force Systems Command's exploratory development program to predict the noise environment of flight vehicles. The work was directed under Project 1471, "Aero-Acoustic Problems in Air Force Flight Vehicles", Task 147102, "Prediction and Control of Noise Associated with USAF Flight Vehicles". Capt. R. P. Paxson of the Aero-Acoustics Branch was the task engineer.

The authors wish to thank their colleagues Messrs. Dieter Nowak, Jerry Coble, Frank Keeney, Ingo Borchers, Gunter Schrecker, Jim Goodman and Lt. Douglas Marshall for their valuable assistance during the course of the research project.

The program was monitored by and under guidance of Dr. B. H. Goethert, Dean, The University of Tennessee Space Institute.

Manuscript was released by the authors on April 26, 1971 for publication as an AFDL Technical Report.

Publication of this report does not constitute Air Force approval of the report's findings or conclusions. It is published only for the exchange and stimulation of ideas.

Walter J. Mykytow
WALTER J. MYKYTOW

Asst. for Research & Technology
Vehicle Dynamics Division

ABSTRACT

A combined Aerodynamics, Acoustics and Bionics study was conducted in an attempt to discover novel mechanisms to reduce the noise associated with aircraft flight. The strigiformes order of birds, selected in the Bionics effort as possessing characteristics of silent flight, was studied extensively. Three mechanisms producing the potential for acoustic quieting were discovered as a result of this study. These are:

1. Vortex sheet generators,
2. Compliant surfaces and
3. Distributed wing porosity

An experimental program aimed at initiating full scale flight evaluation of these concepts was outlined. The detailed results of these studies are included.

TABLE OF CONTENTS

	Page
I. INTRODUCTION	1
II. BACKGROUND STUDIES	3
1. QUIET FLIGHT.	3
2. SOURCES OF NOISE	4
a. Vortex Cores	4
b. Boundary Layer	4
c. Vortex Noise	5
d. Unsteady Lift	5
3. BIONICS	5
III. ANALYSIS AND DISCUSSION	7
1. MAJOR NOISE SOURCES	7
2. UNIQUENESS OF THE OWL	7
3. SEQUENTIAL APPROACH.	8
4. FINDINGS	9
5. APPLICATIONS TO SAILPLANES	11
6. PROPOSED FLIGHT TEST PROGRAM	14
IV. CONCLUSIONS	15
APPENDIX I - RELATIVE STRENGTHS OF MAJOR AERODYNAMIC SOURCES FOR AN AIRFOIL IN LOW SPEED FLIGHT	24
APPENDIX II - WIND TUNNEL TESTS OF THE OWL WING	68
APPENDIX III - WATER TUNNEL STUDIES	88
APPENDIX IV - ACOUSTIC MEASUREMENTS OF THE AERODYNAMIC NOISE PRODUCED BY FLYING OWLS	96
APPENDIX V - BIONIC STUDY OF SILENT FLIGHT	118
REFERENCES	152

LIST OF ILLUSTRATIONS

Figure		Page
1.	Aural Detection in Jungle Environment.	16
2.	Relative Acoustic Amplitudes of NACA 65 ₂ Airfoil	17
3.	Qualitative Perceived Noise Levels	17
4.	Percentage Attenuation of Compliant Plate with Respect to Hard Plate Spectra of Turbulent Energy at Y/S=0.0033.	18
5.	Photograph Showing Trailing Edge Vibration.	18
6.	Streamline Pattern Over Upper Surface of Owl Wing.	19
7.	Enlarged Photograph of Leading Edge Owl Feather.	21
8.	Double Exposure Showing Changing Flight Configuration.	22
9.	Photograph Showing Arbitrary Leg Position.	22
10.	Influence of Splitter Plate Attitude on Boundary Layer Transition	23
11.	Schematic of Vortex Flow Around a Circular Cylinder.	23
12.	The Coordinate System.	49
13.	Qualitative Comparison of Noise Radiation from a Jet and from a Wake.	50
14.	The Sound Fields Due to Oscillating Lift and Drag on a Circular Cylinder in a Flow.	51
15.	Schematic Diagram of Water Table.	52
16.	The Model Shape.	53
17.	Photographic Techniques.	54
18.	Frequency of Vortex Shedding versus Angle of Attack.	55
19.	$\frac{\sigma_{\text{water}}^*}{\sigma_{\text{air}}^*}$ at the Trailing Edge of the Airfoil versus C_L .	56

Figure		Page
20.	Boundary Layer Thickness at the Trailing Edge of an Airfoil and a Flat Plate versus Velocity in Air.	57
21.	Modification of the Boundary Layer Profile as an Adverse Pressure Gradient is Encountered.	58
22.	Velocity Distribution Over the Lower Surface of the Airfoil for C_L Equal to 0.96, 0.635, and 0.135.	59
23.	W_{vs}/W_{bl} versus Velocity.	60
24.	W_{vs}/W_w versus Velocity.	61
25.	Wind Tunnel Test Facility.	75
26.	Photograph of Wind Tunnel.	76
27.	Flow Calibration.	77
28.	Turbulence Records	78
29.	Turbulence Records	79
30.	Wing Curvature.	80
31.	Wing in the Undisturbed Air.	80
32.	Wing in the Flow.	81
33.	Mid-Span Leading Edge Feathers.	81
34.	Regions of Independent Oscillation.	82
35.	High Speed Photograph of Smoke Stream.	82
36.	Flow at Moderate Angle of Attack.	83
37.	Flow at Large Angle of Attack.	83
38.	Flow Through the Wing.	84
39.	Flow Above the Wing.	84
40.	Trailing Flow.	85
41.	Sketch of Tuft Probe.	85
42.	Flow Pattern at Flight Angles of Attack	86

Figure	Page
43. Sketch of Flow Through Leading Edge Comb.	86
44. Backflow Generation.	87
45. Water Tunnel Test Section Set-Up.	92
46. Vortex Generators.	93
47. Tip Flow From Vortex Generator.	94
48. Tip Flow From Cascade.	95
49. Splitter Plate Attachment.	95
50. The Owl Approaching the Lower Perch in a Gliding Descend After Passing the String Barrier.	99
51. Double Exposure of the Owl during a Gliding Phase. The Measured Flight Speed in this Case is 20.6 ft/s.	100
52. Block Diagram of Test and Analysis Instrumentation.	100
53. System Frequency Response.	101
54. Average Reverberation Time of Test Room.	102
55. Typical Recordings of Linear Sound Signals.	103
56. Linear Sound Signals of the Modified Owl.	104
57. Typical Recordings of Overall Sound Pressure Level. (A, Flight No. 102; B, Flight No. 109)	105
58. Sound Pressure Level of a Gliding Owl.	106
59. Sound Pressure Level of a Gliding Modified Owl.	107
60. Frequency Analysis of the Sound Pressure Level of a Gliding Owl	108
61. Frequency Analysis of the Sound Pressure Level of a Gliding Modified Owl.	109
62. Distance of Observation: 1 meter.	110
63. Distance of Observation: 3 meters.	110
64. Distance of Observation: 10 meters.	111
65. Comparison of Spectrum Shape of Aerodynamic Noise Produced by Owl and Sailplane	112

Figure	Page
66. Basic Construction of a Bird Wing.	133
67. Basic Features of a Feather.	134
68. Floor Plan of Experiment Room.	135
69. Profile View of Experiment Room.	136
70. Dual Flash Photograph of a Gliding Owl.	137
71. Sketch Looking Into Flight Path of Owl at Flash Number 1.	138
72. Sketch Looking Down on Flight Path of Owl.	138
73. Typical Plot of the Movie Data Results.	139
74. Forces on a Bird in Equilibrium Gliding.	140
75. Photograph of an Unmodified Owl Wing.	141
76. Photograph of the Removal of the Leading Edge Comb from an Owl Wing.	141
77. Photograph of an Owl Wing with the Leading Edge Comb Removed.	142
78. Photograph of an Owl Wing with the Trailing Edge Fringe Removed (Top View).	142
79. Photograph of an Owl Wing with the Upper Contour Feathers Removed.	143

LIST OF TABLES

Table		Page
I	Relationship Between Air Velocity and Angle of Attack Necessary on the Water Table	62
II	Frequency of Vortex Shedding	63
III	Theoretical Transition Points for Atmospheric Flight	64
IV	The Results of the Theoretical Calculations of the Boundary Layer Thicknesses	65
V	The Effect of Changing the Power Law Describing the Boundary Layer Profile	66
VI	Compilation of the Theoretical and Experimental Results	67
VII	Test Series I; Acoustic Measurements of Owls December 13, 1970.	113
VIII	Test Series II; Acoustic Measurements of Owls January 10, 1971.	114
IX	Test Series III; Acoustic Measurements of Owls March 4, 1971.	115
X	Data of the Tested Owl	117
XI	Physical Properties of Tested Owl	144
XII	Mean Value and Standard Deviation of Several Aerodynamic Parameters of the Owl	145
XIII	Aerodynamic Data of Gliding Owl From Dual Flash Photographs	146
XIV	Aerodynamic Data of Gliding Owl From Movie Film	149

LIST OF SYMBOLS

a	Acoustic velocity, ft/sec
A	Peak amplitude of vibration, ft.; Coefficient boundary layer, dimensionless
AR	Aspect ratio, dimensionless
c	Local wing chord, ft.; Characteristic length of an airfoil, ft
C	Distance from camera to the floor, ft
C_D	Drag coefficient, $2D/(\rho SV^2)$
C_L	Lift coefficient, dimensionless
d	Diameter or distance, ft.
dB	Decibels, reference 2×10^{-4} microbar
D	Dimension of acoustic source, ft.; Drag, lb.
DX^*, DY^* DZ^*	Distance between X_1^* and X_2^* , etc., ft
f	Characteristic frequency, cps; Frequency of vibration, cps; Vortex frequency, cps
f_n	Natural frequency, cps
f_p	Equivalent parasite area, ft ²
F	Acoustic pressure radiation function, lbs/ft
F_0	Forcing function, lbs
GPR	Glide path ratio, dimensionless
H	Distance from flash unit to the floor, ft
l	Length, ft.
L	Lift per unit span, lbs.; Lift, lb
L/D	Lift-to-drag ratio
m	Mass per unit span, slugs per foot
M	Volume of test chamber, ft ³

n	Boundary layer power law exponent, dimensionless
N	Number of data used in standard deviation equation
p	Acoustic pressure, lb/ft ²
P	Position vector, ft
q	Dynamic pressure, lb/ft ²
r ₁₁	Reverberation radius, $5.760M(16\pi T)^{-11/2}$, ft
R	Distance from camera to the wall grid, ft
Re	Reynolds number, dimensionless
S	Reference area, ft ² ; Surface area, ft ²
S _c	Correlation area, ft ²
SPL	Sound pressure level, dB
t	Time, sec; Thickness, ft
T	Reverberation time, sec
U	Velocity, ft/sec
V	Local velocity, ft/sec
V _∞	Remote velocity, fps
V _s	Sinking speed, V/(L/D), ft/sec
W	Acoustic power, ft-lbs/sec; Weight, lb
x,y,z	Position coordinates, ft
X,Y,Z	Position vector coordinates, ft.; Apparent rectangular coordinates of owl, ft.
X*,Y*,Z*	True rectangular coordinates of owl, ft.
X ₁	Parameter value in standard deviation equations
α	Angle of attack, radians (unless otherwise noted)
γ	Damping factor, dimensionless
δ	Boundary layer thickness, ft.

δ^*	Boundary layer displacement thickness, ft.
δ_2	Boundary layer momentum thickness, ft.
ΔD	Actual flight distance, ft
Δt	Time interval between dual flash, sec
η	Proportionality factor, dimensionless
ν	Kinematic viscosity, ft^2/sec
ρ	Air density, slugs/ft^3 ; Density of air, lb_m/ft^3
σ	Standard deviation, dimensionless
ϕ	Glide angle, deg
ω	Characteristic frequency, rad/sec

Subscripts

1	Conditions at first flash
2	Conditions at second flash
1,2	Specified positions or conditions
b δ	Boundary layer
c	Correlation; Coefficient
f	Friction
o	Remote Condition
t	turbulent
$U_{1,2}$	Associated with velocities 1,2
vs	Vortex shedding
w	Wake
∞	Remote condition

SECTION I

INTRODUCTION

From a military standpoint it is desirable that aircraft operate in such a way as to avoid detection. One means by which aircraft are detected is by the noise they generate and propagate to a receiver. Aircraft which have been designed to minimize aural detection are called quiet aircraft. The primary noise associated with quiet aircraft is emitted from the propulsion system and from sources associated with the aircraft in flight (radiated noise from boundary layer turbulence, vortex shedding, wakes, cavities, vibrating panels, etc.). Within aircraft performance limitations, the propulsion system noise can be controlled through design and installation. When these sources are minimized, the noise associated with flight becomes the dominant factor. The attainment of an ultra-quiet aircraft requires that the sources of noise associated with flight be identified and that means of suppressing this noise be developed.

A solution to silent flight is found in nature in birds of the order strigiformes. Species of these birds have evolved with a number of configurations each with the common characteristic of silent flight. Wings of these birds differ from other birds in that they have the following features: (a) a leading edge comb, (b) trailing edge fringe, and (c) a soft and porous upper surface. These characteristics are described in a paper by R. R. Graham (Reference 1).

The technical effort on this project was directed toward discovery of new phenomena and development of engineering information pertinent to the design of a quiet aircraft capable of flying at low altitude in an aurally imperceptible mode. The Bionics approach was taken as the primary element of the research for several reasons. The field of ultra-quiet flight is relatively new and basic studies were felt to be important in their potential for major advances. As in any other scientific study, the precise description of a phenomena may not be as valuable as basic concepts which may arise when considering the conceptual elements of a natural system for use in an applied system. Thus the technical approach employing Bionics under the assumption that "the flight characteristics of the highly specialized Owl were evolved toward the same end as our application and could be simulated in a practical design", opened a new potential for discovery.

The objective defining the work performed under this contract was to conduct an investigation of the noise sources associated with unpowered winged flight and to determine methods of suppressing the noise radiated from these sources. The basic nature of the flow associated with an airplane wing caused this

flight element to be the local point of the study. The only types of flow neglected by concentrating on the wing alone are those accompanying wing/body interference, interaction of an airfoil with a turbulent wake and possibly flow at very high Reynolds Numbers as would be experienced on a long fuselage. The basic mechanisms of noise generation to be studied were therefore reduced to:

- (1) Boundary layer,
- (2) Unsteady lift
- (3) Wakes.

Low speed sailplane flight, between 30 and 100 mph provided the reference Reynolds Number range for the program.

Until recent years, the mechanisms which produce acoustic disturbances in aerodynamic flight were not well known. Extensive research programs (for example, Reference 2-7) have been directed toward predicting and reducing noise in aeronautical systems. However, the ability to design to an acoustic power level requires further developments in noise suppression technology (Reference 8). It is felt that reduction of aircraft noise to an acceptable level will precede the ability to design to a particular level.

The natural flight systems chosen for this research are said to possess the quality of quiet flight. Significant similarities exist among the various species of Owl to suggest the need for a concentrated study of their unique flight methods of reducing noise. Two representative specimens of live Owls were obtained for this research.

This project was organized in a manner to best utilize the talents of a team of specialists in Bionics, Aerodynamics and Acoustics. In the early phases, the three teams worked independently, both for speed and for broadening the scope of possible approaches. During the remaining phases, the teams worked as a unit, using the Bionics approach for narrowing the possibilities and allowing concentrated effort on the most promising ideas. Though this report is assembled to reflect the three distinct elements, the contents of each reflect the integrated program.

Finally, having discovered quieting mechanisms of silent flight, practical techniques were to be applied to a typical sailplane airfoil section in preparation for future system installation on a piloted sailplane. Design specifications of these elements were also to be developed.

SECTION II

BACKGROUND STUDIES

1. QUIET FLIGHT

Flight within the atmosphere is accompanied by an interchange of energy between the vehicle and the surrounding air. The concept of a quiet aircraft requires the reduction of the noise produced by this interchange to a level not noticeable by unsuspecting but alert personnel.

The aural detection of an aircraft depends on several factors. These include: (1) the intensity and radiation pattern of the noise generated by the aircraft, (2) the spectrum and real time character of the generated noise, (3) the distance separating the aircraft and the observer, (4) the atmospheric absorption, (5) the background noise present in the observer's environment, and (6) the sensitivity of the observer to the received noise. In Reference 2, methods are presented for developing aural detection criteria considering the masking effects of the background noise and the hearing sensitivity of the observer (Factor 5 and 6 above). Figure 1 shows an aural detection curve for a daytime jungle. The aural detection levels presented have been modified by replacing the threshold of hearing curve given in Reference 2 with that given in Reference 3. As can be seen in Figure 1, an alert observer should be able to sense a sound pressure level¹ (SPL) of -4 dB for a 4000 Hz tone in the absence of background noise. However, he is restricted to a considerably reduced sensitivity at other frequencies. In addition, the presence of background noise tends to mask other noise signals and, as shown in Figure 1, the masking level of the jungle background noise determines the aural detection level for frequencies over 125 Hz.

As indicated in Reference 4, the aural detection range of an aircraft is determined by comparing the spectrum levels of the received noise signal from a given altitude with an aural detection level curve. The maximum amount by which the signal exceeds the detection curve determines the aural detection range. For example, consider the flight of a sailplane over an observer in a jungle environment. A one-third octave band spectrum of the received noise signal from such a sailplane at an altitude of 125 feet (from Reference 4) is shown in Figure 1. In Reference 4, it is shown that the spectrum level of the sailplane's noise

¹All sound pressure levels (SPL) in this report are referenced to 0.0002 microbar.

signal exceeds the detection level curve by a maximum of 18 dB at 310 Hz with the resulting aural detection range being approximately 1000 feet over a quiet jungle.

The capacity to provide aurally nondetectable flight at a given altitude thus depends on the ability to attenuate the aircraft noise signature such that the received noise signal is below the aural detection level curve for a given environment.

2. SOURCES OF NOISE

The study of ultra-quiet flight introduces the need to consider all of the potential types of noise. The characteristics of directivity and multiple source summing may amplify the influence of subtle contributors. The relative importance of the primary sources of noise has been studied for missions wherein silence is a prerequisite. Normally the propeller/engine noise is sufficiently large to mask the remaining noise sources. However, with the recent successes in low speed propulsion system quieting, the airframe produced sources predominate. These are discussed in minimum detail in the following paragraphs.

a. Vortex Cores

The vortex sheet which develops at a point of steep spanwise lift slope is normally quiet strong and wrapped tightly. Its core is downstream of an element such as a wing or flap tip and is usually low in axial energy because of a local flow separation upstream. The rotational energy of the core may also be quite low. The surrounding vortex sheet is at an elevated energy level and induces high velocities at the interface boundary. The potential nature of the main vortex implies no acoustic disturbances, yet interaction with a region of another energy level provides a noise source, dependent on the incipient nature of the interaction.

b. Boundary Layer

As the vehicle boundary layer transitions to turbulent flow, unsteady pulsations occur and are transmitted into the surrounding field. The extent of this problem is a function of the aerodynamic configuration, Reynolds Number, attitude and surface roughness. A broad band acoustic radiation signal is generated by the resulting boundary layer sources. Control of noise would certainly accompany the ability to shape the boundary layer configuration.

c. Vortex Noise

The natural consequence of three-dimensional lifting surface performance is the generation of an extensive sheet of distributed vorticity. The exact character of this sheet is not well known for arbitrary wings and the individual vorticity elements may have axial as well as lateral components. As they are in a partly viscous region, little can be said of their closure. Thus, their life may be extremely short, being accompanied by a rapid energy exchange. Periodicity is not always a property of this source, though for simple cases its effects may be described analytically.

d. Unsteady Lift

Most forms of noise are accompanied by an unsteady flow process. The development of unsteady lift implies a changing circulation about a body which may be a consequence of a fluctuating induced angle of attack of a rigid surface or a vibrating surface in a steady flow. The existence of such changing circulation about the airfoil may produce noise. Fluctuating circulation may be excited by the classical Karman street or broad band turbulence introduced into wake at the wing trailing edge.

Though these contributors to acoustic disturbance act in varying degrees and may be coupled by some aerodynamic interface, they may be considered as independent for such a basic investigation.

3. BIONICS

Bionics is the study of nature's solutions to the problems of living systems, suggesting the application of these solutions to man-made systems. Ultra-quiet flight may be presenting problems which fall in the realm of novel science. Upon searching the field of aeronautics for solutions, the sailplane was first considered but as Figure 1 shows, it falls short of being imperceptible in a jungle environment.

The science of Bionics offers a well adapted and very effective aerodynamic system for silent flight through the species of Owl. Over millions of years of development, this species has produced many specialized configurations with varying degrees of body solidity, aspect ratio, planform shape, L/D 's, gross weight and performance. However, virtually every member of the species has the common characteristic of silent flight. This implies a successful development toward this common goal. If this is truly a primary objective of this evolution scheme, as it has

been described, considerable optimization has taken place and much can be learned through a detailed engineering and scientific study of the present species of Owl.

Special emphasis will be placed in the study of the Owl's wing-feather structure. For instance, its leading edge contains small feathers with the appearance of hooked combs. It is probable that these as well as other unique elements combine to reduce noise generation.

SECTION III

ANALYSIS AND DISCUSSION

1. MAJOR NOISE SOURCES

The prediction of acoustic disturbances originating in low speed aircraft flight was studied. References 6 through 11 show that the technology is not completely developed. In the early phases of the project it was found necessary to establish a level of importance on the major noise sources. A method described in detail in Appendix I was used. The results are shown in Figure 2. Both the boundary layer and unsteady lift noise components were found to warrant the first consideration. The wake generated noise was found to be of negligible consequence in the low speed range of interest in this research.

2. UNIQUENESS OF THE OWL

For many years, the Owl has been proclaimed to be a silent flyer. His three elements of uniqueness are:

- (1) The leading edge comb,
- (2) The trailing edge fringe,
- (3) The downy upper surface of the feathers.

In addition, a wing porosity exists which is a consequence of the soft feather structure.

In some way these elements must work together to suppress audible acoustic disturbances originating from the turbulent boundary layer and unsteady lift as well as the other possible sources.

The Owl is known to have three distinct phases of flight which must be silent. These are:

- (1) The flapping, or propulsion and guidance phase,
- (2) The gliding phase, and
- (3) The phase of configuration change during touch-down.

All of these phases must be very silent as his prey is wary and the Owl flight is comparatively quite slow and clumsy. This research was concentrated primarily on the gliding phase though the

contribution of the Owls unique qualities to the other phases was always kept under scrutiny.

3. SEQUENTIAL APPROACH

The goals of the project were set out in the beginning to be obtained by the following approach:

- (1) Develop an acoustical measurement system capable of measuring very short duration, low level acoustic properties.
- (2) Obtain and calibrate a reverberation chamber large enough to test the Owl's silent gliding flight phase.
- (3) Study the unique characteristics of the Owl flight with a team composed of Aerodynamicists, Acousticians and Bionics experts, using Zoologists for consultation in certain specialized areas.
- (4) Train the Owls to fly in a manner acceptable for recording the spectral distribution of his radiated noise.
- (5) Develop an acoustic data reduction technique for for short duration noise measurements.
- (6) Develop a wind tunnel with sufficiently smooth flow to test mounted wings of a small species of Owl.
- (7) Perform water tunnel experiments, using a sailplane airfoil section, to search for practical means of simulating the noise suppression mechanism of the Owl.
- (8) Test other species of birds to verify the quiet nature of Owl flight.
- (9) Modify the wings of the living owls and acoustically monitor their flight to show the effect of removing the quieting mechanisms.
- (10) Define the silencing mechanisms of the Owl and make recommendations for sailplane experiments to verify their validity.

In depth descriptions of this approach are included in Appendices I-V.

4. FINDINGS

When the first acoustical data reduction was completed for the Owl flights, it was seen that the Owl had a significant acoustic radiation. The interesting part was that the noise spectrum was shifted strongly toward low frequencies range. In fact, it was seen to nearly match the human perception threshold curve at a distance of three meters. The Owl does not radiate the broad band type noise developed by sailplanes as depicted qualitatively in Figure 3 and discussed in depth in Appendix IV.

Appendix V shows the acoustic quieting of the Owl to be accompanied with a very poor flight performance. For example, the lift-to-drag ratio of the Owl is less than five while the albatross may reach peak values above thirty.

It was thus decided to search for boundary layer and unsteady lift noise suppression mechanisms which were not necessarily aerodynamically efficient but could shift the acoustical noise spectrum to low frequencies as accomplished by the Owl. The wind tunnel studies aided in this matter. The tests of the small Owl wing mounted in a wind tunnel showed a wing instability to occur at approximately 15 cycles per second. This experiment is described in Appendix II. This frequency was seen to correspond to the peak noise radiation measured in the reverberation chamber for the live Owls. Strobe light studies of the small wing mounted in the wind tunnel showed an aeroelastic compliance of a rather complex nature at this frequency. Reference 12 was consulted concerning boundary layer turbulence attenuation by compliant surfaces. The result was that compliant surfaces shift the boundary layer turbulence frequency spectrum to lower levels.

A curve from Reference 13 is shown in Figure 4. It shows the turbulent boundary layer attenuation of a compliant surface with reference to a solid surface. This curve is qualitatively the same as the attenuation which would accompany the comparison of the Owl with the sailplane referred to the same total noise energy level. This conclusion promoted the water tunnel studies described in Appendix III. Figure 5 shows the compliant nature of the Owl wing in gliding flight. The flutter of the feathers on the upper surface was borne out in further wind tunnel and gliding flight tests.

The value of the leading edge comb to the silent flight of the Owl was discovered. In essence, the leading edge comb is a vortex sheet generator (not a classical vortex generator) which works in combination with the leading edge slot and tip feathers to promote attached laminar flow over the entire outer half of the wing span. The mechanism was thoroughly probed and is described in detail in Appendix II. A sketch of the boundary layer streamline pattern is shown in Figure 6. It must be emphasized that the region of counter-rotating flow is not separated but a reversed laminar flow which fills the void

induced by the diverging streamlines near the leading edge slot. The pressure drop created by the flow around the slot adjacent to the vortex sheet generator allows the air to easily negotiate the 180 degree turn and flow smoothly in the pattern shown. It is hard to depict the three-dimensional flow in a sketch; however, approximately four millimeters above the wing the flow is in the chordwise direction and quite comparable to that over a conventional airplane wing. These conditions can exist only with the aid of the special vortex sheet. The wake is very thin at the trailing edge. The weak nature of the induced trailing vortex sheet implies a gentle lift drop-off toward the tip. The very complicated flow pattern found here was seen to allow the existence of laminar tip flow up to an angle of attack near 30 degrees. This is unusual performance for an airfoil with an unswept thin leading edge. The fact that the stagnation line is along the comb at small angles of attack seems to offer an additional design advantage for high speed airplanes.

An exploded view of the leading edge feather possessing the vortex sheet generator is shown in Figure 7. Note the soft downy substance on the upper surface. This material also covers the region of contact between the feathers. No proof of its function could be made. However, two qualities were found which possibly shed light on their function. These are:

- (1) The downy surface allows a uniform film of air to pass between the feathers so that an evenly distributed porosity could be produced. This flow between the feathers could produce a chordwise boundary layer thickening for reduced noise at the trailing edge.

The second explanation, is:

- (2) The downy surface produced lubrication which allowed the wings to be quietly folded into an assault position right before touchdown as shown in Figure 8. The wings on the live owls could be forcefully extended and closed with a very orderly and quiet motion of the sliding feathers. As another point of interest in Figure 8, note the different attitudes of the leading edge slot as depicted in the shadow on the floor.

In effect, the second possibility was not felt to be important in the gliding flight phase other than its contribution to compliance.

One other interesting observation of the owl's flight was his virtual disregard for the position of his legs. Figure 9 shows such a configuration. Of the numerous photographs taken, his leg position seems somewhat arbitrary. If this is the case in his quiet flight mode he must possess a versatile silencing mechanism. This could be in the form of the long, compliant and very fine feathers attached over his legs and in his base region.

5. APPLICATIONS TO SAILPLANES

A design for application of the silencing mechanisms of the Owl to an existing sailplane was not simple. In fact, after considering the influence of tip modifications to the lateral-direction stability and control as well as to the stall characteristics of the vehicle, recommendations concerning the applications of tip vortex sheet generator will be withheld pending exhaustive wind tunnel evaluation. This is due to the lack of existing analytical capability for calculating the three-dimensional flow involving boundary layer interaction. However, it was felt that though the structure of the flow induced by the application of compliant surfaces was extremely complicated, the immediate application to a sailplane for flight testing would not be excessively dangerous.

A series of water tunnel experiments were conducted, as described in Appendix III, to determine a simple, first look at the influence of a type of compliance on the acoustic and aerodynamic performance of the sailplane. A splitter plate was extending from the trailing edge of the wing and a "best" length was found. This length was 12% of the local wing chord. Figure 10 shows how the splitter plate, if mounted flexibly from the trailing edge, might simulate a compliant surface. Notice that as the plate is moved up, the point of turbulent boundary layer transition moves forward on the upper surface and rearward on the lower surface. Conversely, as the plate is moved down, the reverse occurs. The limitation on the success of a sailplane modification program will depend on how well the splitter plate can regulate the flow in this fashion. No doubt, compliance extending further onto the wing would have had more influence. However, since so little was known of the phenomena for quieting, such an extensive study was felt to be beyond the scope of this research. A limitation on the splitter plate approach is that the overall wing streamwise movements compared to those of the splitter plate will be very small. The owl's compliance is such that the entire wing will deform under the influence of the trailing edge motion.

The observations made in the study of the splitter plate were as follows: As the turbulent boundary layers developed on the upper and lower surfaces a closed loop aerodynamic control system was developed. When the airstreams along the upper and lower surfaces coalesce at the trailing edge, an alternate vortex shedding develops. This may occur at a single frequency or over a broad range of frequencies, depending on the Reynolds Number. Figure 11 shows this action for a cylinder. The same type of system develops behind an airfoil except the frequency is higher. The experiments by Strouhal [15] show this to be

$$f_o = 0.185 \frac{V_{\infty}}{d} \quad (1)$$

where f_0 is the vortex frequency in cycles per second, V_∞ is the velocity in feet per second and d is the cylinder diameter in feet. For application to the airfoil, d becomes the boundary layer thickness at the trailing edge.

By adjusting the stiffness of the trailing edge attachment the frequency of oscillation of the splitter plate can be tuned to a predominant wake frequency and thus be driven to amplitudes of at least the thickness of the boundary layer. The prediction of this amplitude will be limited because the variation in total pressure across the path of the plate travel will add a non-linear aerodynamic spring rate.

The amplitude of motion assuming a constant, quasi-steady, aerodynamic spring rate would be;

$$A = \frac{F_0/m(2\pi f)^2}{\{[1-(f/f_n)^2]^2 + [2\gamma(f/f_n)^2]^2\}^{1/2}} \quad (2)$$

where f is the forcing frequency, f_n the natural frequency, m is the effective plate mass (including the local air mass) and γ is the damping factor. It was seen that the prediction of the amplitude would be difficult if the nonlinear terms were included.

Consider the design of the splitter plate attachment where the hinge has small damping. In this case, Equation 2 may be approximated by;

$$A = \frac{F_0/m(2\pi f)^2}{1 - (f/f_n)^2} \quad (3)$$

This equation says that if the forced frequency of vibration, f , of the splitter plate is above the system natural frequency, the displacement will be out of phase with the force. If the forcing frequency is small, compared to the natural frequency they will be in phase. In a very rough sense, this action implies an attenuation of the unsteady lift at high frequency and an amplification at low frequencies in a broad band turbulence wake through the phasing of the camber change with the induced downwash.

For the purposes of analysis of this approach, assume the attachment spring constant to be zero. The average velocity in the region of motion is $V_\infty/2$ and the lift curve slope for the splitter plate is 2π . For harmonic motion, the oscillating lift on the splitter plate becomes

$$L = \frac{\pi a c_p V_\infty^2}{4} \sin(2\pi f)t \quad (4)$$

per unit span. Where α is the effective angular deflection, c is the chord length, ρ the air density, f the vibration frequency and t the time. If the effective system mass and the lift are assumed to act at the 2/3 chord position of the splitter plate, the natural frequency of motion becomes

$$f = \frac{1}{2\pi} \sqrt{\frac{dL/d\alpha}{2/3 \text{ cm}}}$$

or, using Equation 4,

$$f = \frac{V_{\infty}}{4} \sqrt{\frac{\rho}{\pi m}} \quad (5)$$

Next, by setting the natural frequency of the splitter motion (Equation 5) equal to the wake vorticity frequency (Equation 1),

$$0.185 \frac{V_{\infty}}{d} = \frac{V_{\infty}}{4} \sqrt{\frac{\rho}{\pi m}} \quad (6)$$

From this, the mass per unit span of the splitter plate becomes

$$m = 0.6 \rho d^2 \quad (7)$$

Even for thick boundary layers, this equation implies the need for a very light weight splitter plate if a flexible hinge is used. Even if the plates were made from a light material such as balsa wood, some additional spring stiffening would still have to be added at the hinge line to increase the system's natural frequency to the level of Equation 1.

By assuming the net boundary layer thickness at the trailing edge to be around one-tenth foot and assuming a flight velocity of 100 ft. per second, the fundamental wake frequency would be around 180 cps. Therefore, a range of frequencies up to fairly high values should be employed.

The preceeding analysis was very rough and provides only a starting point for a design. The available theory is not sufficient to predict such parameters as splitter plate chord length, mass distribution or elasticity distribution, though a more rigorous analyses might provide more insight into the motion that might be expected.

6. PROPOSED FLIGHT TEST PROGRAM

Based on the above findings, the following flight test program is suggested in order to evaluate the splitter plate concept of compliance simulation.

Strips of 1/16 inch thick balsa wood with a chordwise dimension of 0.12c should be hinged to the trailing edge in a very flexible manner. The grain of the wood should be aligned in the streamwise direction. The spanwise dimension would be one foot. In the first trials, several flight tests should be run using only a few strips being mounted at about the 1/4 span position in the same manner on both wings.

These first tests will determine the durability of the plates and the attachment techniques. A good grade of cloth tape should be sufficient to hold the plates in place. It is expected that the second bending mode may be set up in the plates so their life span may not be very long. A broad speed range should be traversed in the sailplane with merely visual observations being made during and after each flight. Should the attachment and performance of the plates be satisfactory, additional ones may be installed incrementally between high speed runs. As more plates are added, the top flight speed should be reduced as a flutter prevention precaution. In no case should the plates be installed outboard of the 75% span or the inboard edge of the aileron, whichever is the smaller without a detailed flutter analysis.

Acoustic measurements may be made upon establishing the new configuration. Strips of shim stock may be added to increase the stiffness. But again, the stiffening should be started inboard and extended to the outboard regions of the wing with small increments of stiffening being made between flights. A small amount of camber may be added to the splitter plates if another flow position of the plate is desired.

SECTION IV

CONCLUSIONS

Extensive aerodynamic and acoustic studies were made of the owl wing in an attempt to isolate the mechanisms which reduce his noise level. The research succeeded in exposing three mechanisms which could aid in suppressing noise due to unsteady lift and turbulent boundary layer. These are:

- (1) Laminar, attached flow over the outboard half of the wing produced largely by the influence of vortex sheet generators.
- (2) Shift in frequency spectrum, compared with solid surfaces, to the lower range by the action of compliant surfaces.
- (3) A thickening of the boundary layer and a reduction in the velocity gradients at the trailing edge by the action of a porosity distributed over the wing.

Splitter plates at the trailing edge were found to strongly influence the boundary layer transition and mixing near the trailing edge. A flight test program was proposed to evaluate the splitter plates in reducing noise. Care must be taken to isolate the effects of the splitter plate alone and the degree of compliance it simulates.

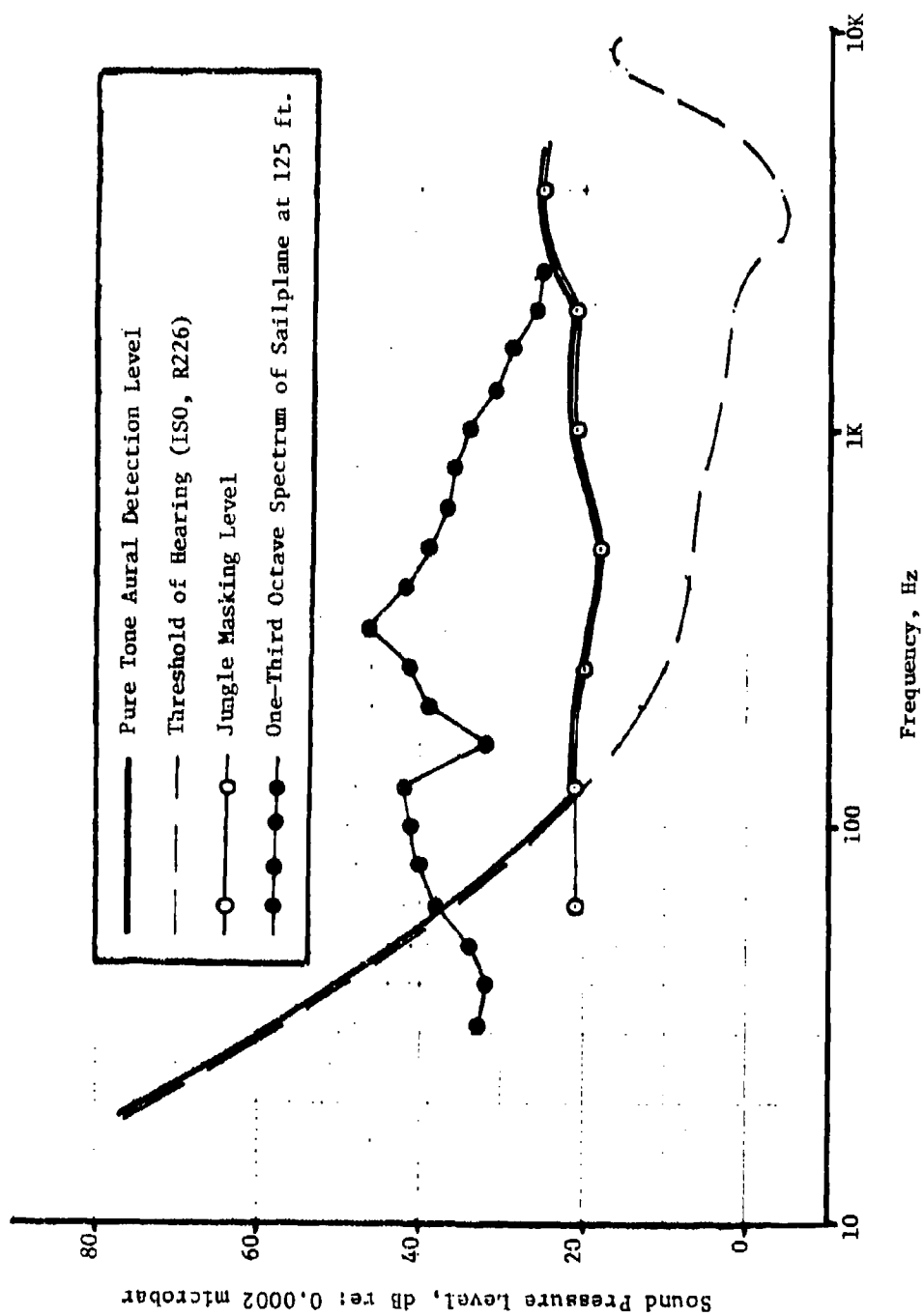


Figure 1. Aural Detection in Jungle Environment.

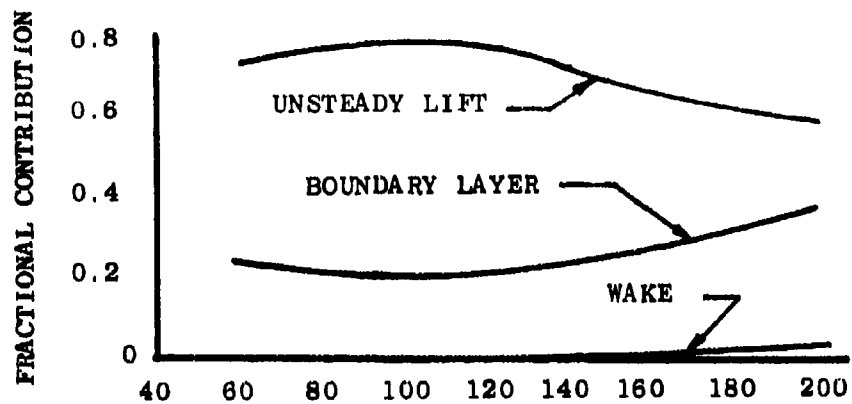


Figure 2. Relative Acoustic Amplitudes of NACA 65₂ Airfoil.

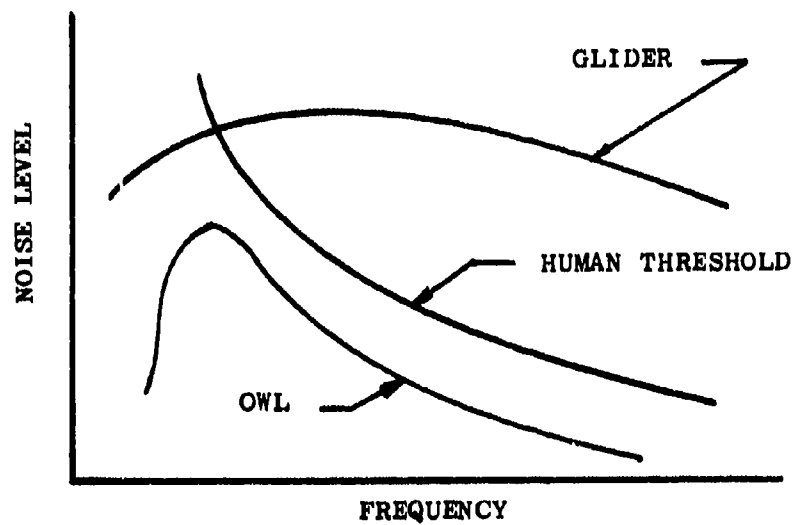


Figure 3. Qualitative Noise Levels

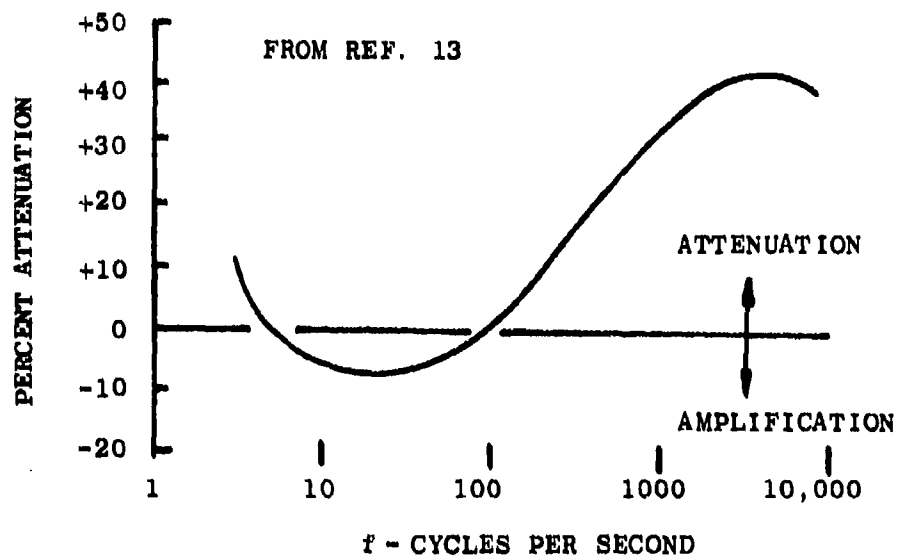


Figure 4. Percentage Attenuation of Compliant Plate with Respect to Hard Plate Spectra of Turbulent Energy at $Y/S=0.0033$.

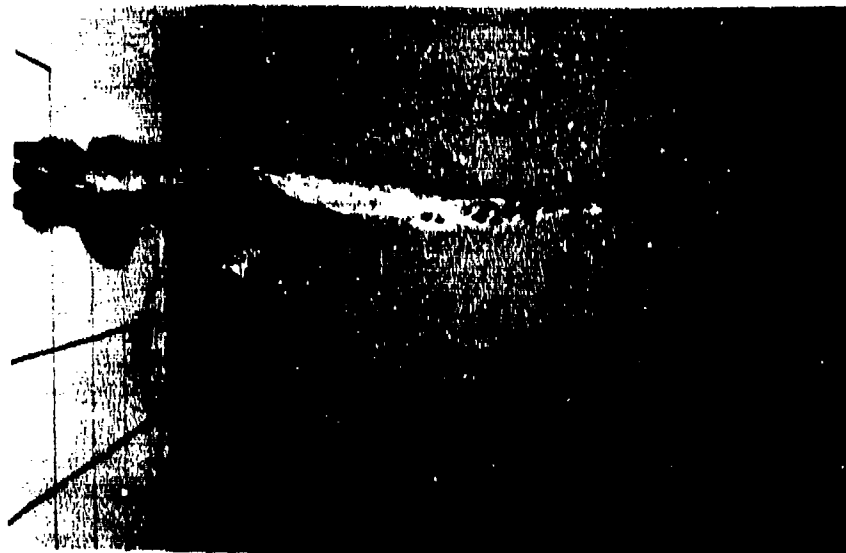


Figure 5. Photograph Showing Trailing Edge Vibration.

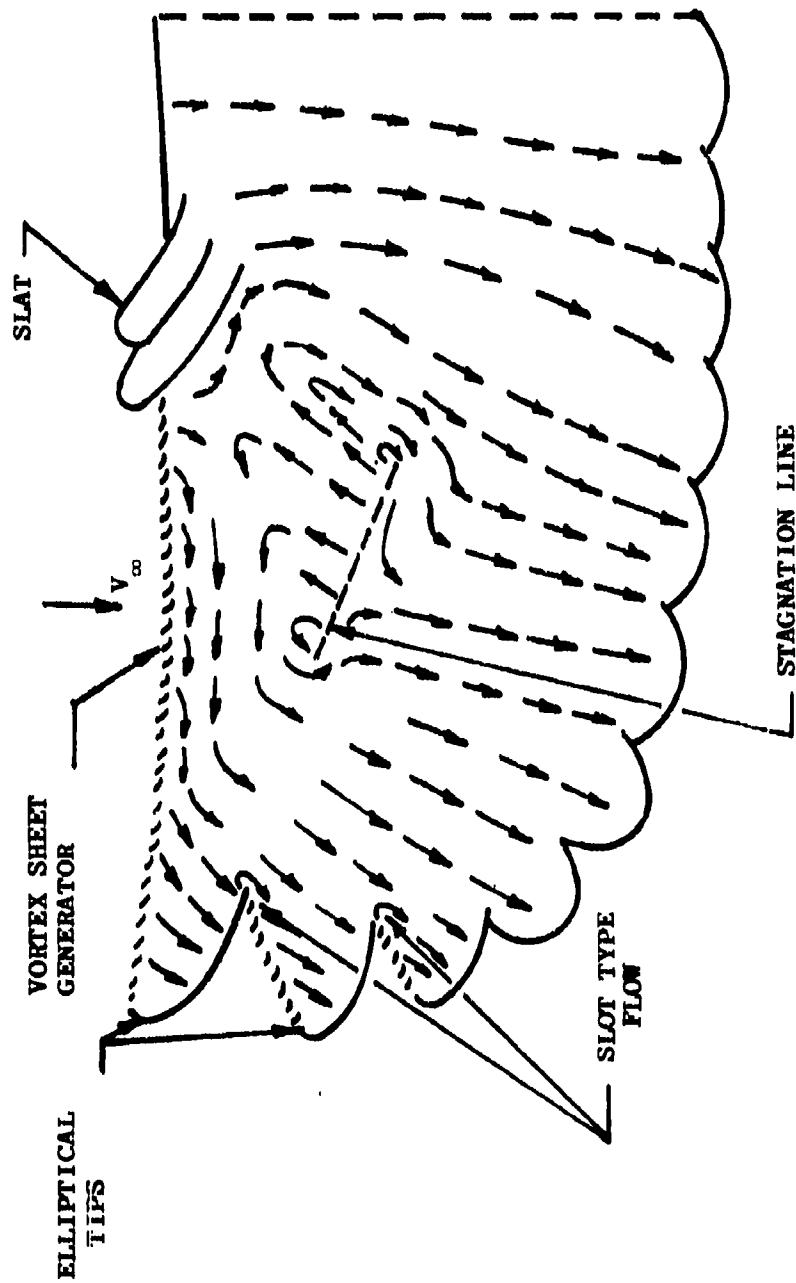


Figure 6. Streamline Pattern Over Upper Surface of Owl Wing.

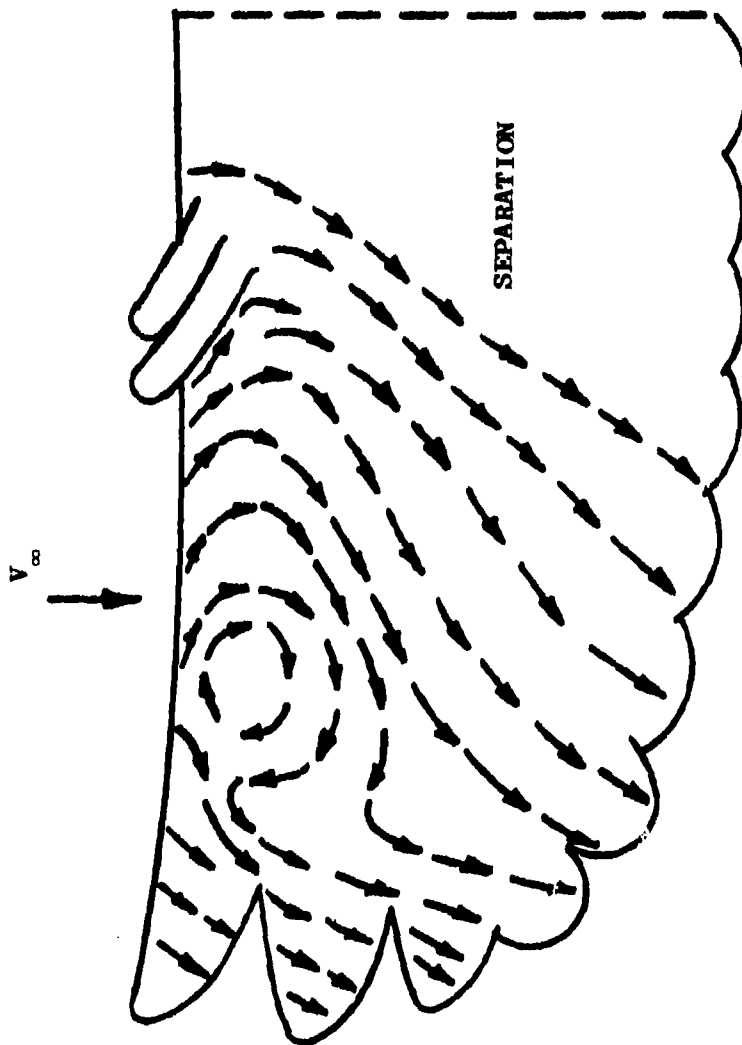


Figure 6 (Concluded). Flow with Comb Removed.

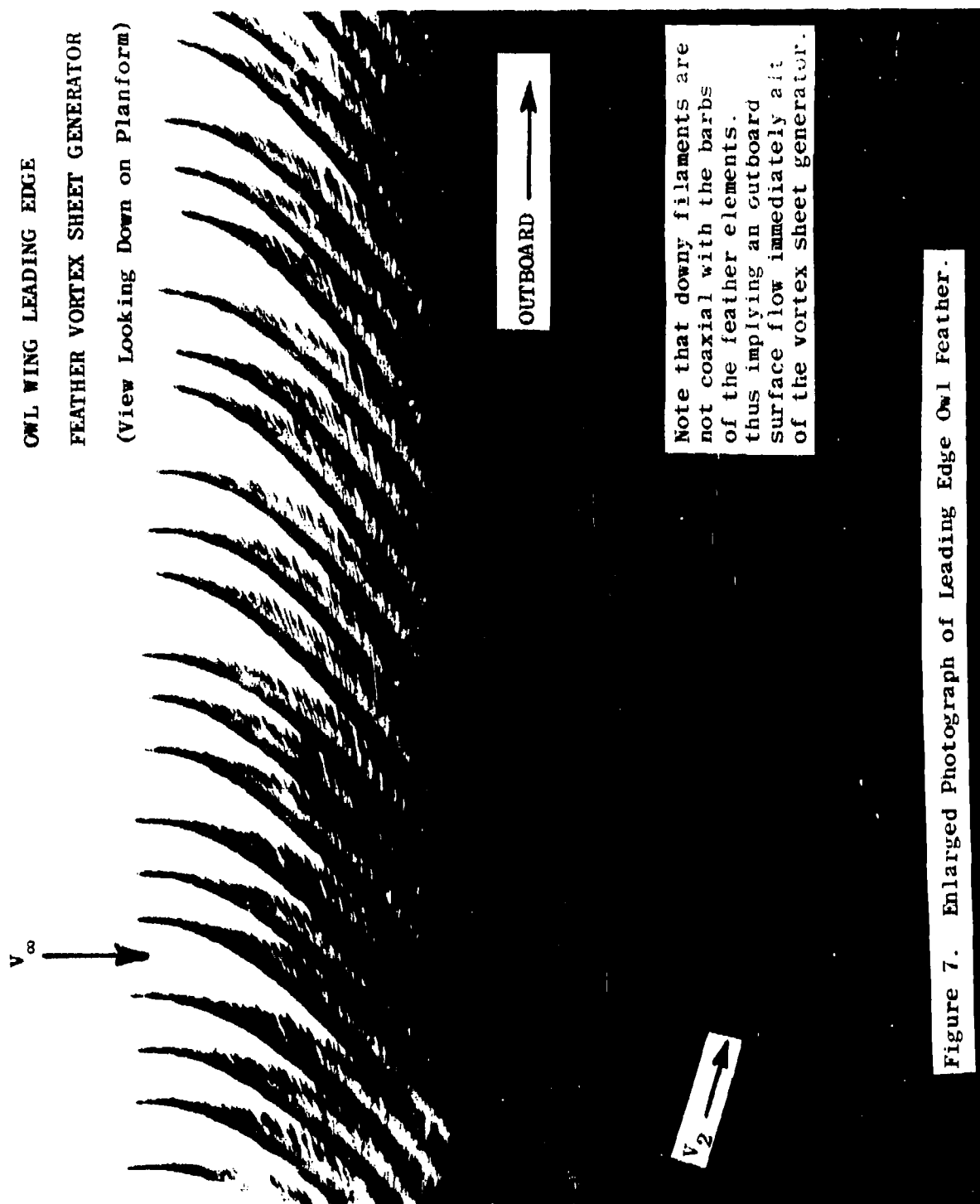


Figure 7. Enlarged Photograph of Leading Edge Owl Feather.



Figure 8. Double Exposure Showing Changing Flight Configuration.

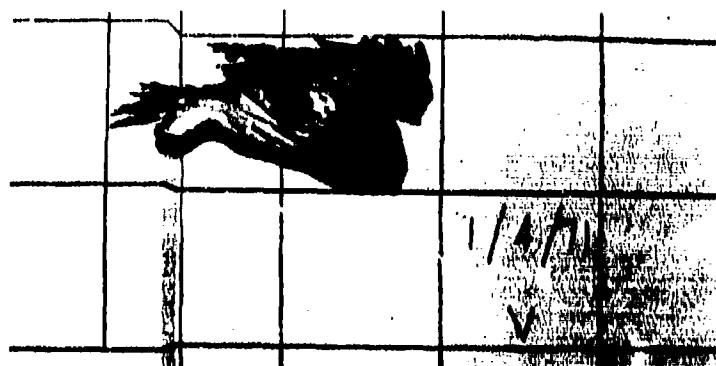


Figure 9. Photograph Showing Arbitrary Leg Position.

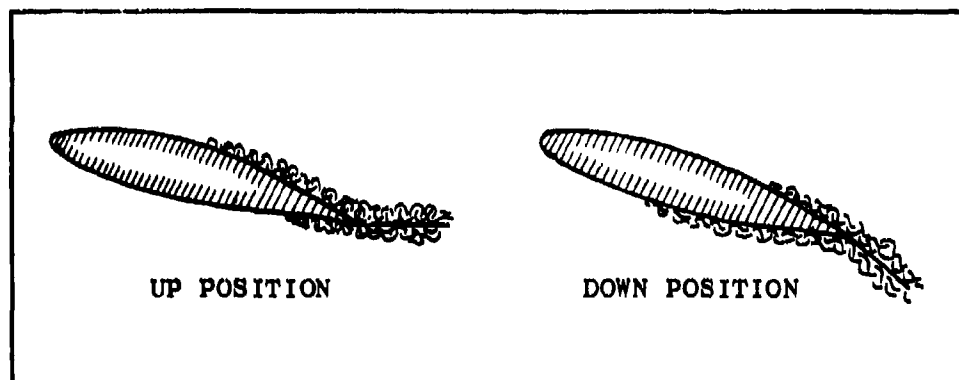


Figure 10. Influence of Splitter Plate Attitude on Boundary Layer Transition

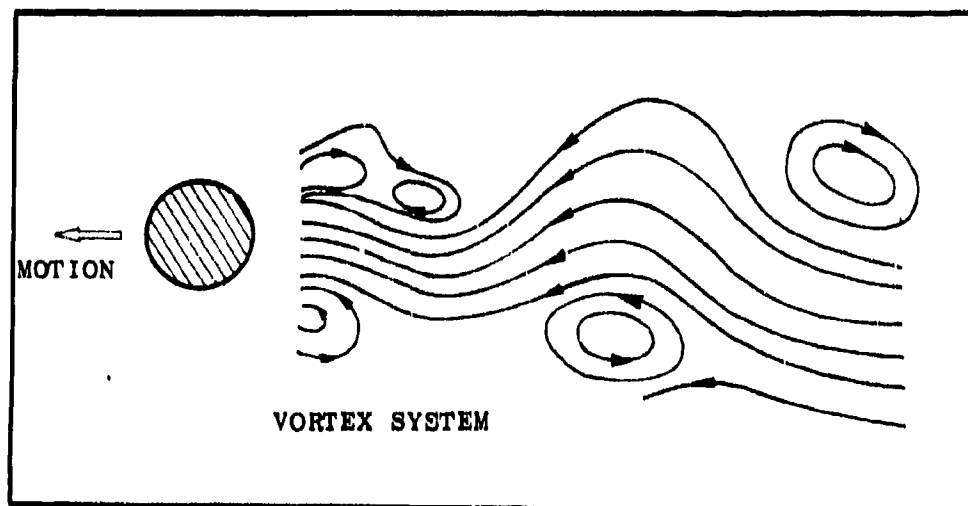


Figure 11. Schematic of Vortex Flow Around a Circular Cylinder.

APPENDIX I

RELATIVE STRENGTHS OF MAJOR AERODYNAMIC SOURCES FOR AN AIRFOIL IN LOW SPEED FLIGHT

1. INTRODUCTION

a. Background

The purpose of this work finds its origin in the increasing interest in achieving silent flight. It is limited to the investigation of the aerodynamic noise caused by the turbulent boundary layer, lift fluctuations caused by vortex shedding at the trailing edge, and the wake resulting from the movement of the wingform through the air. For this work an engineless, high performance sailplane, the Standard Austria SH1, was used as an example. The wing cross section of interest was the Eppler 266 laminar flow airfoil.

b. Objective

The goal of this study was to identify the noise sources of the Eppler 266 airfoil as contained in the wing planform of the Standard Austria SH1 and to determine their relative magnitudes in the low subsonic regime. The Reynolds number and Mach number ranges were restricted to approximately 1,200,000 to 3,750,000 and 0.05 to 0.185, respectively. The primary objective in accomplishing this goal was to qualitatively predict the frequency spectrum and the relative power output of the sound generated by turbulent boundary layer, the lift fluctuations caused by the vortex shedding at the trailing edge of the airfoil, and the wake by theoretical means. This study should then provide the basis for continued investigation and the future flight test of the sailplane to record the noise generated by an area of the wing (excluding the wing tip, aileron deflection, and fuselage effects). By correlating the results of this study and future tests, the actual noise level of the predominant sound source should be identifiable.

c. The Approach

This study relies heavily on the theoretical and experimental efforts of such notables in the area of turbulent boundary layer research as Harrison, Doak, Sharland, Willmarth, and others. The results of their mathematical solutions to the noise problem are presented without elaborating on the actual mechanical details of how they were derived. Likewise, the

experimental results from wind tunnel and water tunnel tests recorded in open literature are used without explaining the techniques through which the data were obtained. The theoretical equations for determining the acoustic output resulting from vortex shedding and the wake are also presented in a similar manner, with the exception that values for the frequency of the vortex shedding and the boundary layer thickness at the trailing edge of the airfoil are obtained by original efforts. The frequency of the vortex shedding is obtained through flow visualization techniques provided by the hydraulic analogy of low subsonic two-dimensional flow represented on the water table to steady air flow. The boundary layer thickness is obtained theoretically with a numerical integration of the potential theory velocity distribution over the airfoil. Finally, the data received from the above techniques and experiments recorded in the literature are placed in the appropriate equations in order to predict the relative noise levels generated by the boundary layer, vortex shedding, and wake. These theoretical predictions should make possible the qualitative overview of the Eppler 266 cross section as a noise generator.

2. GENERAL THEORY AND GOVERNING EQUATIONS

a. The Acoustic Output of the Boundary Layer

The pressure fluctuations at a far field point in a flow due to the radiated sound from a source with an arbitrary surface shape (refer to Figure 12) is proportional to the following integral [16]

$$\int_S \frac{f(\bar{x}', t' - \frac{|\bar{x} - \bar{x}'|}{a_0})}{|\bar{x} - \bar{x}'|} dS'$$

where

$$F(\bar{x}', t' - \frac{|\bar{x} - \bar{x}'|}{a_0})$$

is the source function and

$$t' - \frac{|\bar{x} - \bar{x}'|}{a_0}$$

is the retarded time between source fluctuation and field point response. With the assumption that the field point is a large distance from the source such that $|\bar{x}| \gg D$, and the dimension of the source is small compared to the wavelength of the sound generated, one may replace the retarded times

$$t' = \frac{|\bar{x} - \bar{x}'|}{a_0}$$

by

$$t' = \frac{|\bar{x}|}{a_0}$$

Hereafter the retarded time

$$t' = \frac{|\bar{x}|}{a_0}$$

will be referred to as t . However, when the source function is random, such as that which exists in a turbulent boundary layer, statistical methods become necessary in order to determine the pressure at the field point. The autocorrelation is the statistical tool available to characterize the function. In the space domain the autocorrelation compares the source function at a point to the source function at surrounding points at a specific time and thus enables the formulation of a mean value for the source function in the neighborhood of the point. This mean is formulated from $F(\bar{x}', t)$ and $F(\bar{x}' + \Delta\bar{x}, t)$ in the following operation:

$$\frac{1}{S} \int_0^S F(\bar{x}', t) \cdot F(\bar{x}' + \Delta\bar{x}, t) dS' = \overline{F(\bar{x}', t) \cdot F(\bar{x}' + \Delta\bar{x}, t)}$$

and since $\bar{x}'' = \bar{x}' + \Delta\bar{x}$, then

$$\overline{F(\bar{x}', t) \cdot F(\bar{x}' + \Delta\bar{x}, t)} = \overline{F(\bar{x}', t) \cdot F(\bar{x}'', t)}$$

Doak [17] has taken these general concepts and the work of Curle [18] and Lighthill [19] and established an expression for the source function of a turbulent fluid on an infinite plane.

From this function Doak derived a formula estimating the power radiated from a turbulent boundary layer on a flat plate at low Mach numbers:

$$W = \frac{1}{6\pi\rho_0 a_0^3} \int_S \int_S \frac{\partial p}{\partial t}(\bar{x}', t) \frac{\partial p}{\partial t}(\bar{x}'', t) dS' dS'' \quad (1)$$

where $\partial p/\partial t(\bar{x}', t)$ and $\partial p/\partial t(\bar{x}'', t)$ represent the source function at time t at the points described by position vectors \bar{x}' and \bar{x}'' , respectively. The differentials dS' and dS'' indicate the neighborhoods of \bar{x}' and \bar{x}'' and are integrated over the entire surface, S , of the body.

One of the key assumptions upon which the derivation depends is the presence of low Mach numbers, and/or that the turbulent eddies in the fluid are small compared to the wavelength of the sound generated. Doak demonstrates that, in fact, the Mach number and the ratio of the turbulent eddy size to the acoustic wavelength are identical dimensionless parameters. Thus the presence of low Mach numbers allows--as Lighthill [19] has pointed out--the neglect of the different times of the emission of waves from \bar{x}' and \bar{x}'' .

The integrated covariance term

$$\int_S \frac{\partial p}{\partial t}(\bar{x}', t) \frac{\partial p}{\partial t}(\bar{x}'', t) dS''$$

may, according to Doak, be expressed in terms of a correlation area such that

$$\int_S \frac{\partial p}{\partial t}(\bar{x}', t) \frac{\partial p}{\partial t}(\bar{x}'', t) dS'' = \left\{ \frac{\partial p}{\partial t}(\bar{x}', t) \right\}^2 S_c(\bar{x}'; \frac{\partial p}{\partial t}) \quad (2)$$

where

$$\left\{ \frac{\partial p}{\partial t}(\bar{x}', t) \right\}^2$$

denotes a mean square of the source function at a point at time t and where $S_c(\bar{x}', \partial p/\partial t)$ is a correlation area over which this mean square pressure fluctuation has been derived and depends only on the point in question and the source function at that point.

The equation for power output, W , may now be written:

$$W = \frac{1}{6\pi\rho_0 a_0^3} \int_S \left\{ \frac{\partial p}{\partial t}(\bar{x}', t) \right\}^2 S_c(\bar{x}'; \frac{\partial p}{\partial t}) dS'. \quad (3)$$

According to Sharland [20]

$$\left\{ \frac{\partial p}{\partial t}(\bar{x}', t) \right\}$$

and S_c as a function of $(\bar{x}'; \frac{\partial p}{\partial t})$ may be replaced by

$$[p(\bar{x}', t)]^2 \cdot \omega^2 \cdot S_c(\bar{x}', p)$$

where ω is the characteristic frequency of the pressure fluctuation. Substitution into Equation (3) for

$$\left\{ \frac{\partial p}{\partial t}(\bar{x}', t) \right\}^2 S_c(\bar{x}', \frac{\partial p}{\partial t})$$

renders the form

$$W \approx \frac{1}{6\pi\rho_0 a_0^3} \int_S [p(\bar{x}', t)]^2 \cdot \omega^2 \cdot S_c(\bar{x}', p) dS' \quad (4)$$

Since for flight test, the microphone will be so situated that it will predominantly receive the noise generated from the bottom of the airfoil, the assumption will be made that the airfoil is nearly symmetrical and thus the bottom surface area is equal to one-half of the total surface area. Therefore, the sound radiated by the turbulent boundary layer into the lower semi-space should be one half of Equation (4):

$$W \approx \frac{1}{12\pi\rho_0 a_0^3} \int_S [p(\bar{x}', t)]^2 \cdot \omega^2 \cdot S_c(\bar{x}', p) dS. \quad (5)$$

Here $[p(\bar{x}', t)]^2$ may be interpreted as the mean square pressure fluctuation of the turbulent boundary layer. According to Harrison [21], the quantity

$$[p(\bar{x}', t)] / \frac{1}{2} \rho_0 U_0^2$$

is equal to a constant for a Strouhal number, based on the boundary layer displacement thickness δ^* , less than or equal to 0.2. Harrison obtained a value of 9.5×10^{-3} for this constant

which is high according to the measurements of Willmarth [22] and others. A generally accepted value for this constant in the Mach number range of this study is 6×10^{-3} and will be utilized in the appropriate equations. This means that $(\bar{p})^2 = 36 \times 10^{-6} q^2$, where q is the dynamic pressure, $1/2 \rho_o U_o^2$.

According to Bull and Willis [23], the value for $\omega^2 S_c$ should be of the order $1/2 U_o^2$ [20]. Substituting these values into Equation (5) gives:

$$W = 1.2 \times 10^{-7} \frac{\rho_o U_o^6}{a_o^3} \int_S dS' = 1.2 \times 10^{-7} \frac{\rho_o U_o^6}{a_o^3} S_{b1} \quad (6)$$

where S_{b1} is the lower surface of the wing covered by the turbulent boundary layer.

This equation for estimating the acoustic power output of the turbulent boundary layer on a flat plate should be applicable to the lower surface of the Eppler 286 airfoil. Doak [17] states that a surface may be considered locally flat if the radius of curvature of the surface is large compared to the wavelength of the sound generated by the turbulent boundary layer. Since the lower surface of the airfoil could be approximated by a circle with a large radius, the surface may be considered locally flat except possibly at low frequencies of 100 cycles per second and below.

b. Lift Fluctuation Caused by Vortex Shedding as a Noise Source

The boundary layer noise, according to Sharland [20], will be rather small in comparison to a larger order noise source created by the fact that for a plate of finite size, the "larger scale vorticity in the boundary layers on the two sides of the plate is not instantaneously symmetric." He contends that vortex shedding will occur at the trailing edge and, therefore, lift fluctuations are present. Sharland states that Equation (5) may be simplified when one realizes that the pressure fluctuations may be thought of in terms of local lift fluctuations per unit area. This idea relies on the assumption that the normal pressure fluctuations on the surface are large compared to the tangential stresses. Therefore,

$$p(\bar{x}', t) = C_L q = C_L (\bar{x}', t) \frac{1}{2} \rho_o U_o^2$$

and

$$\frac{\partial p}{\partial t}(\bar{x}', t) = \frac{\partial C_L}{\partial t} \frac{1}{2} \rho_o U_o^2$$

assuming the fluctuating component of the velocity is small when compared to the mean velocity. Then

$$\overline{\left[\frac{\partial p}{\partial t}(\bar{x}', t) \right]^2}$$

may then be written

$$\frac{1}{4} \rho_o^2 U_o^4 \overline{\left[\frac{\partial C_L}{\partial t}(\bar{x}', t) \right]^2}.$$

Substituting back into Equation (5) results in the following:

$$W = \frac{\rho_o}{48\pi a_o} \int_S U_o^4 \overline{\left[\frac{\partial C_L}{\partial t}(\bar{x}', t) \right]^2} S_c(\bar{x}', \frac{\partial C_L}{\partial t}) dS'. \quad (7)$$

Assuming then that

$$\overline{\left[\frac{\partial C_L}{\partial t}(\bar{x}', t) \right]^2} \cdot S_c(\bar{x}', \frac{\partial C_L}{\partial t}) = \overline{[C_L(\bar{x}', t)]^2} \cdot f^2 \cdot S_c(\bar{x}', C_L)$$

where f is the characteristic frequency of the lift fluctuations and

$$\overline{[C_L(\bar{x}', t)]^2}$$

the mean square of the fluctuation lift coefficient, then

$$W = \frac{\rho_o}{48\pi a_o} \int_S U_o^4 f^2 \overline{[C_L(\bar{x}', t)]^2} \cdot S_c(\bar{x}', C_L) dS'. \quad (8)$$

The description of this integral in terms of flow parameters necessitates a certain degree of knowledge about the flow mechanics by which the lift fluctuations are produced. Sharland [20] contends that the source strength can be ascertained by considering the order of magnitude of the parameters involved. He states that the lift fluctuations can be related to time fluctuations in the boundary layer thickness at the trailing edge of the airfoil. On this basis, it is suggested that the root-mean-square of the fluctuating lift coefficient should be of the order of $-1/5$ power of the Reynolds number [20]. The frequency of the lift fluctuations should be approximately the same as the frequency of the vortex shedding at the trailing edge. Sharland [20] contends that the correlation area as a function of (x', C_L) should be "governed by the size of the larger eddies at the trailing edge."

Thus if

$$[C_L(\bar{x}', t)]^2 \approx Re^{-0.4}, *$$

then

$$W = \frac{P_o}{48\pi a_o^3} \int U_o^4 \cdot f^2 \cdot (Re)^{-0.4} S_c(x', C_L) dS'. \quad (9)$$

Since $[U_o^4 f^2 (Re)^{-0.4} S_c(x', C_L)]$ is assumed constant during the integration,

$$W \approx \frac{P_o}{48\pi a_o^3} U_o^4 \cdot f^2 \cdot (Re)^{-0.4} S_c \cdot S_{v_s}, \quad (10)$$

where S_{v_s} is the entire lower surface of the wing.

Since f , the characteristic center frequency of vortex shedding, is not attainable from existing theory for streamline bodies, it must be ascertained experimentally. In Section 3 of this report an experiment is described which utilizes the flow visualization scheme provided by a water table in order to establish this shedding frequency. The correlation area S_c may be estimated if the larger eddies at the trailing edge are assumed to be approximately the same size as the boundary layer

* For small angles of attack only.

thickness at the trailing edge. Since the experimental measurement of the actual boundary layer thickness is extremely difficult, a theoretical approximation of this thickness is necessary. The method of obtaining this thickness is discussed in Section 4 of this report.

c. The Acoustic Output of the Wake

Since no direct data exists for the estimation of the noise produced by a wake, qualitative efforts to predict the noise generated by this sound source have been made. Franken [24] has argued that the wake of a subsonic vehicle is a region of high shearing forces, flow separation, and turbulence. Franken notes that these are the identical flow characteristics which occur in the jet stream of a gas reaction motor. Thus he makes an analogy between the two in qualitative terms. He observes that in jet radiation the velocity profile is directed downstream away from the jet engine and the most intense sound radiation is likewise downstream. However, since in wake turbulence the velocity profile is directed upstream towards the moving vehicle, he reasons that likewise the most intense sound radiation should be directed upstream as depicted in Figure 13.

Franken contends that the acoustic output of the wake is a small fraction of the power contained by the mechanical system generating the wake. The power of this system may be estimated by the equation

$$W = \eta DU_0$$

where D is the drag, U_0 is the free stream velocity (forward speed of the vehicle), and η is a factor of proportionality. The drag for a sailplane may be written in terms of an equivalent parasitic area f_p and the dynamic pressure q [3].

$$D = f_p q = f_p \left(\frac{1}{2} \rho_0 U_0^2 \right)$$

where

$$f_p = \frac{\bar{W}}{q(\text{GPR})} \left[1 - \frac{\text{GPR}(\bar{W})}{q} \left(0.01158 + \frac{0.3185}{AR} \right) \right] \quad (11)$$

and GPR is the glide path ratio at a specific velocity, \bar{W} is

the total weight of the aircraft and occupant, S is the total wing surface area, and AR is the aspect ratio. Then

$$W = \eta U_0 \left(\frac{1}{2} \rho_0 U_0^2 \right) f_p.$$

According to Franken, η , based on the analogy with subsonic jets, is assumed to be of the order $10^{-4} M_0^5$ where M_0 is the free stream Mach number. Substituting for η renders the final form for the acoustic energy of the wake:

$$W \approx 10^{-4} M_0^5 U_0 \left(\frac{1}{2} \rho_0 U_0^2 \right) f_p. \quad (12)$$

Interestingly enough, this produces an eighth power velocity dependence for the acoustic power output from a wake.

d. Frequency Spectra

(1) Boundary Layer

The turbulent boundary layer frequency spectrum, according to Skurdzyk and Haddle [25], can be assumed to arise from a Gaussian (a random distribution function) energy spectrum. The pressure spectrum is then derived by a series of integrations and the result resembles a Gaussian spectral distribution with a pronounced drop off above the frequency described by $f = U_0/\delta_s$ where U_0 is the free stream velocity and δ_s is the smallest boundary layer thickness.

From the derivation of the low frequency spectrum, a patch of turbulence may be thought of as being a pulse with a diameter equal to the width of the turbulent patch. If this patch is considered to have a width approximately equal to the thickness of the boundary layer, then the spectrum should turn out to be constant up to a space wavelength approximately equal to the largest boundary layer thickness and then decrease as $(\sin x/x)$. The high frequency spectrum is supposed to behave as specified by the "equilibrium laws of turbulence," of which the Kolmogorov law predicts that at high frequencies the energy spectrum decreases inversely as $3/2$ the power of the space wavelength. Thus the spectral density may be expected to be nearly constant at low frequencies from U_0/δ_1 (where δ_1 denotes the largest boundary layer thickness) up to a high frequency of U_0/δ_s and then decrease approximately as the inverse of the $3/2$ power of

of the wavelength. Therefore, the spectral density of the boundary layer noise in the audible range of the human ear would be expected to be the result of broad band type noise.

(2) Vortex Shedding

A sizable amount of consideration has been given to the solid stationary circular cylinder in a flow [26]. The general findings of these investigations show that the vortex shedding from the cylinder due to the viscosity of the flow medium creates an unsteady lift force on the cylinder, causing an opposite circulation and hence a lift. This fluctuating lift generates a distinctive sound field perpendicular to the flow with the frequency $f = S_t U_0 / d$ where S_t is the Strouhal number and d is the diameter of the cylinder. A weaker sound field of twice the frequency of the noise generated by the fluctuating lift and parallel to the flow is produced by the fluctuating drag resulting from the lift variation as shown in Figure 14. For an airfoil in a flow, one would expect a similar acoustic phenomenon; the most intense sound, due to the fluctuating lift, being radiated perpendicular to the flow while a much weaker sound field, due to the fluctuating drag being spherically radiated parallel to the flow. At higher angles of attack the sound spectrum produced by the airfoil should center about a pre-dominant characteristic frequency, while at lower angles of attack, as more randomness appears in the fluctuations, a broader band noise should appear.

(3) Wake

The wake of the cylinder at low Reynolds numbers (300 to 10,000) results in the regularly spaced vortices of the Karman sheet. At higher Reynolds numbers the Karman sheet dissipates rapidly and the orderly progression of individual vortices disappear. According to Lighthill [19], the velocity fluctuations in the turbulent wake produce a field of quadrupole noise sources which radiate broad band noise whose intensity varies as U_0^8 . Likewise, the frequency spectrum of the noise generated by the moving airfoil should reflect the presence of wide band noise with no particular frequency predominating.

e. Comparison of the Equation for the Acoustic Output of the Aerodynamic Noise Sources

Consider the ratio of the acoustic output due to lift fluctuations caused by vortex shedding to the acoustic output of the boundary layer, i.e., W_{vs}/W_{bl} :

$$W_{vs} = \frac{\rho_o}{48\pi a_o^3} U_o^4 f^2 (Re)^{-0.4} S_c S_{vs}, \quad (10)$$

$$W_{bl} = 1.2 \times 10^{-7} \frac{\rho_o U_o^6}{a_o^3} S_{bl}. \quad (6)$$

Now forming W_{vs}/W_{bl} ,

$$W_{vs}/W_{bl} = \frac{17.4 \times 10^4}{\pi} \left\{ \frac{f}{U_o} \right\}^2 S_c (Re)^{-0.4} \frac{S_{vs}}{S_{bl}}. \quad (13)$$

S_{vs} , the sound radiating area due to the lift fluctuations, is the entire area of the lower portion of the wing, S . S_{bl} is that area of the bottom of the wing covered by the turbulent boundary layer and is equal to $S(1-x_1/\bar{c})$ where x_1/\bar{c} is the transition point of the boundary layer from laminar to turbulent flow expressed as a decimal fraction of the mean aerodynamic chord \bar{c} . Therefore, $S_{vs}/S_{bl} = 1/(1-x_1/\bar{c})$.

If the correlation area is assumed to be the size of the larger turbulent eddies at the trailing edge of the airfoil [20], S_c can then be approximated by a circular area, the width of which is of the same scale as the trailing edge boundary layer thickness, δ , on the lower side of the airfoil:

$$S_c = \pi (\delta/2)^2 = \frac{\pi}{4} \delta^2.$$

Substituting in Equation (13) for S_{vs}/S_{bl} and S_c renders the final form,

$$W_{vs}/W_{bl} = \frac{4.35 \times 10^4}{(1-x_1/\bar{c})} \left\{ \frac{f}{U_o} \right\}^2 \delta^2 (Re)^{-0.4}. \quad (14)$$

Now consider the ratio of the acoustic output due to the lift fluctuations caused by vortex shedding to the acoustic output of the wake, i.e., W_{vs}/W_w :

$$W_{vs} = \frac{\rho_o}{48\pi a_o^3} U_o^4 f^2 (Re)^{-0.4} S_c S_{vs}, \quad (10)$$

$$W_w = 10^{-4} M_o^5 U_o (\frac{1}{2} \rho_o U_o^2) f_p. \quad (12)$$

Now forming W_{vs}/W_w where S_c is again considered to be $\pi/4 \delta^2$,

$$W_{vs}/W_w = 1.04 \times 10^2 \left\{ \frac{f}{U_o} \right\}^2 \frac{(Re)^{-0.4}}{M_o^2} \delta^2 \frac{S}{f_p}, \quad (15)$$

where f_p is the parasitic area. As previously mentioned, f_p for a sailplane may be expressed by Equation (11). The glide path ratio (GPR) of the Standard Austria SH1 is 32:1 at a speed of 57 miles per hour. The weight of the pilot and aircraft for the preliminary flight test was approximately 715 pounds. Using these values and an aspect ratio of 16.7 in Equation (11) renders an f_p of 1.12 square feet. Substituting the area of the wing for S (146 square feet) and 1.12 square feet for f_p , then

$$W_{vs}/W_w = 1.36 \times 10^4 \frac{(Re)^{-0.4}}{M_o^2} \left\{ \frac{f}{U_o} \right\}^2 \delta^2. \quad (16)$$

The common unknown parameters for both W_{vs}/W_w and W_{vs}/W_{b1} are $\{f/U_o\}^2$ and δ^2 . Once these parameters are known then the relative strengths of the aerodynamic noise sources may be qualitatively judged.

3. THE WATER TABLE EXPERIMENT

a. Theory Behind the Experimental Approach

The purpose of the water table experiment is to ascertain the quantity $\{f/U_o\}^2$ by establishing the characteristic frequencies of vortex shedding at the trailing edge of the airfoil at various angles of attack. To accomplish this task the flow pattern about the sailplane wing is simulated by the two-dimensional flow of the water table. The characteristic frequency of the vortex shedding at the trailing edge of the airfoil in water may then be correlated to the frequency in the air through the Strouhal number. The Strouhal number is a dimensionless parameter which describes flow periodicity. The number is defined by $St = fl/U_o$ where f is the frequency of the flow, l is a characteristic length, and U_o is the free stream velocity. For this study the characteristic length is the boundary layer displacement thickness, δ^* , at the trailing edge of the airfoil. By matching the Strouhal number in the

air and on the water table, the frequencies may be correlated:

$$\frac{f_{\text{air}} \delta_{\text{air}}^*}{U_{\text{air}}} = \frac{f_{\text{water}} \delta_{\text{water}}^*}{U_{\text{water}}}$$

if

$$\bar{n} = \frac{\delta_{\text{water}}^*}{\delta_{\text{air}}^*} \cdot \frac{1}{U_{\text{water}}}$$

then

$$f_{\text{air}} = \bar{n} f_{\text{water}} U_{\text{air}}$$

In this manner the Strouhal number compensates for the differences in velocity and in the Reynolds number of the two flows. The missing parameter $\{f_{\text{air}}/U_{\text{air}}\}^2$ for the comparison of the acoustic output of the aerodynamic noise sources is thus equal to $\{\bar{n} f_{\text{water}}\}^2$. Hence, the purpose of the water table is to provide a flow regime from which the frequency of the vortex shedding at the trailing edge of the airfoil may be correlated to the frequency of the vortex shedding or lift fluctuations in actual flight at different velocities. The method of obtaining values for $\delta_{\text{water}}^*/\delta_{\text{air}}^*$ is discussed in part (d) of this section.

The determination of f_{air} requires that the angle of attack of the airfoil on the water table be varied as one attempts to simulate different velocities in the air. Thus the determination of how variations in angle of attack in actual flight are related to velocity changes is important to the correlation of the periodic flow disturbances at the trailing edge to the acoustic output of the airfoil.

It is possible to relate angle of attack to velocity through the lift coefficient. If one knows how C_L varies with angle of attack, then the velocity can be obtained through the equation:

$$L = C_L \frac{1}{2} \rho U_o^2 S.$$

Assuming lift, (L), equal to weight, (\bar{W}), then

$$C_L = \frac{2\bar{W}}{\rho U_o^2 S}.$$

Thus if one knows the velocity and how C_L varies with angle of attack, then it is known how the effective angle of attack varies with velocity. Since the water table gives only a two-dimensional model of the flow regime and the effect of induced velocities due to the vortex system of the three-dimensional wing is not present, then the effective angle of attack is equal to the geometric angle of attack. For this experiment Table I defines the angle of attack necessary on the water table to simulate a certain angle of attack in the air associated with a specific velocity. The derivation of the C_L versus angle of attack curve given in this table was developed experimentally from the specified glider in flight.

b. Mechanics of the Experiment

(1) The Water Table

For this experiment, the water table located in the hydrodynamics laboratory of The University of Tennessee Space Institute was utilized. The main table assembly consists of a 3 feet, 9 inch by 6 feet test section made of 0.75 inch thick plexiglass, 3 inch high walls, a settling and a discharge tank, and a 2 inch thick fibrous mesh located in the upstream edge of the test section (refer to Figure 15). The fibrous mesh smoothed out the flow and removed bubbles which formed on the water's surface in the settling tank before they could be transported downstream. Recirculation of the water from the discharge tank to the settling tank is accomplished by a Weinmann water pump with a 3 horsepower electric motor. The maximum capacity of the pump is 650 gallons per minute. The water table assembly is attached to an iron frame which has built-in floor screws that enable the adjustment of the slope of the table. Water for the table is supplied by a 2 inch water pipe located just above the discharge tank. Once the proper level of water is obtained on the test section, the flow may be adjusted by changing the flow rate through the recirculation pump. This adjustment is accomplished through the use of throttling valves on the pump.

(2) The Model

The model was constructed from a large section of 2 inch thick plexiglass. A pattern of the Eppler 266 cross section was produced from a 4-1/2 inch scale drawing which was photographically enlarged to a 27 inch chord length. This chord length is approximately the upper limit for a model on the water table and still preserve the flow without wall interference affecting the near field around the model. The large chord length was chosen in order to obtain the closest possible Reynolds number to those expected in actual flight. The pattern was then placed on the plexiglass and cut, ground, and sanded to a smooth close tolerance finish. A 7 inch enlargement of the 4-1/2 inch scale

drawing is included in Figure 16. The inner unshaded airfoil is the NACA 652414 which was employed by the Standard Austria S 1963. The outer airfoil is the Eppler 266 which is utilized by the later Standard Austria SH1 1964.

(3) Lighting Technique

A light source consisting of a bank of six standard fluorescent tubes was placed underneath the water table in order to illuminate the test section. A large sheet of translucent tracing paper was taped underneath the plexiglass test section. This paper served two purposes: first, it diffused the light, thus producing a good background for picture taking; second, a reference grid and lines to designate specific angles of attack orientations were drawn on the paper. The model could then be aligned and realigned over these lines, thus providing a simple, accurate method of varying the angle of attack. The grid proved to be of great value when reviewing the pictures of the model in the flow by providing a reference by which the scale of the disturbances created in the flow might be judged.

(4) The Dye

A dye was used in order to visualize the streamlines close to the model. The dye for this experiment was potassium permanganate crystals dissolved in water. This solution is a dark red liquid which was easily photographed when introduced into the flow. Once the model was properly aligned at the correct angle of attack and positioned in the center of the test section approximately 14 to 18 inches downstream of the fibrous mesh (in order to minimize wall effects and to capitalize on the smoothest possible flow), smooth, steady flow of the desired velocity achieved, and the desired water level attained (approximately 1-7/8 inches at the leading edge of the model and 1-15/16 inches at the trailing edge), then the dye was introduced into the flow. The dye was allowed to enter perpendicular to the flow in a steady stream through small rubber tubing connected to a gravity feed dye dispenser located high on the laboratory wall. When an overall view of the flow near the model was desired, the dye was allowed to enter the water about 2 inches in front of the leading edge of the model in such a position that the dye would pass through the stagnation point and then spread out over both the top and bottom surfaces of the model. If just the flow at the trailing edge was to be viewed, then the dye was allowed to enter the flow next to the lower surface of the model, approximately 3 inches upstream of the trailing edge.

(5) Photographic Techniques

The two cameras used in this experiment were the Minolta K7 8mm for motion pictures and the 35mm Agfa Karat for still photographs. There were two basic photographic methods utilizing these cameras which were especially adaptable to the water table. Although the table is equipped with a large 5 feet by 6 feet mirror mounted at a 45 degree angle over the test section, the method of simply mounting the cameras on a tripod and taking photographs directly into the large mirror was not applicable since much smaller focal lengths were required for close-up lenses, focal lengths of approximately 12 inches and smaller became necessary. Focusing directly into the large mirror could not produce focal lengths less than 36 inches. To solve the problem, two pieces of 1/2 foot by 8 feet by 1/2 inch thick plexiglass were placed 7-1/2 inches above the test section. The cameras were mounted to one while a 4 inch by 6 inch mirror was mounted at a 45 degree angle on the other (refer to Figure 17). For still photographs the 35mm camera was then focused into the mirror with the focal length being varied by changing the distance from the mirror to the camera. The entire length of the model could be photographed in detail by moving the mirror and camera from position to position along the plexiglass supports and adjusting the focal length.

For motion pictures of the flow, the Minolta K7 was mounted to the plexiglass support by a screw at the base of the hand grip and tilted to a position perpendicular to the area of the flow desired to be photographed. A support cable from the hand grip was then attached to the top of the large mirror mounted above the table (not shown in Figure 17). With the close-up lens attached, the camera could be focused manually by looking through the viewfinder and adjusting the "zoom" lens. This camera arrangement was especially advantageous because it allowed for the simple modification of the field of view around the model while still maintaining excellent support of the camera.

(6) Measurement of the Water Velocity

In order to obtain the water velocity, a simple but reliable method is apparent. Directly above the test section a meter stick was placed parallel to the flow. Small pieces of paper were then placed on the water surface upstream of the meter stick and allowed to be transported downstream by the flow. The time the paper took to traverse the length of the meter stick was timed with a stop watch. The times of several runs at the same throttle setting were then averaged and the result divided into the one meter distance to establish the velocity. This approach seemed quite satisfactory since the run times generally fell in the near vicinity of one another.

(7) Reynolds Number

The Reynolds number is described by three parameters: U_0 (the free stream velocity), l (the characteristic length of the model, and ν (the kinematic viscosity of the fluid). In this experiment, all three parameters could be varied. Since $Re = U_0 l / \nu$, increasing U_0 and l will increase Re while increasing ν will decrease Re . The Reynolds number may be modified through the free stream velocity by adjusting the throttling valves on the recirculation pump and by increasing or decreasing the table slope with the floor screws. The length of the model may also affect the Reynolds number. In addition to the main 27 inch model, an 18 inch and an 11-1/2 inch model were constructed. By placing these different models on the table, the Reynolds number may be modified simply and quickly. Finally, since kinematic viscosity is a function of temperature, the action of the pump's stator blades against the water will increase the temperature of the water with time and thus modify the Reynolds number. Since little control is possible over this variable, one can only record the increase of the temperature with a thermometer and thus note this automatic change in the Reynolds number.

c. The Still Photograph Experiment

The purpose of the still photograph experiment is to obtain the transition point of the boundary layer from laminar to turbulent flow for the 27 inch model on the water table. This information will then be used to obtain theoretically the boundary layer displacement thickness at the trailing edge of the model in the water flow.

For this experiment, the angle of attack of the model was varied from -2.3 to 10.4 degrees. Different water velocities and water temperatures were used to vary the Reynolds number on the table. Both black and white and color pictures were taken of the model. Some of the best photographs of the transition region resulted from color pictures of the model when dye was injected into the boundary layer by a hypodermic syringe. Even though the Reynolds number was varied between 1.38×10^5 and 2.56×10^5 , for angles of attack between -2.3 and 5.9 degrees, the transition region remained at approximately 21 inches downstream from the leading edge of the 27 inch model. This figure represents a transition of about 0.78 of the chord length.

d. The Motion Picture Experiment

The frequency of the vortex shedding at the trailing edge of the airfoil was studied for angles of attack of -2.3, -1.9,

2.8, 4.25, and 5.9 degrees. The close-up lens on the 8mm camera allowed the inspection of approximately a 3 inch diameter area immediately behind the trailing edge. At the higher angles of attack the pattern of shedding vortices is quite pronounced and dissipates relatively slowly when compared to the smaller vortices which dissipate immediately at the two negative angles of attack. However, even at 5.9 degrees, the vortices have generally decayed beyond recognition as distinctive eddies by the time they reach the limit of the camera's field of view. For the three positive angles of attack the vortices are approximately 1/4 to 3/8 inch in diameter when first formed downstream of the trailing edge, but soon decay to larger and rather formless swirls of approximately 1 inch in diameter within the time it takes for the vortices to be conveyed 1/10 to 1/12 foot downstream. The vortices at the two negative angles of attack are smaller and their cycle between creation and decay are much more difficult to follow. These vortices dissipate very rapidly and are not nearly as well formed. This is to be expected, however, since these vortices result from a flow juncture at the trailing edge which is far more symmetric than those for the higher angles of attack where separation occurs on the upper surface and creeps toward the leading edge as the stall angle is approached. Thus at the positive angles of attack the counterclockwise rolling up of the flow from the bottom surface of the airfoil just downstream of the trailing edge is quite distinctive, while at the negative angles of attack this forming of the vortices is not nearly as visible.

The data presented here is the result of over 300 feet of 8mm film being placed on a microfilm reader and inspected frame by frame to arrive at the various frequencies for the stated angles of attack. The results of these efforts are presented in Table II and Figure 18.

The frequencies of the vortex shedding for the same angle of attack at the velocities shown in Table II appear to vary by the ratio of the velocities. Logically, one would expect this correlation to exist since the boundary layer structure for the various velocities are quite nearly identical since the Reynolds numbers are nearly matched. Therefore, by matching the Strouhal number, then

$$\frac{f_{U_1} \delta_{U_1}^*}{U_1} = \frac{f_{U_2} \delta_{U_2}^*}{U_2},$$

and since

$$\delta_{U_1}^* \approx \delta_{U_2}^*,$$

then

$$f_{U_1} = f_{U_2} \frac{U_1}{U_2},$$

where the subscripts U_1 and U_2 denote the respective values associated with the two velocities.

4. BOUNDARY LAYER THICKNESS

This section deals with the method by which the boundary layer thicknesses at the trailing edge of the Eppler 266 airfoil can be theoretically determined with the aid of the computer. This study is concerned only with the boundary layer that is formed on the lower surface of the airfoil; however, the method is applicable to both top and bottom surfaces. Once the computer program is established, this method allows for the varying of the Reynolds number, lift coefficient, and flow medium (specifically air and water).

The basic formula for computing the various boundary layer thicknesses is found in Schlichting's Boundary Layer Theory [27] in the chapter dealing with the incompressible two-dimensional turbulent boundary layer with a pressure gradient. This equation deals with the momentum thickness and from it the boundary thickness and displacement thickness may be computed if the velocity profile is assumed to be of the form $U/U_\infty = (y/\delta)^{1/n}$, known as a power law. In this case of the power law, the boundary layer thickness may be expressed in the following ratios:

$$\delta^*/\delta = \frac{1}{1+n}, \quad \delta_2/\delta = \frac{n}{(1+n)(2+n)}$$

where δ^* is the boundary layer displacement thickness, δ is the boundary layer thickness, and δ_2 is the momentum thickness.

Schlichting [27] provides the following formula for the momentum thickness which is the basis for the various desired thicknesses:

$$\delta_2/l = \left(\frac{U}{U_\infty}\right)^{-3} \left\{ C_1^* + \left(\frac{C_f}{2}\right)^{(n+1)/n} \int_{x_t/l}^{x/l} \left(\frac{U}{U_\infty}\right)^{3+2/n} d\left(\frac{x}{l}\right) \right\}^{n/(1+n)} \quad (17)$$

Here (U/U_∞) denotes the potential theory velocity ratio which varies over the surface of the airfoil. But in Equation (17),

$$\left(\frac{c_f}{2}\right)^{(n+1)/n} = A \left(\frac{U_\infty \ell}{\nu}\right)^{-1/n}, \quad (18)$$

where A is a constant established by the n which is chosen to represent the boundary layer velocity profile (assuming a constant profile along the entire length of the turbulent boundary layer) and

$$C_1^* = \left[\frac{1}{2} c_{f_\ell} \left(\int_0^{x_t/\ell} \left(\frac{U}{U_\infty}\right)^5 d\left(\frac{x}{\ell}\right) \right)^{1/2} \right]^{(n+1)/n}, \quad (19)$$

where c_{f_ℓ} is the coefficient of skin friction for a flat plate at zero angle of attack with a Reynolds number (Re) defined by $U_\infty \ell / \nu$. However,

$$c_{f_\ell} = \frac{1.328}{\sqrt{\text{Re}}} + \frac{2.326}{\text{Re}} \quad (20)$$

and x_t/ℓ is the transition point from laminar to turbulent flow as a nondimensional fraction of the chord length.

For turbulent flow $4 < n < 6$, where $n = 4$ is valid for low Reynolds numbers and $n = 6$ is valid for high Reynolds numbers. The corresponding constant A for $n = 4$ is 0.016 and for $n = 6$ is 0.0076. Choosing $n = 5$ for the Reynolds numbers in the one to three million range and linearly interpolating the constant A between the values for $n = 4$ and $n = 6$ produces an $A = 0.0118$. For the Reynolds numbers on the water table, $n = 4$ is chosen with an $A = 0.016$.

The remaining values which must be known to establish the desired boundary layer thicknesses are the velocity distribution along the bottom of the airfoil and the transition point from laminar to turbulent flow in the boundary layer. First, consider the velocity distribution along the bottom surface of the airfoil.

The velocity ratio, U/U_∞ , distribution is composed of three parts. First is the U/U_∞ distribution over the basic thickness form at zero angle of attack. This will be denoted by U_0/U_∞ . Any thickness ratio may be obtained from the nearest thickness form by linear scaling with the following equation [28]:

$$\left(\frac{U_0}{U_\infty}\right)_{t_2} = \left[\left(\frac{U_0}{U_\infty}\right)_{t_1} - 1 \right] \frac{t_2}{t_1} + 1. \quad (21)$$

The second component corresponds to the design load distribution of the mean line and will be denoted by $\Delta U_o/U_\infty$. For any other camber or design lift coefficient the $\Delta U_o/U_\infty$ may be obtained by a direct ratio. The third component corresponds to the additional load distribution due to angle of attack and will be designated by $\Delta U_\alpha/U_\infty$. For velocity distributions at lift coefficients other than the design lift coefficient, the ratio may be determined by multiplying the $\Delta U_o/U_\infty$ at the design lift coefficient by $(C_L - C_{L1})$. Thus, the final ratio for the lower surface is

$$\frac{U}{U_\infty} = \left(\frac{U_o}{U_\infty} - \frac{\Delta U_o}{U_\infty} - \frac{\Delta U_\alpha}{U_\infty} \right), \quad (22)$$

and for an airfoil which is built up from another basic camber and thickness form:

$$\frac{U}{U_\infty} = \left\{ \left[\left(\frac{U_o}{U_\infty} \right)^{t_2} - 1 \right] \frac{t_2}{t_1} + 1 \right\} - (\text{camber ratio}) \frac{\Delta U_o}{U_\infty} - (C_L - C_{L1}) \frac{\Delta U_\alpha}{U_\infty} \quad (23)$$

For this study, the velocity distribution on the lower surface of the Eppler 266 airfoil is constructed from the thickness form of the NACA 66₁-012 with a new thickness of 17% [29]. The mean line is the NACA 66 with a camber ratio of 0.0326/0.060. Thus the new design lift coefficient is:

$$(0.0326/0.060) (\text{NACA 66 mean line design coefficient})$$

and is equal to 0.413.

The final unknowns for evaluating the trailing edge boundary layer thicknesses at various velocities are the transition points from laminar to turbulent flow in the boundary layer. Using Equation (24) for the instability points for a symmetrical airfoil renders a reasonable approximation for these points [23]:

$$x_1/c = 0.0537 (C_L + 1.02) - 0.0493 (C_L + 1.36) \log Re. \quad (24)$$

Using Equation (24) in the lift coefficient range between 0.097 and 0.960 renders the following values, as stated in Table III.

For the range of the various lift coefficients above and a constant Reynolds number of approximately 1.845×10^5 , it was determined that transition on the water table remained approximately constant at 0.78 of the model's chord length. This figure was arrived at through a photographic study of the airfoil on

the water table when the flow was seeded with dye (refer to Section 3).

With this information, a computer program was constructed using Schlitching's equation for the momentum thickness which necessitates the numerical integration of the velocity distribution over the lower surface of the airfoil. The results of this procedure are later presented in this section in the form of tables and graphs (refer to Table IV and Figures 19 and 20).

There is a weakness in the assumption that the velocity profile of the turbulent boundary layer is constant along the entire length of the wing section. In reality, as the flow encounters an adverse pressure gradient, the profile will change. The profile closely resembles a power law soon after transition, but is modified by an adverse pressure gradient in such a manner that the profile can be approximated by a power law with a smaller $1/n$ term (refer to Figure 21). The result is a change which lessens the steepness of the profile. In order to check the magnitude of the effect of this changing profile on the answers given by the computer, the exponent of the power law was varied.

The amount that the exponent should vary in order to simulate actual flow conditions depends upon the severity of the actual adverse pressure gradient. In Figure 22 the velocity distribution is plotted for a lift coefficient equal to 0.980, 0.635, and 0.135. These three lift coefficients reflect a wide-spread sampling of the velocity regime in which the sailplane flies. From Figure 22 it is easily seen that the flow begins to decrease in velocity at $x/c = 0.7$ for all three lift coefficients. Thus from $x/c = 0.7$ to the trailing edge of the airfoil the flow encounters an adverse pressure gradient. For the lift coefficients of 0.635 and 0.135, a nearly zero pressure gradient exists from the transition point to 70% of the chord. For a lift coefficient equal to 0.98, a gentle favorable pressure gradient exists from transition at $x/c = 0.4$ to $x/c = 0.5$, where a near zero pressure gradient exists until $x/c = 0.7$. From $x/c = 0.7$ to the trailing edge all three encounter approximately the same moderate adverse pressure gradient. On the basis of the near zero pressure gradient from transition to $x/c = 0.7$ and for the relatively moderate adverse pressure gradient which is experienced by the flow--for this lift coefficient range--from $x/c = 0.7$ to the trailing edge, it is assumed that the actual profile of the boundary layer will at all times lie between the limiting power laws of $U/U_\infty = (y/\delta)^{1/5}$ and $U/U_\infty = (y/\delta)^{1/4}$. Table V compares the values given by the computer for the boundary layer displacement thickness for the power law exponent equal to $1/4$ and $1/5$. On the basis of the comparison shown in Table V, it will be assumed that a constant velocity profile equal to the power law $U/U_\infty = (y/\delta)^{1/5}$ will produce a high estimate of the actual boundary layer thicknesses. This estimate is utilized during the remainder of this study.

5. RESULTS AND CONCLUSIONS

Now that the necessary information is available to establish values for $\{n_{\text{water}}\}^2$ and δ^2 , the comparison of the relative importance of the aerodynamic sound sources of the Eppler 286 airfoil throughout the flight velocity range of the Standard Austria SH1 is possible with aid of the ratios $W_{\text{vs}}/W_{\text{bl}}$ and $W_{\text{vs}}/W_{\text{w}}$ derived in Section 2. Tables and plots of $W_{\text{vs}}/W_{\text{bl}}$ versus Velocity and $W_{\text{vs}}/W_{\text{w}}$ versus Velocity are presented in Table VI and in Figures 23 and 24.

From these ratios of acoustic energies, a qualitative summary may be made of the aerodynamic sound sources of the Eppler 286 airfoil

- (1) When one speaks of what is the predominant sound source, the velocity regime of the flight must be considered.
- (2) In general, the most predominant sound source in the range from 60 to 210 feet per second appears to be that of the unsteady lift caused by vortex shedding at the trailing edge of the airfoil.
- (3) At the lowest and the highest speeds in the aircraft's velocity range, however, the turbulent boundary layer appears to be an important contributor to the overall acoustic output of the airfoil.
- (4) At low speeds, the wake appears to have very little effect on the total acoustic output of the airfoil, but as the velocity exceeds 150 feet per second, the wake rapidly becomes more influential to the overall sound energy generated by the airfoil moving through the atmosphere. At velocities above the range of the Standard Austria SH1, the wake may possibly be the most predominant aerodynamic source of conventional subsonic aircraft.
- (5) One would expect the frequency spectra of the sound generated by the aircraft in the approximate velocity range of 74 to 100 feet per second to show peaks at the characteristic frequencies of vortex shedding, but also to reflect the broad band nature of the sound generated by the turbulent boundary layer. At the higher frequencies, however, the influence of the broad band nature of the wake, turbulent boundary layer, and the increased randomness of the lift fluctuations predominates.

It should be noted that although the equations used for the acoustic output of the turbulent boundary layer (W_{bl}), wake (W_w), and lift fluctuations (W_{vs}) are dimensionally correct, they have been applied to a very specific situation and their real significance lies in their relative values with one another rather than their absolute magnitudes. Again, the derivation of Equation (1) is highly dependent on the presence of low Mach numbers and thus would lose validity in a higher velocity regime than that considered in this study. Also, a characteristic frequency of vortex shedding from a streamline body would not be expected unless highly unsymmetrical flow in the boundary layers of the upper and lower surfaces at the trailing edge is present. At the higher velocities where small angles of attack are present, the increased randomness of the unsteady lift forces makes the concept of a characteristic frequency more difficult to apply. Thus a time average of the fluctuations is the best estimate that can be expected for such orientations. Therefore, for any exact calculations of the absolute acoustic output at angles of attack near zero lift, this method becomes questionable. However, for a first order approximation of the relative source strengths, this formulation of W_{vs} , W_{bl} and W_w should provide a good deal of insight into the parameters affecting the achievement of ultra-quiet flight.

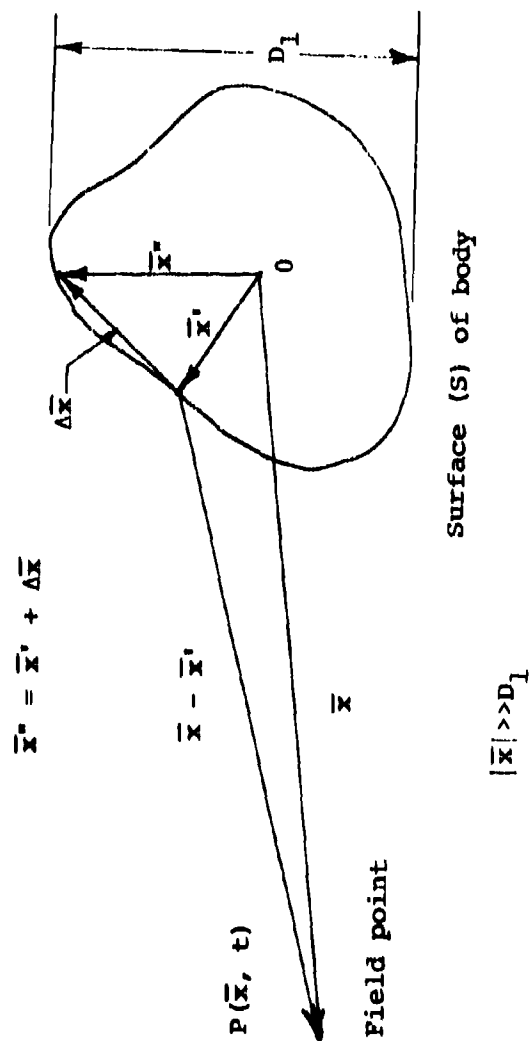


Figure 12. The Coordinate System.

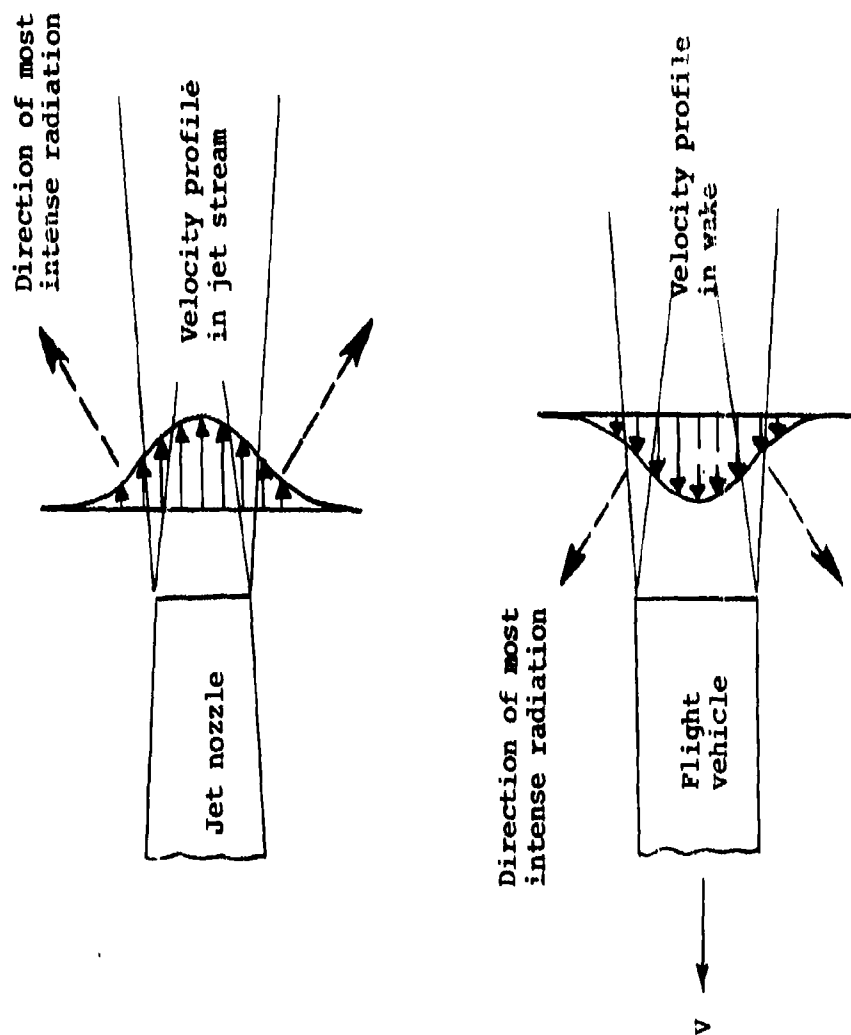


Figure 13. Qualitative Comparison of Noise Radiation from a Jet and from a Wake.

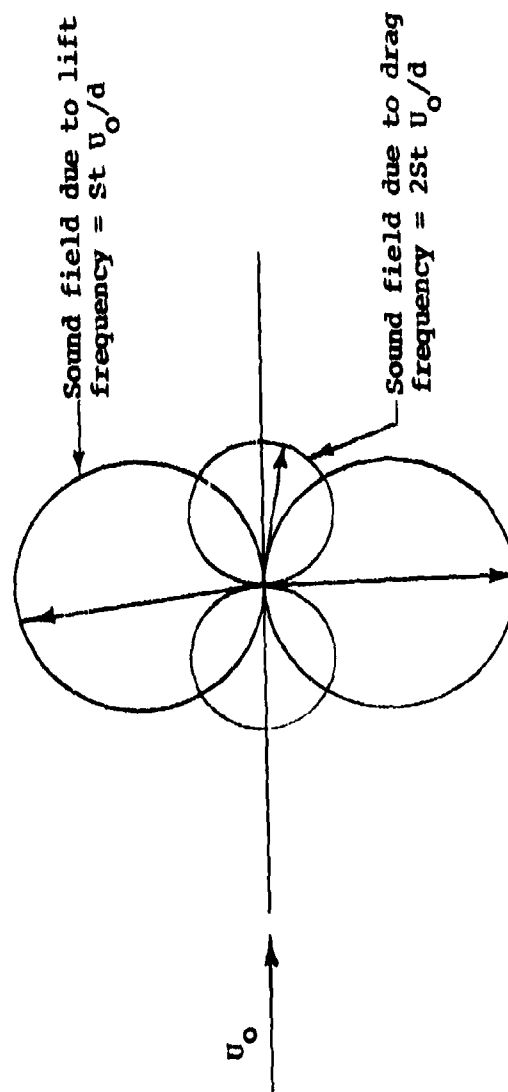


Figure 14. The Sound Fields Due to Oscillating Lift and Drag on a Circular Cylinder in a Flow.

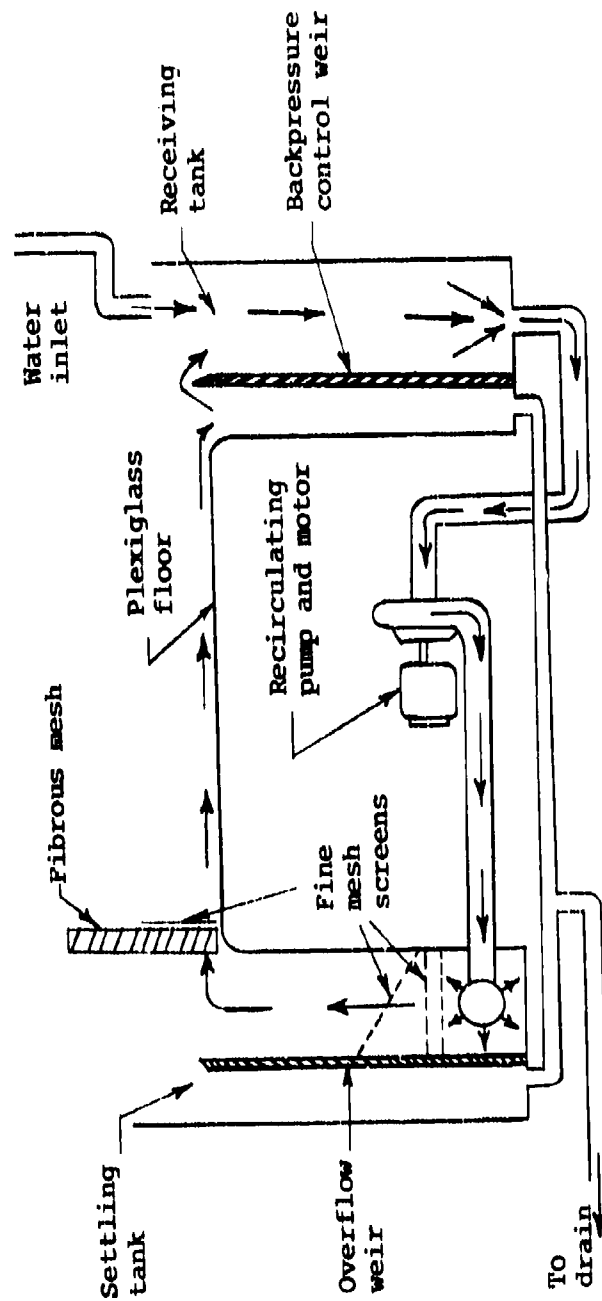
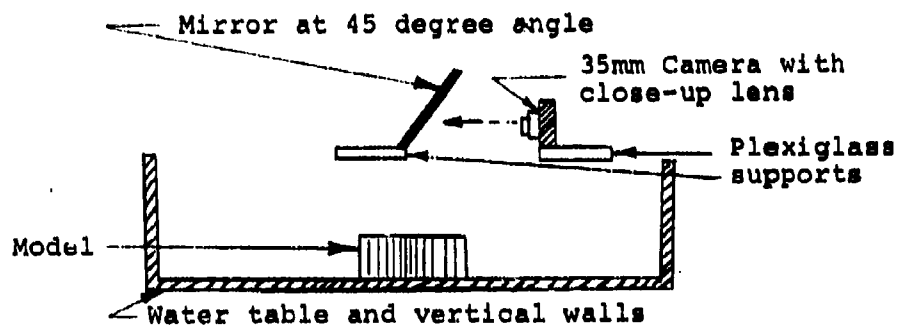


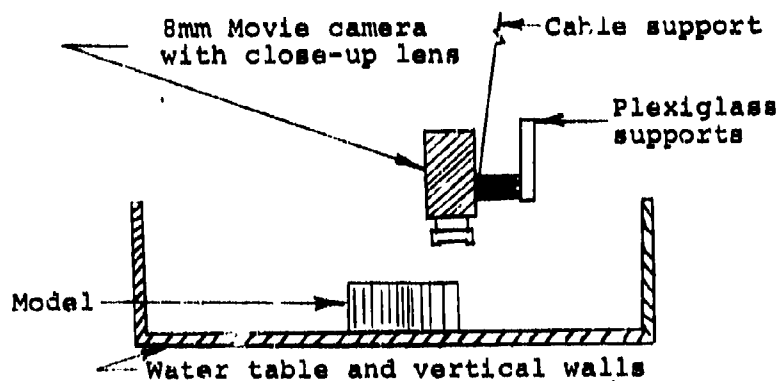
Figure 15. Schematic Diagram of Water Table.



Figure 16. The Model Shape.



a. Configuration for Still Photographs



b. Configuration for Motion Pictures

Figure 17. Photographic Techniques.

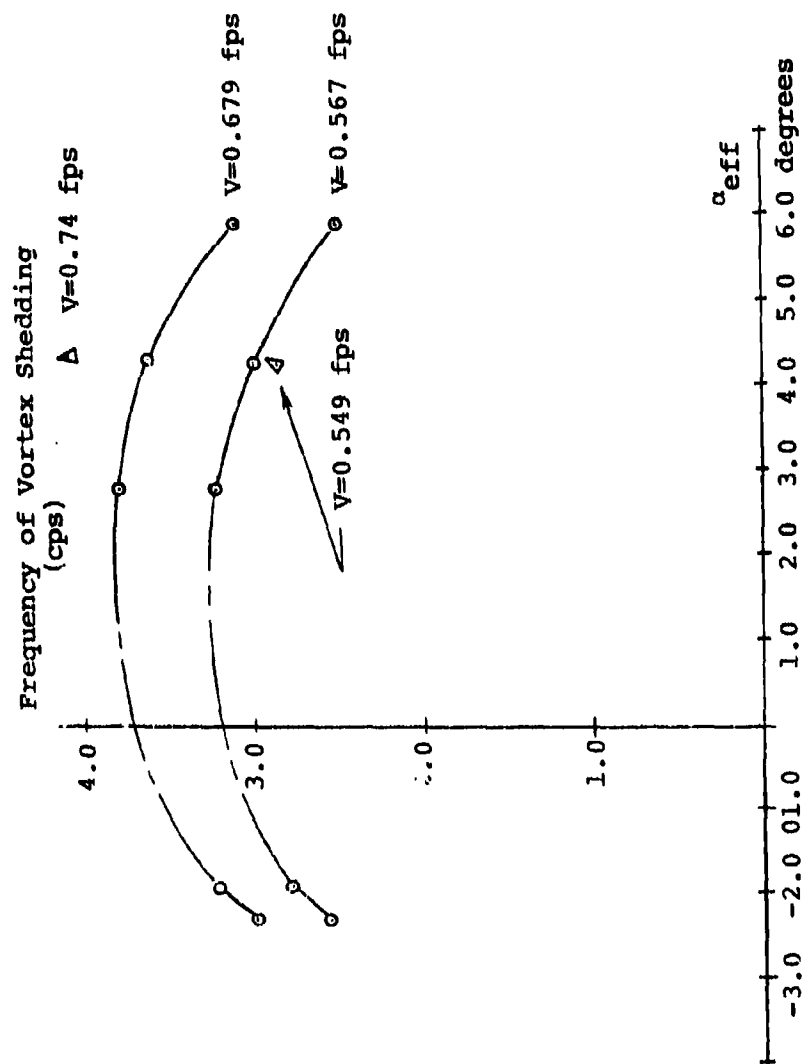


Figure 18. Frequency of Vortex Shedding versus Angle of Attack.

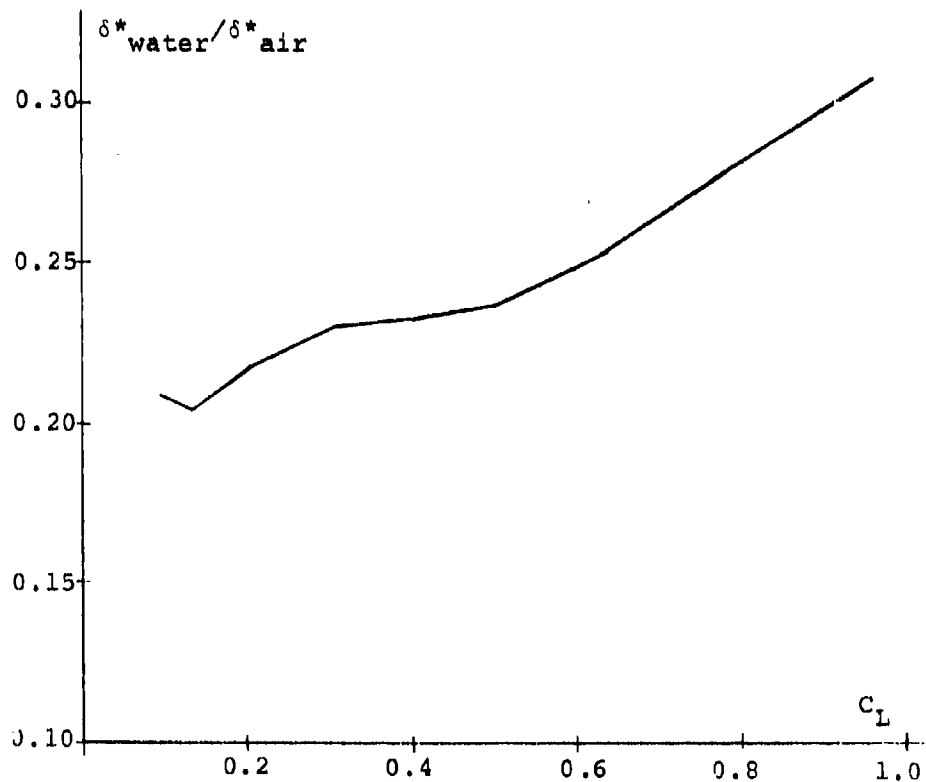


Figure 19. $\delta^*_{\text{water}}/\delta^*_{\text{air}}$ at the Trailing Edge of the Airfoil versus C_L .

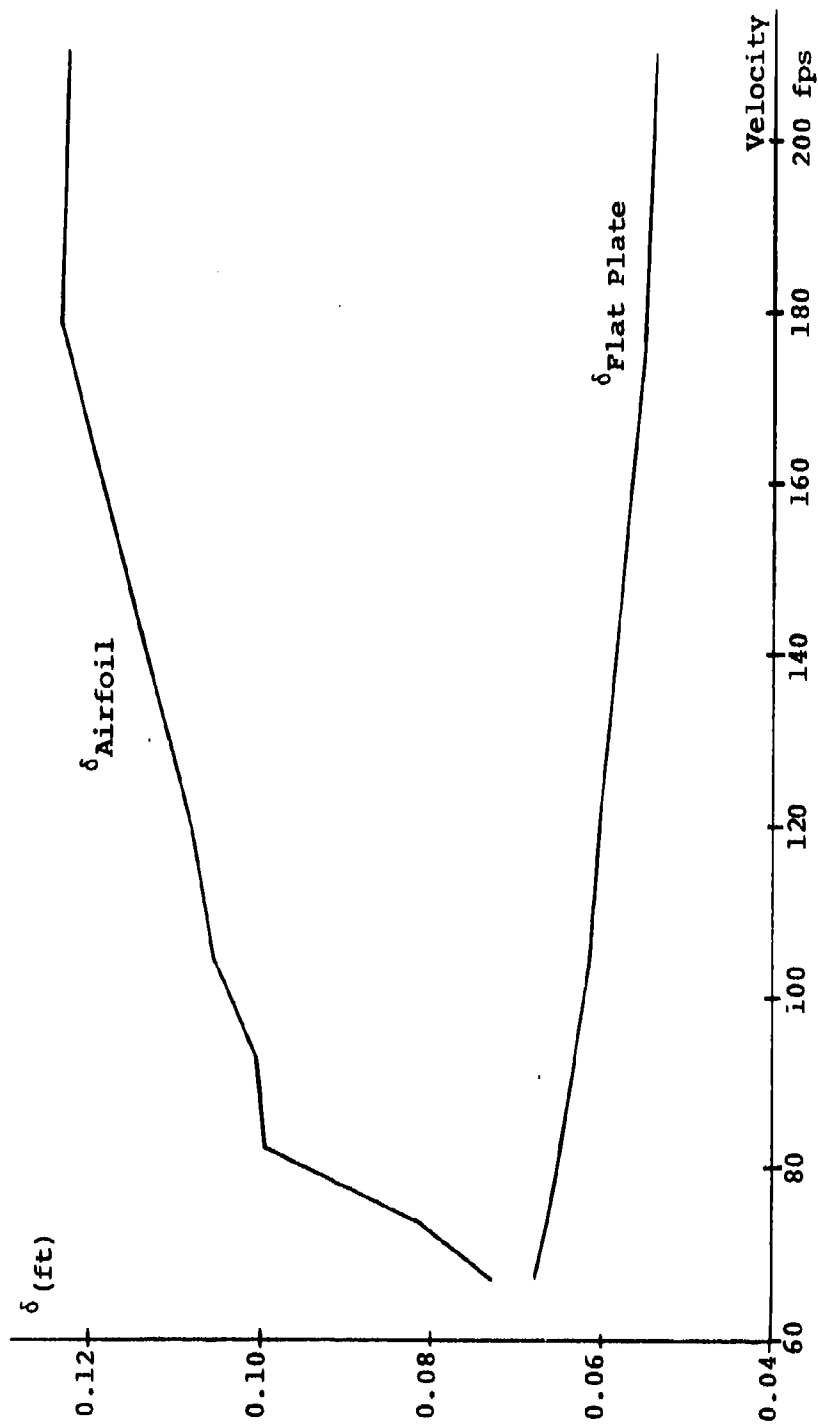
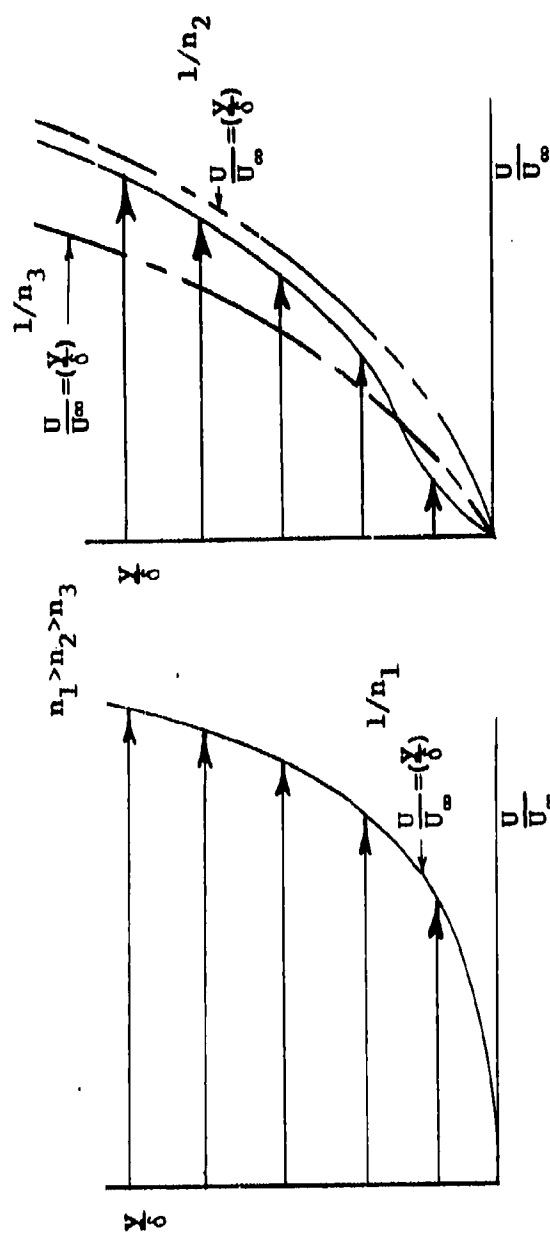


Figure 20. Boundary Layer Thickness at the Trailing Edge of an Airfoil and a Flat Plate versus Velocity in Air.



The profile soon after transition very closely resembles a power law.

As the adverse pressure gradient is encountered, the profile changes and may be approximated by a power law with a smaller exponent.

Figure 21. Modification of the Boundary Layer Profile as an Adverse Pressure Gradient is Encountered.

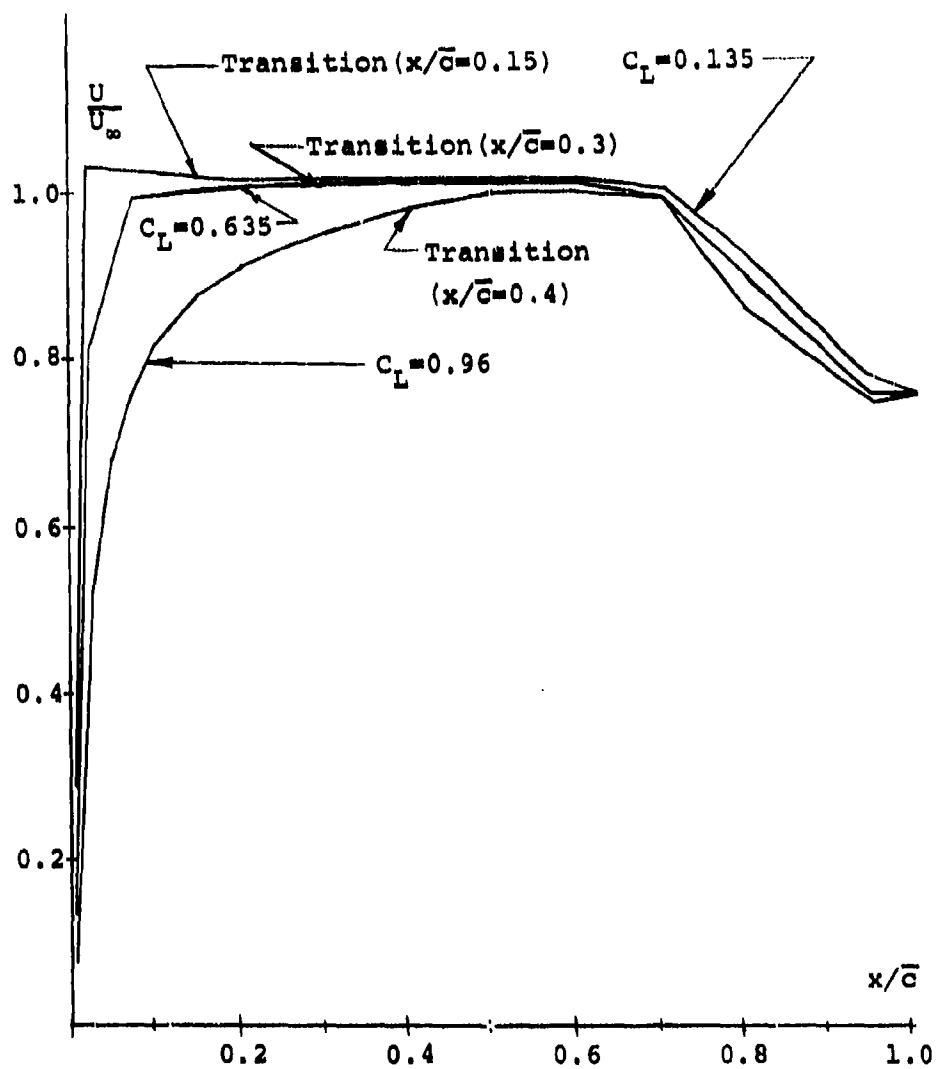


Figure 22. Velocity Distribution Over the Lower Surface of the Airfoil for C_L Equal to 0.96, 0.635, and 0.135.

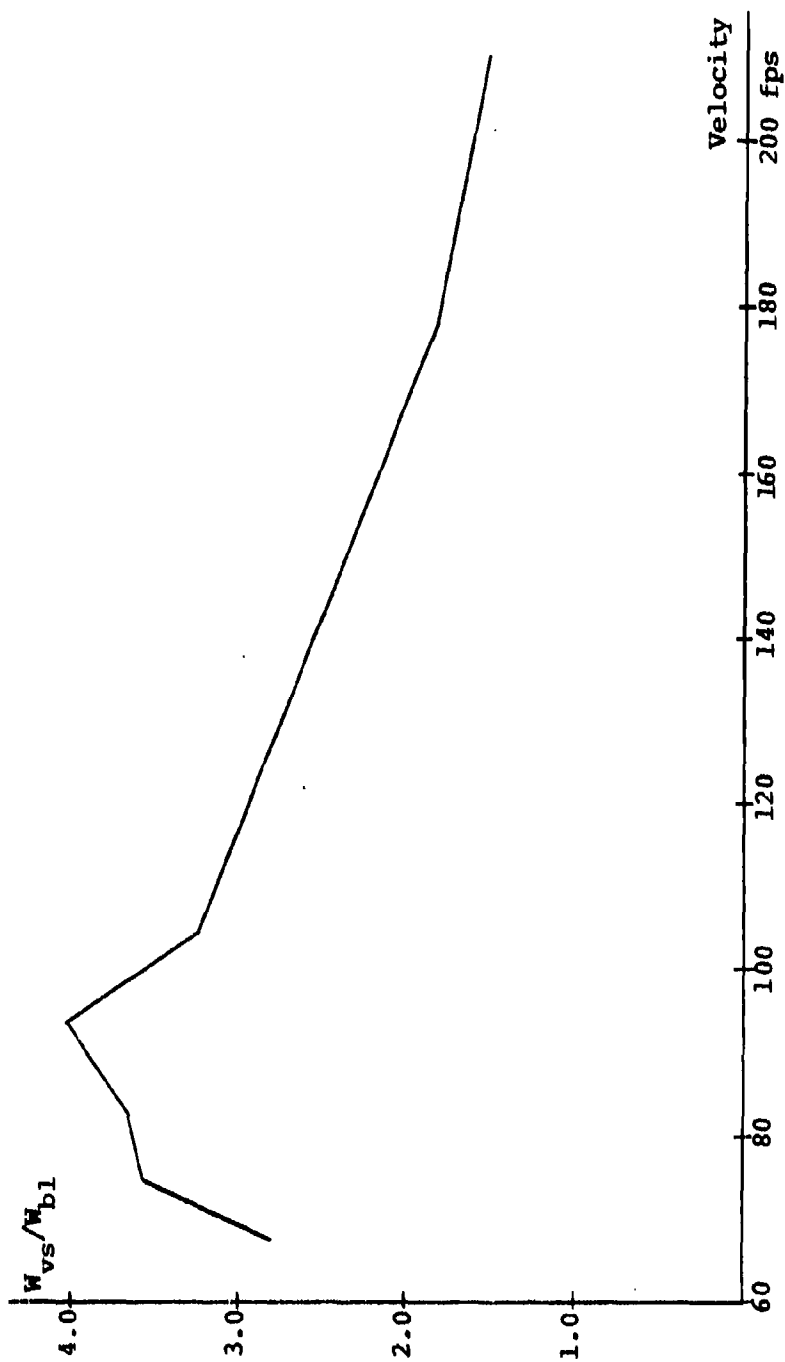


Figure 23. W_{vs}/W_{bl} versus Velocity.

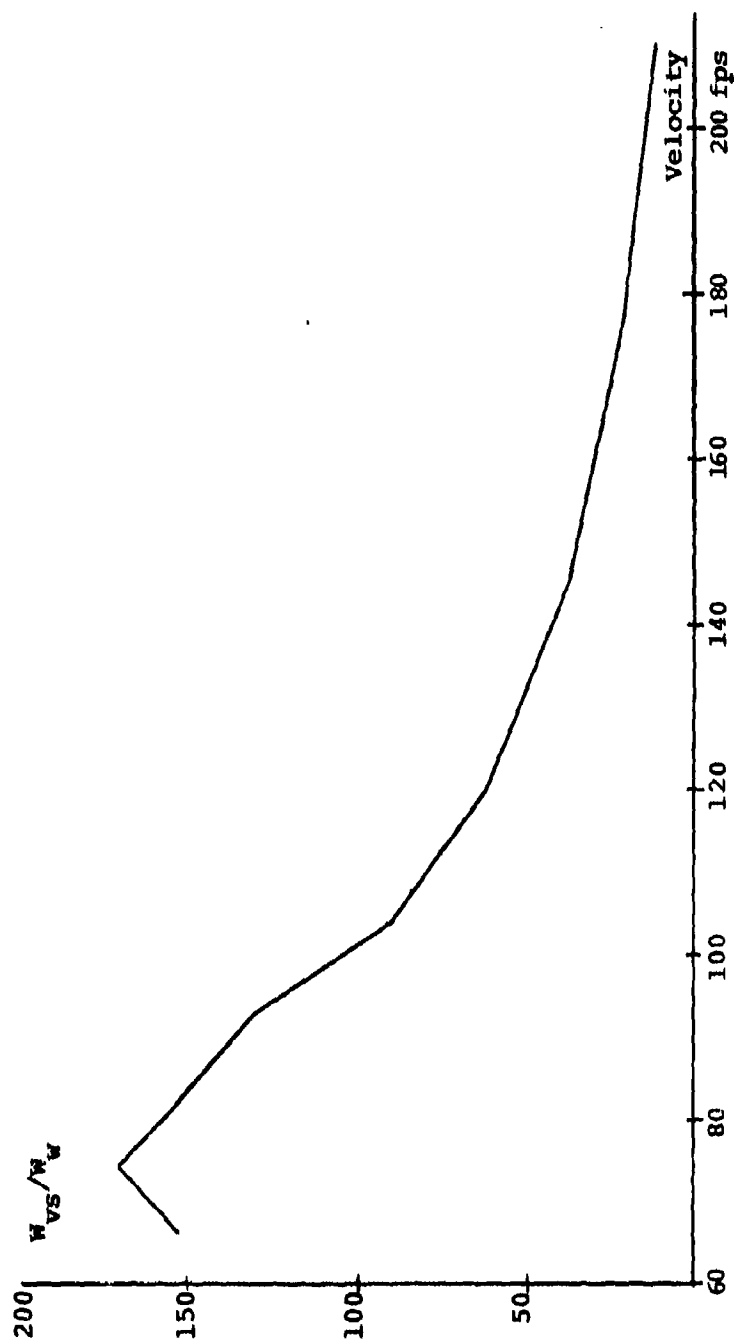


Figure 24. W_{VS}/W_W versus Velocity.

TABLE I
RELATIONSHIP BETWEEN AIR VELOCITY AND ANGLE OF ATTACK
NECESSARY ON THE WATER TABLE

Velocity in Air (fps)	C_L	Effective Angle of Attack on the Table
66.8 (stalled)	0.960	10.4°
66.8 (unstalled)	0.960	5.9
74.3	0.780	4.25
82.3	0.635	2.8
178	0.135	-1.9
210	0.097	-2.3

TABLE II
FREQUENCY OF VORTEX SHEDDING

Angle of Attack, Degrees	V=0.549 fps Re=1.39 x 10 ⁵	V=0.567 fps Re=1.435 x 10 ⁵	V=0.679 fps Re=1.845 x 10 ⁵	V=0.740 fps Re=1.875 x 10 ⁵
5.9	---	2.50 cps	3.1 cps	---
4.25	2.86	3.00	3.63	4.1
2.8	---	3.21	3.8	---
-1.9	---	2.79	3.23	---
-2.3	---	2.57	3.00	---

TABLE III
THEORETICAL TRANSITION POINTS FOR ATMOSPHERIC FLIGHT

C_L	Reynolds Number	Approximate x_1/\bar{c}
0.097	3.75×10^6	0.14
0.135	3.18	0.15
0.200	2.61	0.20
0.300	2.14	0.23
0.400	1.86	0.25
0.500	1.66	0.27
0.635	1.46	0.30
0.780	1.32	0.35
0.960	1.18	0.40

TABLE IV
THE RESULTS OF THE THEORETICAL CALCULATIONS OF THE BOUNDARY LAYER THICKNESSES

C_L	δ^*_{water}	δ^*_{air}	$\frac{\delta^*_{\text{water}}}{\delta^*_{\text{air}}}$	δ_{air}	δ_{air}^2
0.960	0.00372 ft	0.01216 ft	0.306	0.0730 ft	0.00530 ft ²
0.780	0.00382	0.01377	0.278	0.0825	0.00680
0.635	0.00391	0.01544	0.253	0.0926	0.00859
0.500	0.00399	0.01687	0.236	0.1011	0.01023
0.400	0.00406	0.01748	0.232	0.1048	0.01098
0.300	0.00412	0.01804	0.228	0.1081	0.01170
0.200	0.00418	0.01929	0.217	0.1157	0.01336
0.135	0.00423	0.02063	0.204	0.1239	0.01531
0.097	0.00425	0.02043	0.208	0.1225	0.01500

TABLE V
THE EFFECT OF CHANGING THE POWER LAW DESCRIBING THE
BOUNDARY LAYER PROFILE

C_L	δ^*_{air}	δ^*_{air}	Percent Difference
	(where $\frac{U}{U_\infty} = (\frac{y}{\delta})^{1/4}$)	(where $\frac{U}{U_\infty} = (\frac{y}{\delta})^{1/5}$)	
0.960	0.01150 ft	0.01216 ft	5.4
0.635	0.01440	0.01544	6.6
0.135	0.01858	0.02063	9.9

TABLE VI
COMPILATION OF THE THEORETICAL AND EXPERIMENTAL RESULTS

Velocity	$\{\bar{n}f_{\text{water}}\}^2$	δ^2	w_{vs}/w_{bl}	w_{vs}/w_w
67 fps	1.96	0.0053 ft	2.81	153
74	2.21	0.0068	3.58	172
82	2.02	0.0086	3.66	153
93	1.77*	0.0102	4.04	131
104	1.64*	0.0110	3.24	89.5
120	1.51*	0.0117	2.94	63.5
146	1.22*	0.0134	2.44	37
178	0.94	0.0153	1.84	21.4
210	0.85	0.0150	1.53	11.9

* Interpolated values from Figure 18

APPENDIX II

WIND TUNNEL TESTS OF THE OWL WING

1. OUTLINE

The objective of the aerodynamic experiments with the owl wing was to attempt to discover the aerodynamic mechanisms, if such exist, which were responsible for the silent flight. A small wind tunnel was designed and constructed specifically for testing the wing at low velocities. A wing from a small owl was used so that three-dimensional flow could be studied. Four types of experiments were designed:

- (1) Visual observation of the aeroelastic motions,
- (2) Flow visualization using a smoke generator,
- (3) Measurement of the motions of the wing or its components by use of a strobe light,
- (4) Flow studies over the wing by use of tufts and hot wire instruments.

2. TEST FACILITY

The wind tunnel was designed and constructed from plywood. It consisted of three basic parts:

- (1) The stilling chamber. This is a rectangular box of dimensions 49" x 30" x 30". Three double thicknesses of fine mesh screen wire were used to eliminate large flow irregularities. Between the screens and the blower, the box was filled with plastic wool to reduce the effect of the blower which induces unsteady, turbulent flow. The exhaust from the stilling chamber was a square rigid nozzle with a 10" x 10" exhaust cross section. A smoke generator was placed upstream of the nozzle to inject the smoke prior to acceleration by the nozzle. The source of smoke was cigars placed in the end of a tube through which air was blown. The small plastic mouth piece on the cigar was used as a nozzle.
- (2) The air flow generator was a centrifugal fan. It was powered by a 1/4 horsepower electric motor through the use of a pulley drive arrangement. The rpm could be adjusted to vary the wind speed.

- (3) The model mount system. Immediately downstream of the nozzle a frame outside of the air jet was used to mount the owl wing. The mounting platform could be adjusted to vary the angle of attack, the angle of yaw and the position downstream of the nozzle.

The wind tunnel arrangement is shown in Figures 25 and 26.

3. ANALYSIS OF THE WIND TUNNEL

The wind tunnel experiments on the owl wing were run only at one slower speed. This corresponded to the average flight velocity experienced in the acoustic experiments. The relative velocity profiles and the turbulence data taken for calibration was at an average velocity of 1250 feet per minute. The following is the description of these results; Figure 27 shows the flow calibration. The deviations from the basic calibration speed are shown at each measurement position. A hot wire anemometer was used as the measuring instrument. The edge of the laminar section can be seen. Steady state distortion between -120 and +70 feet per minute were found. The unsteady character of the flow is shown in Figure 28. An oscilloscope trace was photographed depicting the output of the hot wire anemometer. Measurements showed that the average unsteadiness was plus or minus 1.25% in the low frequency range and plus or minus 3.9% at high frequency.

4. HOT WIRE INSTRUMENT

The velocities were measured by a portable Flowtronic, Model 55B1, hot wire anemometer manufactured by the Flow Corporation, Cambridge. It is linearized and indicates the velocity in units of feet per minute. The calibrated measurement range was from 0 to 12,000 feet per minute.

5. STROBE LIGHT

Frequencies of aeroelastic motions of the wing were measured with a Strobetac, Model 631DL, manufactured by the Radio Corporation, Cambridge. Its range is from 1 Hz to 240 Hz.

6. TEST OBJECT

Two owl wings were used. These were both the left and right wings from the same bird. After several photographs were taken

of the live owls from the Bionics study in gliding flight, the planform geometry was established. The two small wings were then made flexible by soaking them in water. Next, they were formed into a life-like shape using the aforementioned photographs for reference. Finally, the wings were dried so that they retained the desired shape. From this configuration the basic data were obtained:

Wing span:	18"
Wing sweep:	0°
Maximum chord:	4.5"
Wing area:	72 sq. in.

7. EXPERIMENTS

a. Visual Observations

The owl wing was fixed rigidly in the model mounting system. The wing root was held with a clamp while the outboard portion of the wing was allowed to remain flexible. Care was taken to simulate the live flight configuration. The following observations were made:

- (A) The wing changed shape upon introduction of the flow velocity because of the elasticity of the feathers. The first three tip feathers curved up to some position which was strongly dependent upon the angle of attack. Figure 30 shows this condition. If the angle of attack was either very small or very large the curvature of the feathers diminished. There was a unique angle of attack where maximum curvature occurred. The trailing edge of the wing also changed its shape in the flow. Figure 31 shows the comparative geometries of the wing in undisturbed and disturbed air. On the leading edge at about the mid-span position, there are two small feathers (see Figure 33). These feathers separate from the wing at a distance which is proportional to the angle of attack.
- (B) The wing oscillates. Some parts of the wing appear to be independent of the total wing system in the manner in which they move. Oscillation is always present in the wing despite the fact that the nozzle flow is laminar. The amplitude of the motion depend on the angle of attack. They achieve their maximum amplitudes at very small and very large angles of attack. There is one angle

of attack where the amplitude of oscillation reaches a minimum.

There are five regions of the wing which appear to maintain independent oscillation. These are:

- 1) The first three feathers of the wing tip,
 - 2) The trailing edge,
 - 3) The leading edge (which is extremely small in amplitude),
 - 4) The surface region near the owl body,
 - 5) The trailing edge near the owl body. These regions are shown in Figure 34.
- (C) Behind the leading edge in region 3 of Figure 34 the surface of the wing is mildly porous. This allows the air to pass through from the lower to the upper surface beneath the small secondary feathers. This is noticed during certain movements of the feathers.

b. Smoke Generator Experiments

The owl wing was tested in the wind tunnel using the smoke generator to study further details of the flow. Photographs were taken to allow detailed investigations of the flow. The angles of attack and position of the smoke generator were varied. Special emphasis was placed upon the flow in the outboard region. Figure 35 shows a high speed picture with an exposure time of 0.001 sec. Vibration of the smoke generator pipe caused the smoke stream to appear turbulent; however, this was not felt detrimental as the flow in the high speed section remained laminar. The exposure time was increased to approximately 1/60 sec. in order to better describe the streamline flow.

Figures 36 and 37 show the flow at a moderate angle of attack and a very large angle of attack. In neither case was the flow separated on the outboard regions of the wing.

Figure 38 shows how the streamlines are shifted outboard on the upper surface. Figure 39 shows that the smoke is separated into two stream, one of which curls to form a helix. Further downstream both parts coalesce to form a large trailing vortex.

Figure 40 shows the wake being turned in, aft of the trailing edge. The flow defined in these pictures is outside of the boundary layer. Flow immediately on the wing surface will be described in detail in a later section.

c. Strobe Light Experiments

In an earlier section of this report a flow oscillation was described. The purpose of the strobe light experiments was to analyze the frequency and the modes of these oscillations. This was accomplished as follows: By focusing the strobe light on the model in a darkened room the model was clearly illuminated. The oscillating parts of the wing appeared blurred. The frequency of the strobe light was slowly changed until the blurring vanished on a particular element being studied. When the moving part appeared to stop the frequency of the strobe light was recorded. This was considered to be the frequency of the oscillating part. The following was discovered: Each part that was found to be in motion fell in a frequency band of between 13.3 to 15.0 Hz. The large and small feathers alike vibrated in this same way. The motion appeared to combine wing bending and torsion in such a way that the leading edge of the wing was very nearly the nodal axis. Though the frequencies were extremely close together the amplitudes and phases were different.

d. Experiments with the Tuft Probe

Several types of probes were used to study the flow. The larger probes were made by attaching a small wool thread to the end of a metal tube (approximately 2 mm in diameter). This type of probe is sketched in Figure 41. Another probe using a small sewing needle was built for purposes of studying flow very near the wing surface. The lengths, d , of the tuft were varied from approximately 4 mm up to approximately 5 cm to study various portions of the flow. A small amount of glue was touched to the end of the tube or needle, and the tuft attached in this way. The glue was of such a plastic nature that the tuft could be separated from the tube proper and be held with the extended filament of the glue to allow extreme flexibility.

By use of a tuft 4 mm in length attached to the sharpened end of the sewing needle the flow direction of the boundary layer was studied. This study was difficult and time consuming due to the intricate mechanism of flow control over the owl wing. Only small vertical displacements of the tufts would indicate large changes in flow direction due to the presence of the complex vortex sheet distribution. For example, approximately four hours of uninterrupted probing were necessary to map the flow field on the outboard half of the wing upper surface. At one location the direction of the streamlines changed 180 degrees over a depth change of about one millimeter. The following conclusions were made concerning the mechanisms of the flow at two angles of attack.

If the wing was at a small angle of attack, the boundary layer performed in the following way: Laminar flow existed

over both the upper and lower surfaces everywhere. An extremely thin flow discontinuity existed behind the wing. The streamlines over the upper surface curved slightly toward the wing root. The streamlines over the inner parts of the wing moved more in the streamwise direction. No effect concerning the leading edge comb could be recognized at this angle of attack. Such flow is seen in Figure 39. Large vortices separated from the tip feathers and appeared in the trailing wake over the entire outboard half of the wing. The leading edge slot was only slightly open. The termination of the large trailing vortex system in the wake occurred directly downstream of the slot.

The flow at large angles of attack corresponding to the flight condition showed an entirely different pattern. This is shown in Figure 42. The leading edge combs became very active in producing the resulting field. No deformation of the comb system occurred at any conditions tested. The leading edge slot was extended away from the wing and at the increased angles of attack. Immediately behind the slot the flow moved inboard; however, the sense of the trailing vortex was as expected (clockwise, looking upstream). This vortex aided in moving the boundary layer flow on the aft portions of the wing outboard. The leading edge combs developed a vortex sheet which allowed the flow in the boundary layer to be initiated in the outboard direction while the flow above the sheet moved in the chordwise direction.

Figure 43 shows how the comb elements are twisted and tapered to provide the development of the sheet. Thus, a vortex system exists from the leading edge slot to all wing positions outboard. The tip feathers also aid in promoting flow in the outboard direction.

Probably the most interesting and unique condition of the flow field was the development of back flow immediately aft of the leading edge comb system. This was definitely not a separated region. The flow was attached and laminar throughout this region. The way this develops may be explained by the sketch in Figure 44. The leading edge comb immediately develops a vortex sheet promoting spanwise flow in the outboard direction on the surface. The leading edge slot being intersected with the upper surface of the wing leading edge develops a low pressure in the region immediately behind its point of intersection, which creates a localized inboard flow. This leaves a region aft of the combs to be filled with the flow containing the comb induced vortex sheet. Somewhat further downstream of the wing the slot induced vortex begins to move the boundary layer flow back in the outboard direction. Flow along the comb induced vortex sheet fills the void that is created by these diverging flows. Upon interaction with the wing the flow moves back toward the leading edge and develops two counter-rotating fields. The streamline flow from these fields is able to escape from this region by the strongly three-dimensional nature of the flow. The entire process occurs in a region of thickness from 4 to 5 mm. Above this (boundary flow) the streamlines move in a more chordwise

direction. Thus the influence of the leading edge combs in combination with the slot and tip feathers produces a vortex sheet system that enables a very complex, yet entirely laminar, flow system to develop.

Another interesting observation was that this system continues to work in this same manner at extremely large angles of attack. Though the tip feathers reach some maximum deflection position at an intermediate angle of attack the leading edge slot continues to open over the increasing angle of attack range. Laminar flow continued to exist even at angles of attack in excess of 30° . Turbulent flow and separation thus are effectively resisted by the three-dimensional flow created by the wing.

The final part of this study was to investigate the owl wing with the leading edge vortex sheet generator removed. The comb was simply cut off with a pair of scissors. The flow over the wing near the surface was mapped. The counterrotating areas were replaced by a single large system with the flow being directed inboard at the leading edge. Flow separation occurred immediately aft of the leading edge and reattachment was seen near the trailing edge with considerable turbulence being induced.

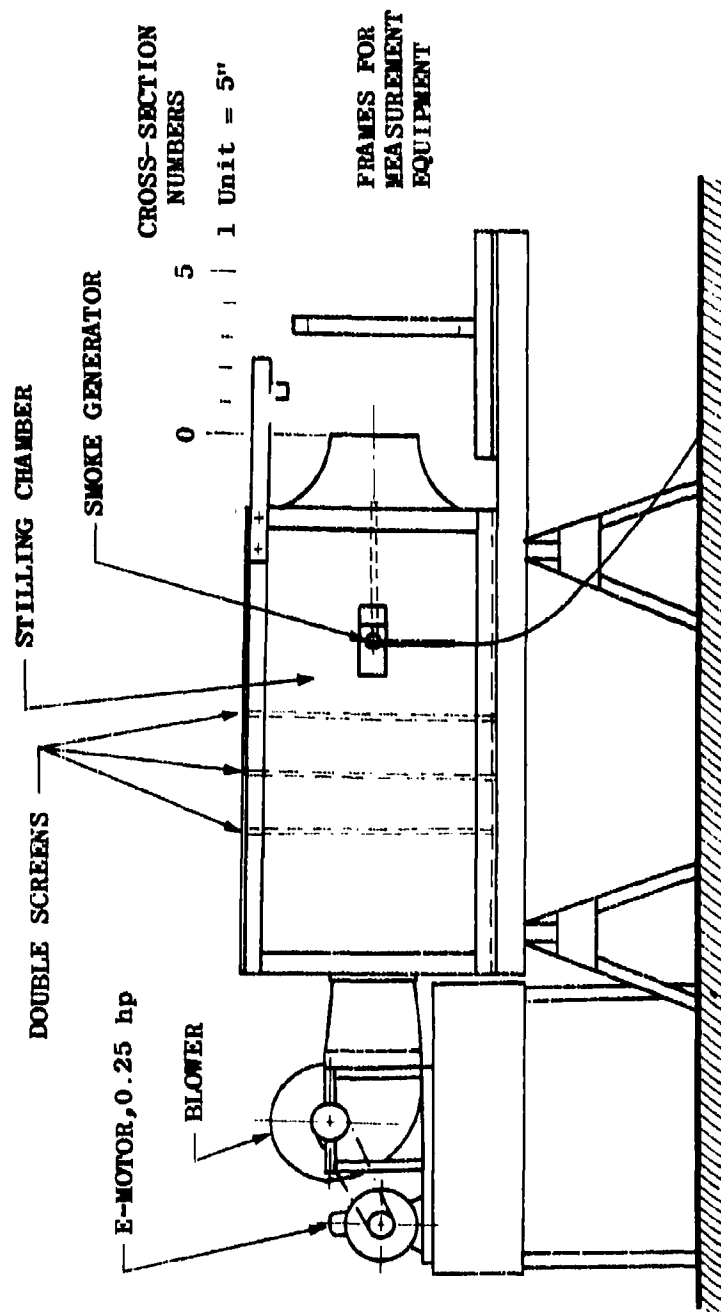


Figure 25. Wind Tunnel Test Facility.

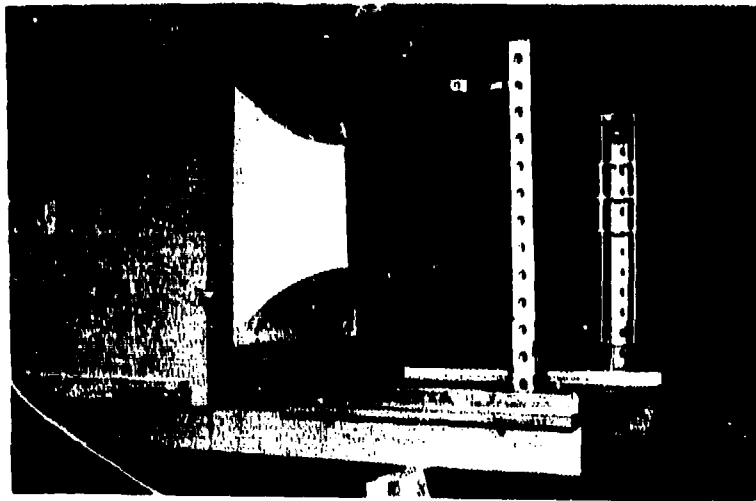
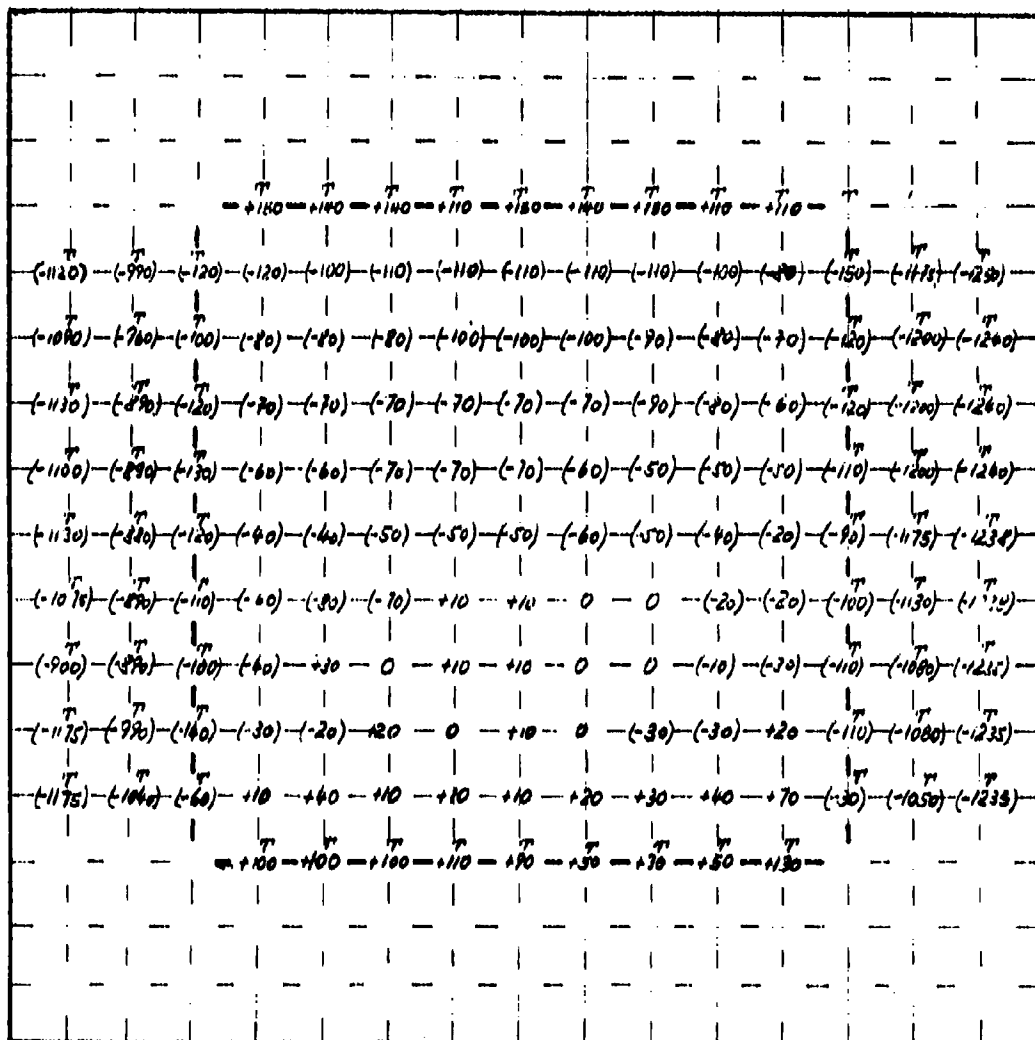
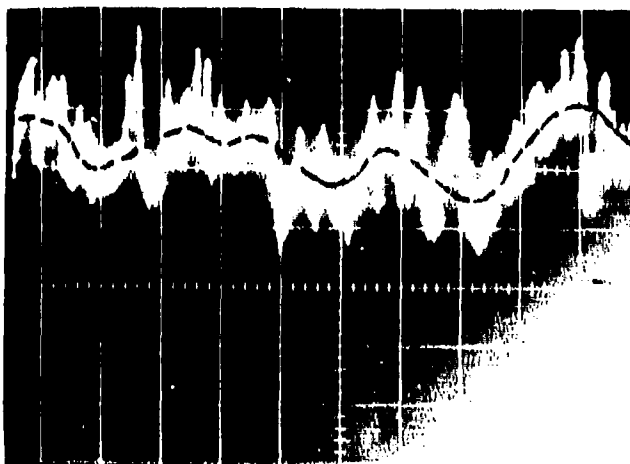


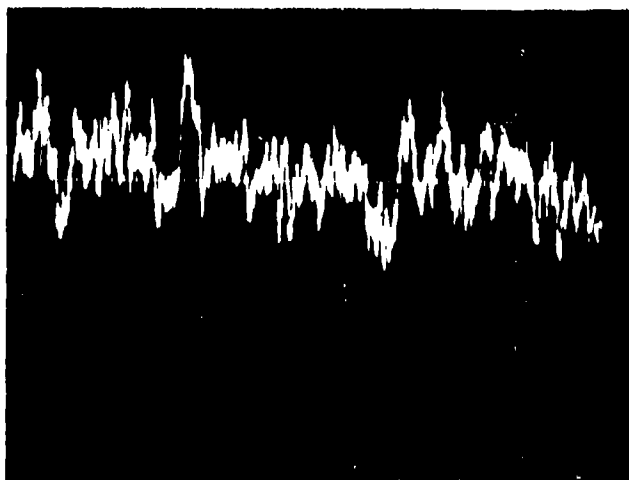
Figure 26. Photograph of Wind Tunnel.





20 ft. pm

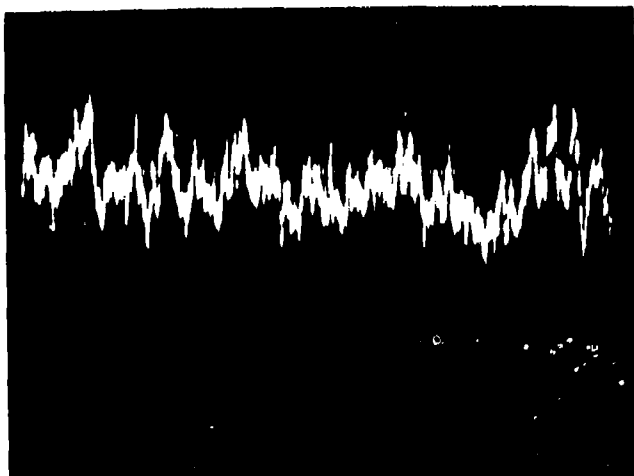
Basic Velocity = 1250 FPM



20 ft. pm

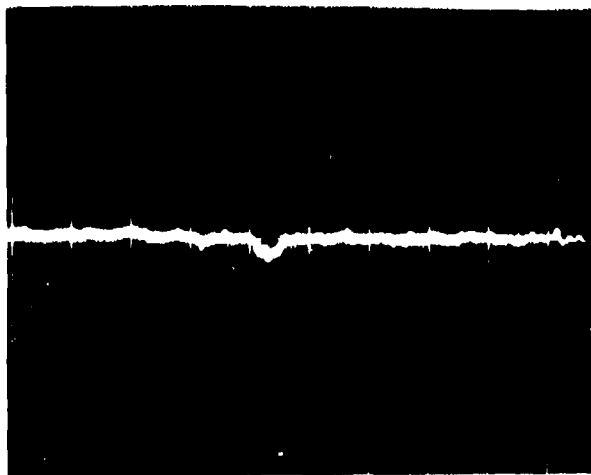
Basic Velocity - 925 FPM

Figure 28. Turbulence Records.



20 ft. pm

Basic Velocity - 950 FPM



400 ft. pm

Basic Velocity - 950 FPM

Figure 29. Turbulence Records.

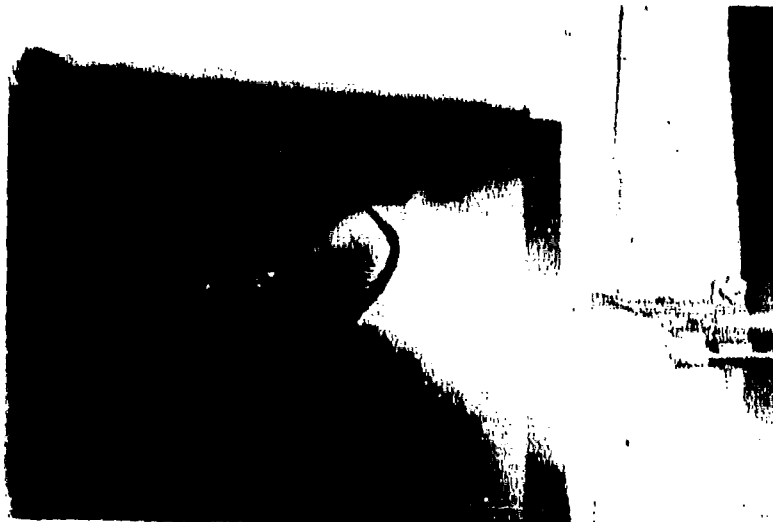


Figure 30. Wing Curvature.



Figure 31. Wing in the Undisturbed Air.



Figure 32. Wing in the Flow.

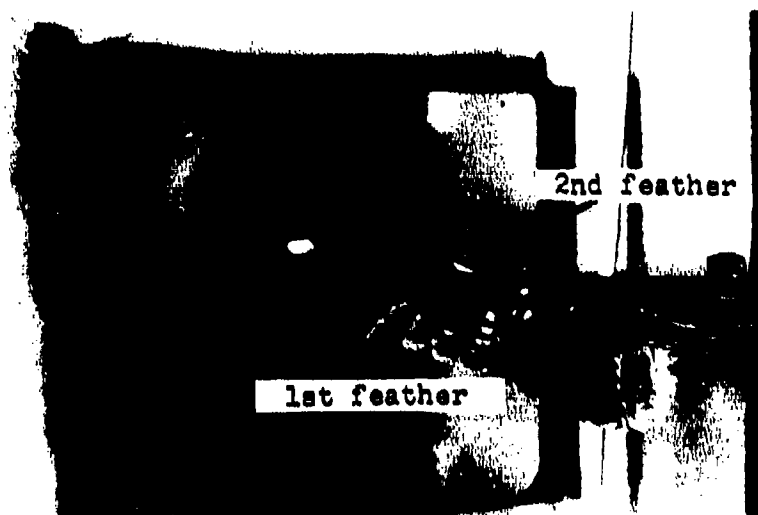


Figure 33. Mid-Span Leading Edge Feathers.



Figure 34. Regions of Independent Oscillation.



Figure 35. High Speed Photograph of Smoke Stream.



Figure 36. Flow at Moderate Angle of Attack.



Figure 37. Flow at Large Angle of Attack.

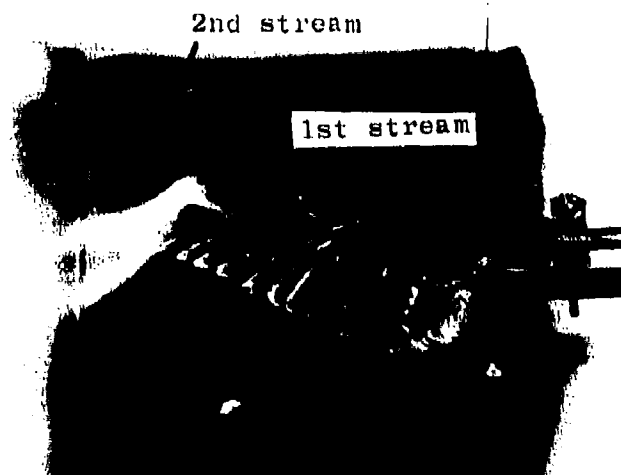


Figure 38. Flow Through the Wing.



Figure 39. Flow Above the Wing.

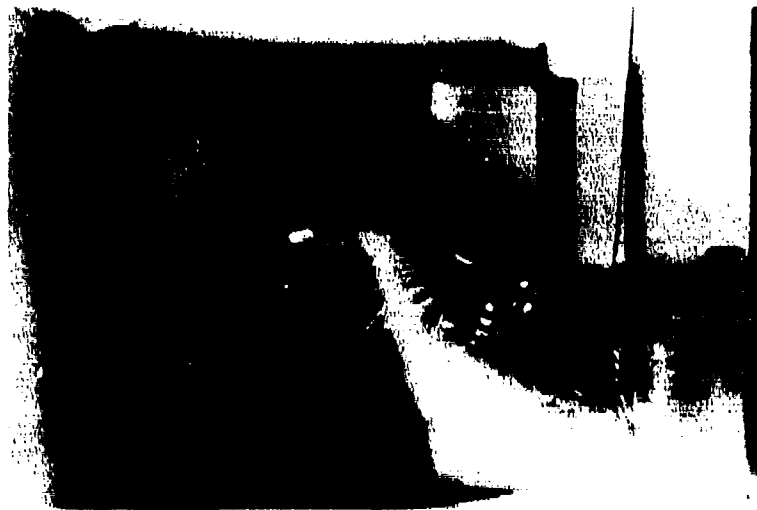


Figure 40. Trailing Flow.

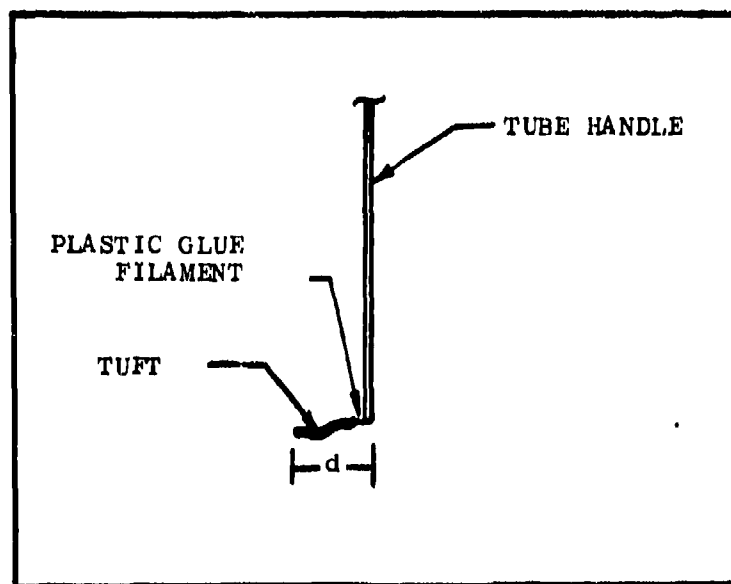


Figure 41. Sketch of Tuft Probe.

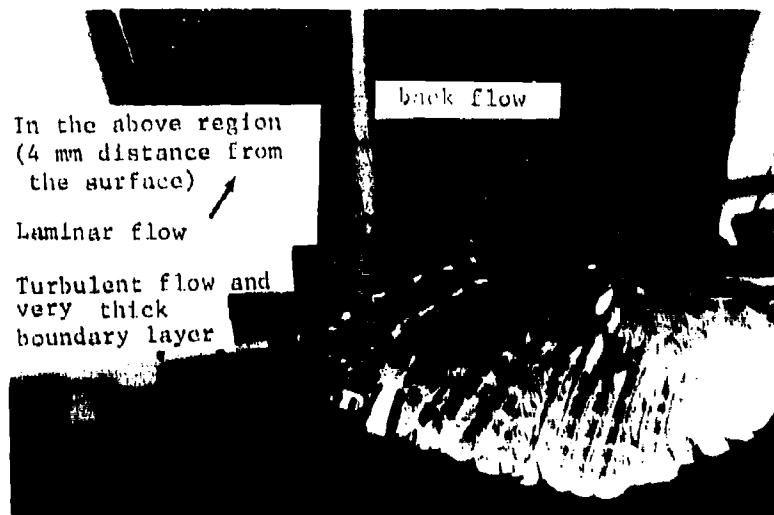


Figure 42. Flow Pattern at Flight Angles of Attack.

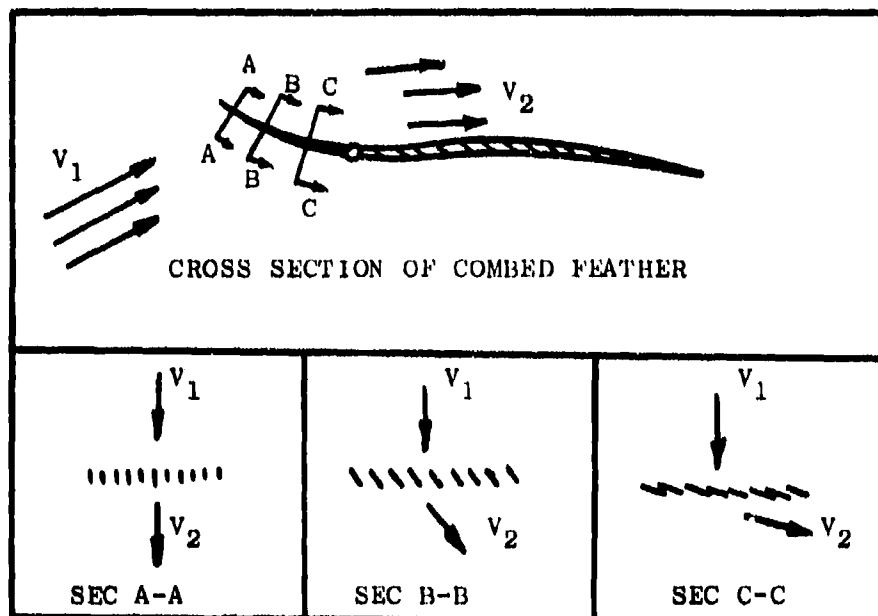


Figure 43. Sketch of Flow Through Leading Edge Comb.

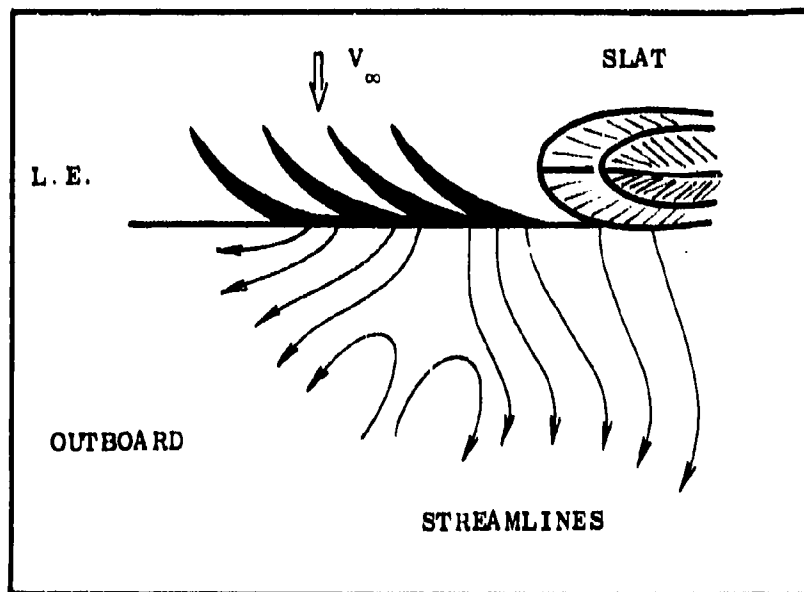


Figure 44. Backflow Generation.

APPENDIX III

WATER TUNNEL STUDIES

A series of fluid flow tests were conducted in The University of Tennessee Space Institute water tunnel to evaluate concepts suggested by the combined Aerodynamic, Acoustic and Bionics studies. The objective of the experiments was to apply various aerodynamic quieting devices to low drag series airfoils and evaluate the resulting flow fields. An additional objective was to develop the quieting modifications in such a way that they could be applied to full scale gliders. That is, when a quieting mechanism was described from the other parts of the program, a practical analog was to be designed and tested for stability, boundary layer performance and wake characteristics. Early phases of the project pointed to the downward fluctuations and boundary layer radiation as the important sources of noise to consider. Thus the flow conditions at the trailing edge were considered to be the most important key to the noise problem.

1. THE WATER TUNNEL

The UTSI water tunnel is a closed return system driven by a 1 HP electric motor through an infinitely variable transmission system. The test section dimensions are 50 x 12 x 18 inches. The top speed with sufficient quality flow for these tests was one foot per second or a Reynolds Number of about 60,000 per foot. The largest airfoil model available had a chord of two feet. Thus to operate at a reasonable Reynolds Number, the tunnel speed had to be increased. This was accomplished by designing a test section insert which dropped the channel width from 12 inches to two inches. This provided Reynolds Numbers in excess of one half million which was considered adequate. The top of the test section was open for easy model access.

A dye probe using potassium permanganate crystals dissolved in water was used for flow visualization. The dye was injected upstream of the nozzle in the low speed section. The dye flow rate could be varied to eliminate unsteady flow resulting from the presence of the probe.

The probe position could be varied vertically for studying different levels of stream flow above and below the model. It could also be moved along the direction of flow into the nozzle so the intensity of the dye could be increased. Figure 45 shows a schematic of the test section arrangement. The flow was sufficiently steady and laminar to provide good visualization.

2. THE MODELS

The models used in these tests were three sizes of NACA 652414 airfoils (Ref., Appendix I). Their chords were 27, 18 and 9 inches. When they were installed in the test section they were sealed to the walls all around to eliminate leakage from the lower to the upper surface. The only tests considered were two dimensional. However, some degree of three-dimensional flow could be simulated.

The angle of attack could be varied over a wide range. Excessive boundary interference was observed when the large model was installed so the 18 and 9 inch models were used for most of the experiments.

3. EXPERIMENTS

Two types of experiments were conducted. These were to investigate the effectiveness of vortex generators simulating leading edge combs and flexible trailing edge devices to simulate wing compliance. The results of these tests are as follows;

(a) Vortex Generators

Several suggestions for vortex generator configurations were provided by the Aerodynamics and Bionics studies. Some of these are depicted in Figure 46. Early in the experiments little was known of the use of the leading edge vortex generator by the owl so nearly arbitrary selections of configurations were made. Various perturbations from these basic shapes were easily made since systems a through e were constructed of 0.015 shim stock and could be easily cut and installed. The trailing wake system was visually observed by use of dye injection to determine its thickness and turbulence. The gradients in the boundary layer at the trailing edge could be observed by pulsing the dye stream. The vortex generator could be placed on the leading edge or any chordwise position on the upper or lower surface. In virtually all configurations tested, the results were somewhat the same. The boundary layer transitioned to turbulent much earlier than on the clean airfoil. The wake turbulence increased and appeared to gain higher frequency components. The wake thickened. The smaller vortex generators seemed to have less effect on the trailing wake thickness. It appeared that no positive sense of direction was being gained by these experiments so they were temporarily stopped.

Next, a closer look was taken at the flow mechanisms induced by vortex generators. The ideal vortex motion immediately downstream of a configuration such as in Figure 46d might appear as shown in Figure 47.

Next, consider the flow pattern if the vanes are staggered with an alternating left and right angle of attack to the flow. The sheet roll-up will be of the same type, yet having only half as many elemental vortices in the wake. Neither of these systems of vortices is stable and both very quickly dissipate into turbulent flow.

Finally, if the vanes are all placed at the same angle of attack to the flow as in a cascade, a vortex sheet such as shown in Figure 48 would be developed. This configuration possesses a high degree of stability.

After the above configurations were made concerning the action of various vortex generating devices, a new type was tried. This was merely a piece of shim stock cut normal to the leading edge at one-eighth inch intervals about one-fourth inch deep and the resulting blades twisted to form a cascade. This system was installed at the leading edge, slightly downstream of the stagnation point. No significant flow improvement was made but a rather crude cross flow on the airfoil surface appeared. Upon close examination of the flow over the wind tunnel mounted owl wing, described in Appendix II, a similar cross flow was noted. Further inspection of the leading edge comb revealed a twisted cascade arrangement with tapered, washed out tips. This system was simulated by taking the vortex generator shown in Figure 46c and twisting each of the elements until the tips had a zero degree angle of attack with respect to the free stream. Care was taken to approximate a linear twist from the root to the tip. Tests of this system showed the development of a distinctly laminar vortex sheet downstream of the comb. The three-dimensional nature of the flow precluded arriving at further conclusions through the use of the water tunnel because of the narrow test channel. The studies on the performance of vortex generators were stopped and referred to the wind tunnel for further analysis.

b. Flexible Trailing Edge Devices

During the course of the research program the important nature of the wing compliance was discovered. The development of a mechanism to produce an optimized wing compliance was felt to be beyond the level of this effort as it would involve very specialized and detailed considerations. However, a mechanism was conceived which could possibly have some merit. This was the use of a flexibly mounted splitter plate along the trailing edge of the airfoil. This arrangement is shown in Figure 49. The plate was taped to the airfoil so that no gap would be present yet a high degree of compliance would exist at the attachment.

The exact mechanism for noise reduction by compliance was not known; however, preliminary tests indicated the sensitivity of the point of boundary layer transition on the wing upper

surface to the position and size of the splitter plate.

The first tests that were made were to establish the plate length. This was done by cambering the plate so that it would move to a predetermined position. A range of such positions was tried until the furthest aft point of boundary layer transition would occur yet the laminar nature of the flow on the lower surface was not destroyed. Several plate lengths were tried until an optimum was found. This corresponded to a plate length of twelve percent of the wing chord. It is expected that this particular dimension will be a function of Reynolds Number. The proof of this method of noise reduction could not be done in the water tunnel. However, the plate did oscillate at a low frequency as was predicted from the study of the Owl flight.

A brief and inconclusive look was taken at the influence of porosity on the boundary layer flow at the trailing edge. A cambered flat plate with lateral slots was placed in the water tunnel. Flow visualization showed that the lower surface could be made fully laminar. The wider the slots were cut, the lower the frequency of the outer boundary layer could be made. However, no conclusion was made regarding the spectral content of the inner layers. The total boundary layer was thickened, however, possibly implying reduced gradients and frequencies. The application of this concept to a thick airfoil would be quite simple.

This concluded the water tunnel experiments.

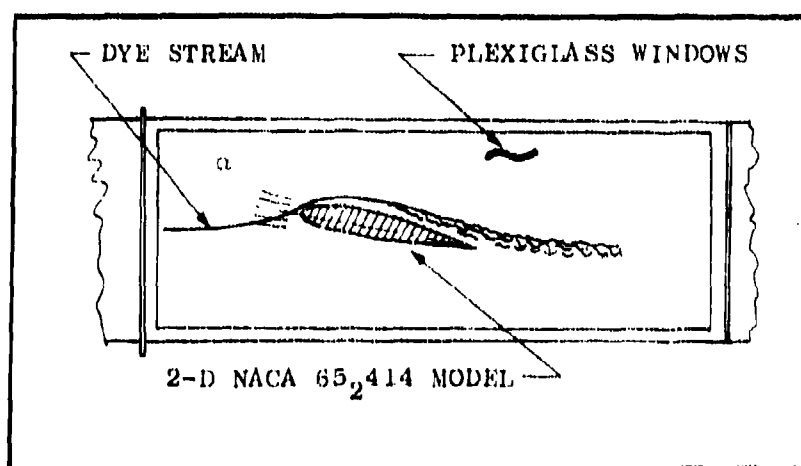
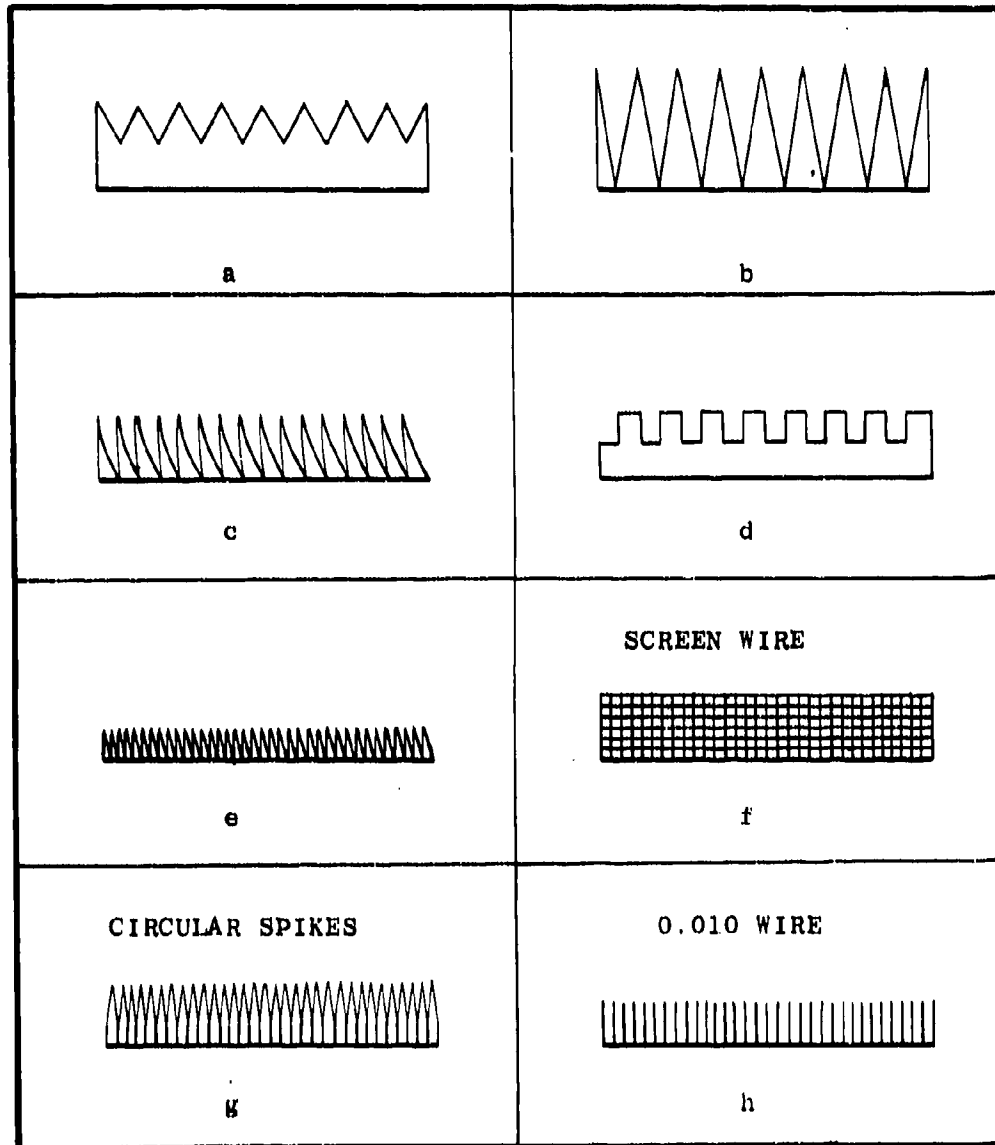


Figure 45. Water Tunnel Test Section Set-Up.



Scale; Full

Figure 46. Vortex Generators.

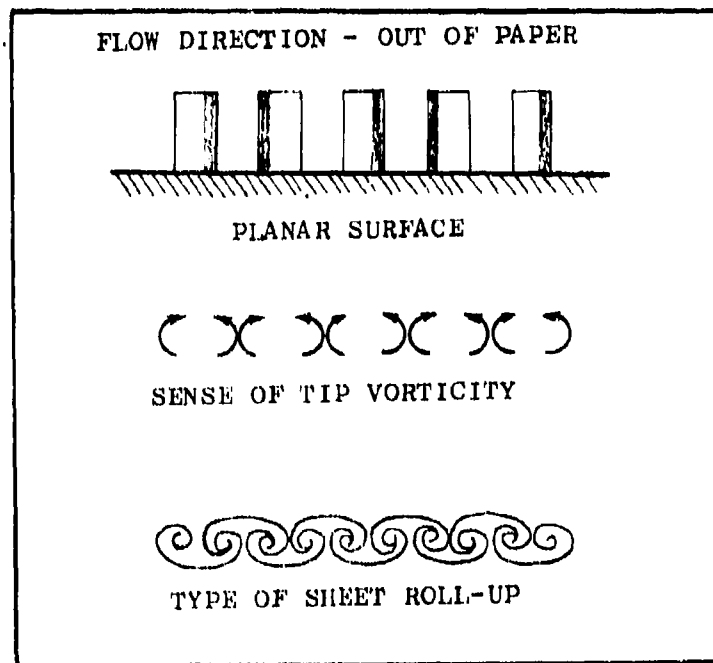


Figure 47. Tip Flow From Vortex Generator.

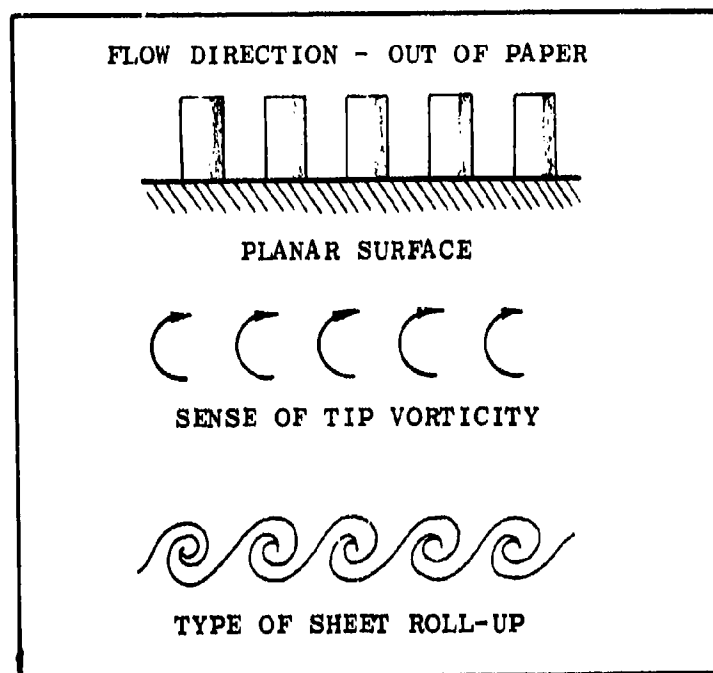


Figure 48. Tip Flow From Cascade.

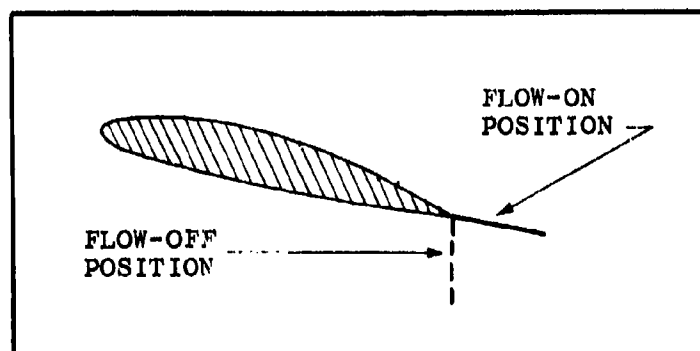


Figure 49. Splitter Plate Attachment.

APPENDIX IV

ACOUSTIC MEASUREMENTS OF THE AERODYNAMIC NOISE PRODUCED BY FLYING OWLS

A series of tests was conducted at The University of Tennessee Space Institute to determine the "aerodynamic noise" produced by owls during flight, especially during gliding approaches. The owl species used in these tests is the Florida Barred Owl (*strigiformes strix varia allen*).

In order to measure the total sound power produced by the flying owl and the spectral distribution of the overall noise signal the reverberation chamber method was selected for these tests. The chamber used was a 240 m³ room with reverberation times varying between approximately 0.8 sec and 0.4 sec in the frequency range 100 Hz to 10 kHz. The lower limiting frequency of this room below which statistical acoustic conditions were degraded was found to be around 100 Hz. The general procedure of obtaining the acoustic data was to record the unmodified noise signal and the overall sound pressure level of the noise produced by the owl flying in the reverberation chamber. Subsequently the noise signal record was frequency analyzed in terms of one-third octave frequency bands.

A particular requirement of these tests was to obtain representative noise samples from only the gliding phase of the observed flights. In all tests the owl was forced to fly from an upper perch in one corner of the room to a lower perch in the diagonally opposite corner. A flight generally consisted of an initial flapping phase followed by a gliding phase and a short flapping during touchdown. As a result of the owl's speed and the dimensions of the test room the observation of the gliding phase was relatively short, generally in the order of 0.6 to 0.8 seconds. By introducing a light string barrier mounted near the middle of the room the test flight configuration became very reproducible. The owl was forced to flap to the string barrier and then to a gliding flight with nearly constant speed to the lower perch. Figures 50 and 51 give more details of the flight conditions.

The resulting acoustical data which are reported here were measured with a single condenser microphone having a sensitivity of 5 mV/microbar and a flat frequency response in the range 2 Hz to 10 kHz. The microphone was positioned slightly above the floor at a sufficiently large distance from the flight path, and for all frequencies well beyond the reverberation radius of the moving noise source. During the flight tests the noise signal and the overall sound pressure level were recorded simultaneously by an FM magnetic tape recorder and a sound level recorder.

The measuring and analysis setup and its frequency characteristics are shown in Figures 52 and 53. The average reverberation time of the test room is given in Figure 54. The one-third octave band spectral analysis in the frequency range below 25 Hz has been made by application of magnetic tape frequency transformation. Samples of the resulting measurements are shown in Figures 55 through 61. On the photographs showing the unmodified noise signal as sensed by the microphone, Figures 55 and 56, a 1 kHz signal traced during part of the flight indicates the gliding phase as judged by the observer in the test room. In identifying the part of the signal produced during the gliding of the owl, evidently the observer's reaction time has to be taken into consideration. The time history record of the overall sound pressure level in decibel is a graphical logarithmic record of the root-mean-square value of the time varying signal shown on the photograph (see Figures 57 through 59). In a follow-up analysis a reproduction of the noise signal only from the gliding phase of the test flight was made and a frequency analysis of this signal in terms of one-third octave bands was obtained. The gliding noise/frequency spectra for the reported flight tests are shown in Figure 60 and 61. The spectral sound pressure level distribution as measured in the reverberation chamber is compared with the ISO, R226, threshold of hearing case for pure tones. The spectra shown are corrected for the ambient noise level observed during the tests. This was done by using the formula

$$n = n_{ospl} + 20 \log \left(1 - 10^{\frac{n_{ospl} - n_{back}}{20}} \right) \quad (1)$$

where n_{ospl} is the measured overall sound pressure level in dB and n_{back} is the background noise level in dB.

The overall sound pressure level data resulting from the reverberation chamber measurements permit the calculation of the total sound power produced by the flying owl (see for example: Kinsler, Frey, Fundamentals of Acoustics, (1967) p. 436). If the values found for the overall produced sound power are used to define a simple spherical source radiating with the same intensity in a free field, an estimate of the sound pressure levels produced by a gliding owl under free field conditions can be obtained. Spectra resulting from such an estimate with absorption effects (air of 50% relative humidity at 20°C) taken into account are shown in Figures 62 through 64 for distances equal to the reverberation radius r_1 , 3 meters, and 10 meters. The reverberation radius has been estimated according to

$$r_1 = [0.163 V (16\pi T)^{-1}]^{1/2} \quad (2)$$

with the chamber volume V measured in cubic meters and the reverberation time T in seconds.

The aeroacoustic data resulting from these tests with gliding owls make it quite understandable that an aural detection of a gliding owl at distances larger than approximately three meters from a human observer is quite unlikely. From the spectra shown in Figures 62 through 64 it can be seen that beyond a propagation distance of three meters the sound pressure levels in all frequency bands up to at least 10 kHz has dropped below the threshold of hearing curve. The produced total overall sound pressure level (40 dB to 50 dB) is relatively high. The relative quietness of the owl flight appears to be rather a result of an appropriate noise energy distribution over the frequency spectrum rather than an overall low noise level. A comparison with a similar noise spectrum from a sailplane overflight in a comparable distance, for example, shows the fundamental difference in the shape of the spectra, see Figure 65. Evidently the overall noise level time history during a test flight, is a periodic signal component which is found to occur in all gliding phases of the analyzed test flights. This periodic component has a dominant frequency of 15 Hz well in the subaudible range of the human ear. The following facts about this periodic component are to be mentioned. The 15 Hz component has never been observed, except during the owl flights where it dominates the noise signal during all gliding phases. Further, the signal in a number of tests exhibits an amplitude modulation as e.g. in the case of Figure 55, with first increasing and then decreasing amplitude. The 15 Hz coincide with the lowest fundamental mode of the reverberant chamber. The measured amplitude is therefore not directly comparable with the amplitudes of the high frequency components. This is due to the fact that at low frequencies pronounced room resonances occur which lead to a non-uniform frequency response of the room. The reverberation time for this frequency range depends strongly on the frequency and a meaningful average reverberation time cannot be defined. At higher frequencies when the sound field becomes "diffuse" the frequency response of the room is more uniform and average reverberation times may be used.

In preliminary wind tunnel tests flutter frequencies of about the same frequency have been observed (see Appendix II).

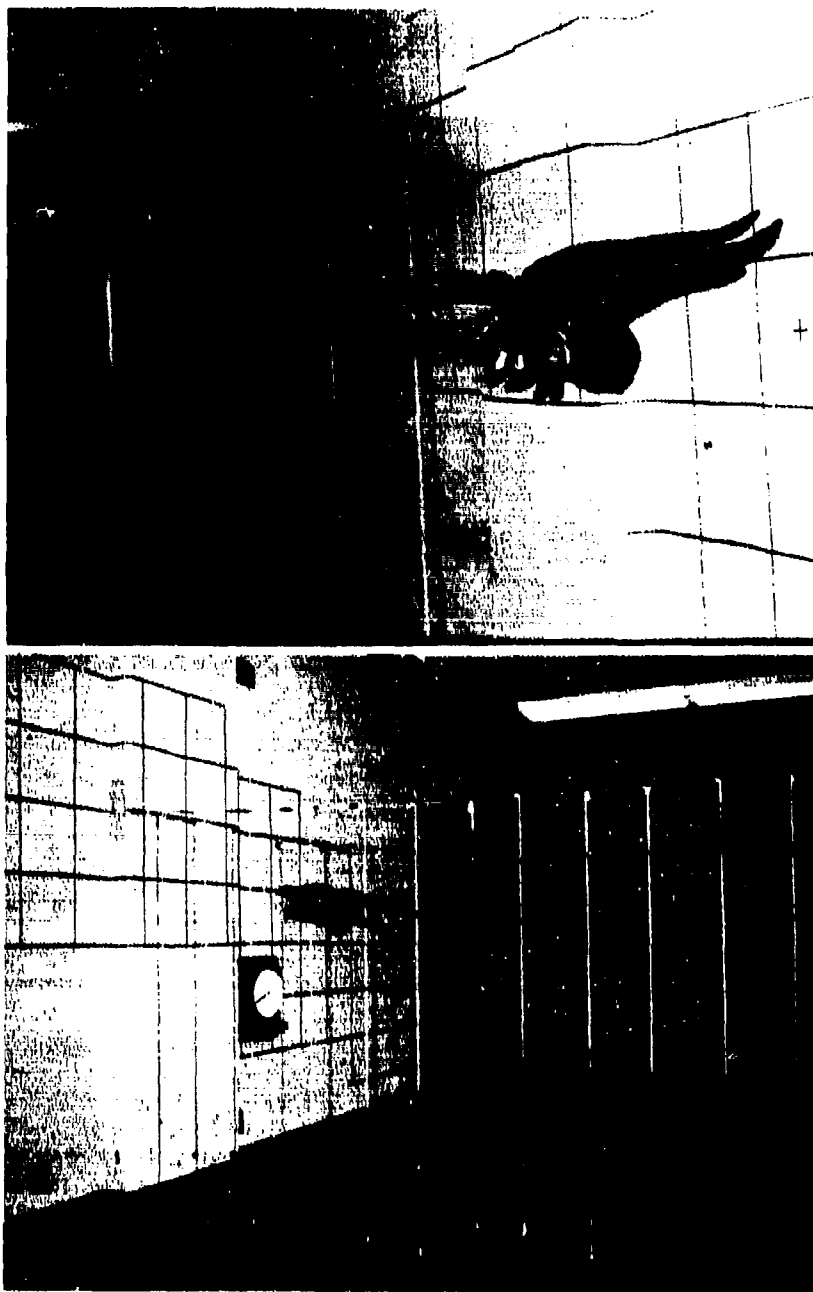


Figure 50. The Owl Approaching the Lower Perch in a Gliding Descend After Passing the String Barrier.

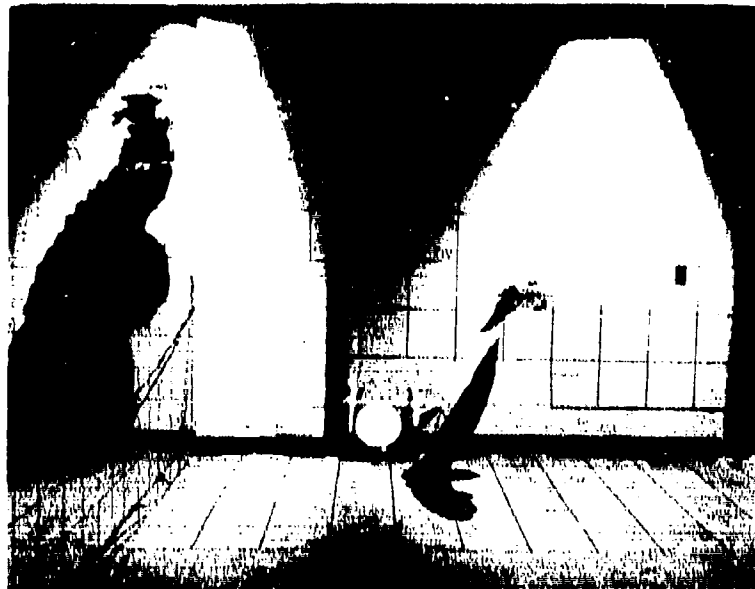
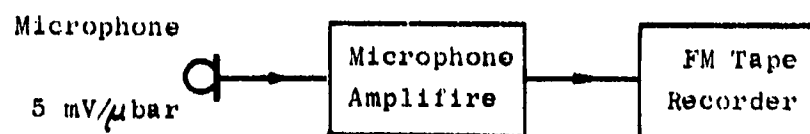


Figure 51. Double Exposure of the Owl During a Gliding Phase.
The Measured Flight Speed in this Case is 20.6 ft/s.

Recording:



Reproducing:

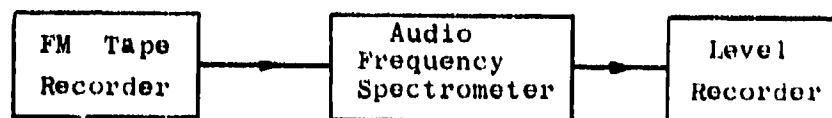


Figure 52. Block Diagram of Test and Analysis Instrumentation.

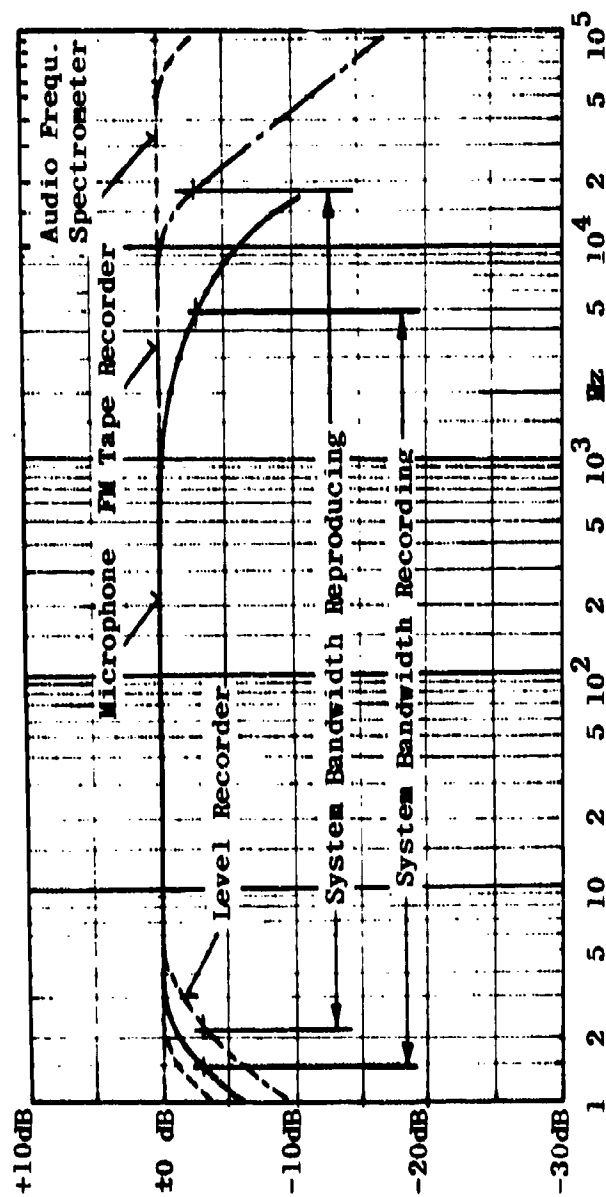


Figure 53. System Frequency Response.

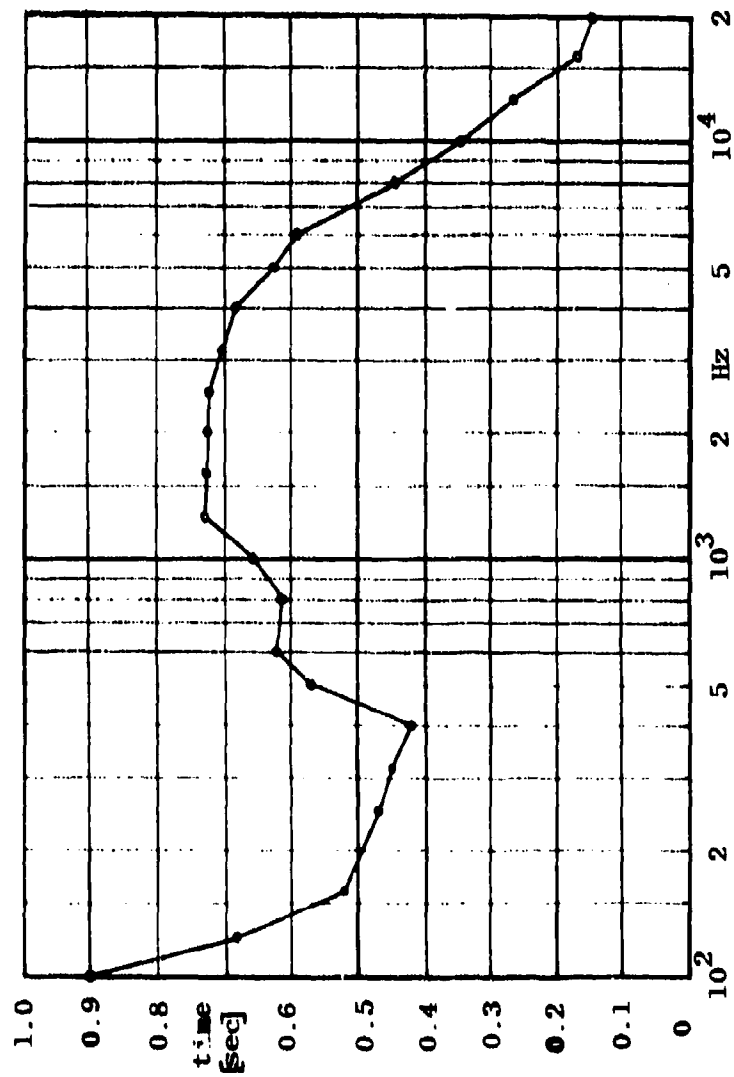


Figure 54. Average Reverberation Time of Test Room.

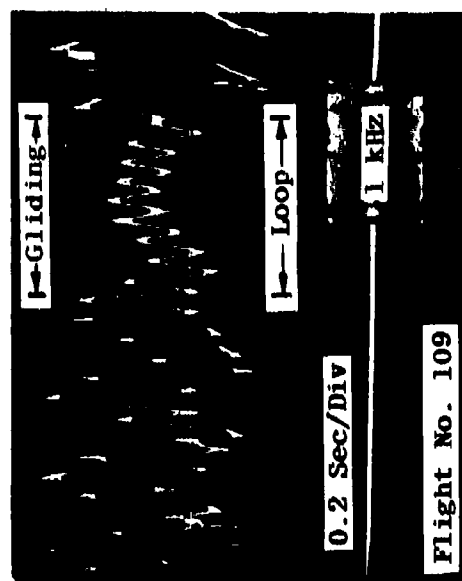
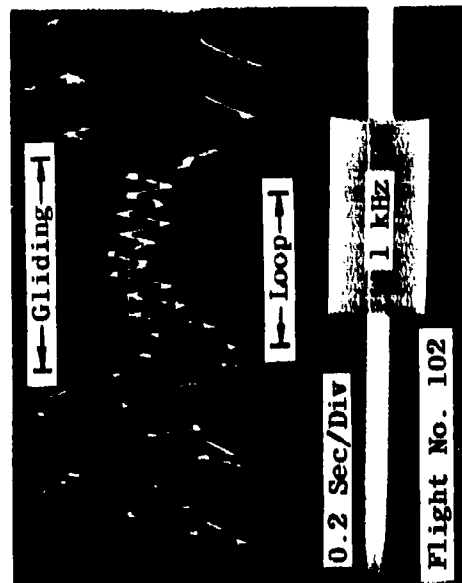
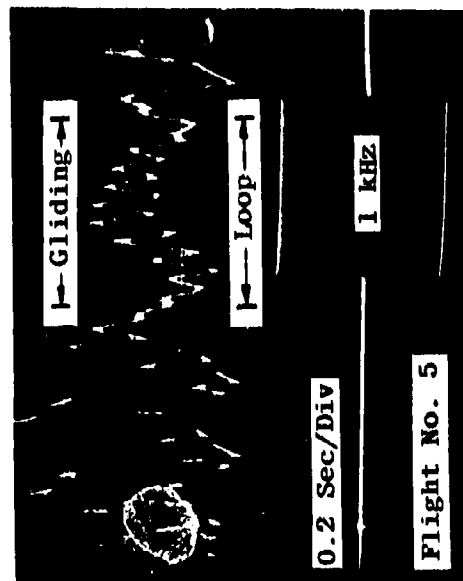
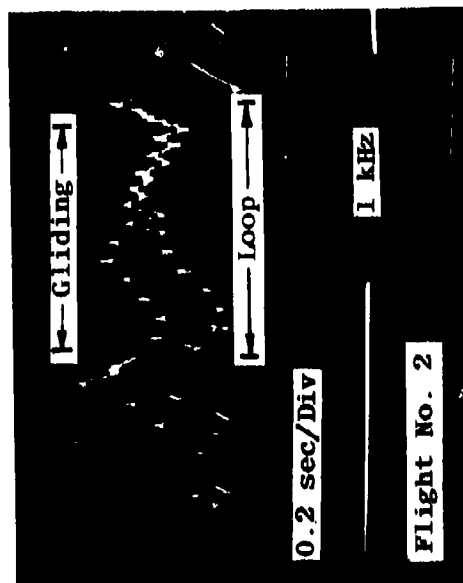
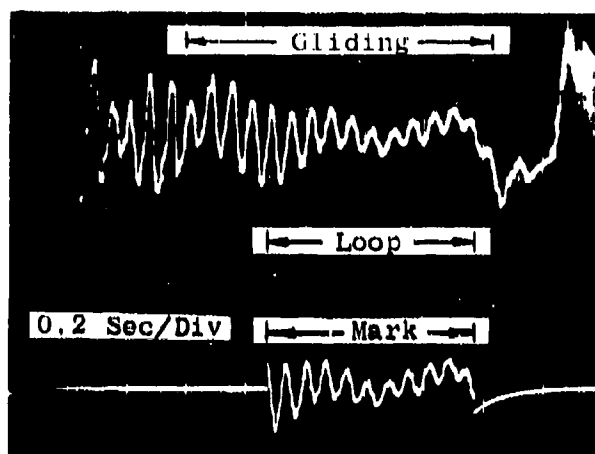
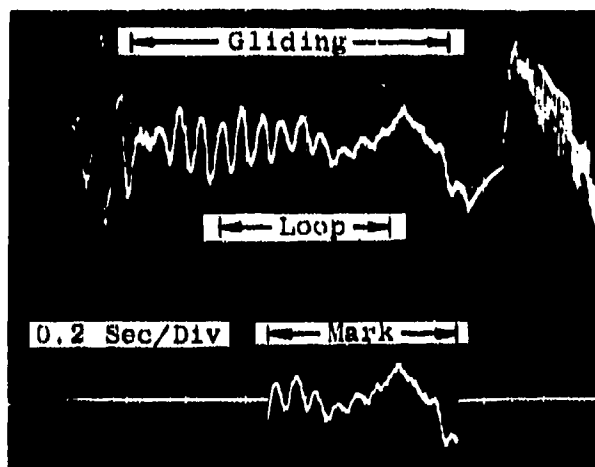


Figure 55. Typical Recordings of Linear Sound Signals.



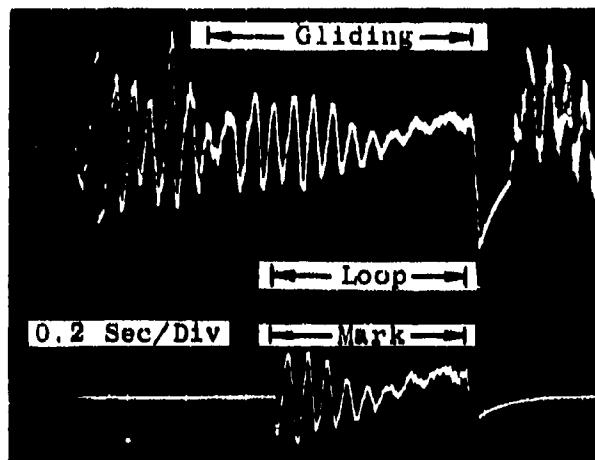
Flight No. 12:

Leading edge removed



Flight No. 14:

Trailing edge removed



Flight No. 17:

Top of wing modified

Figure 56. Linear Sound Signals of the Modified Owl.

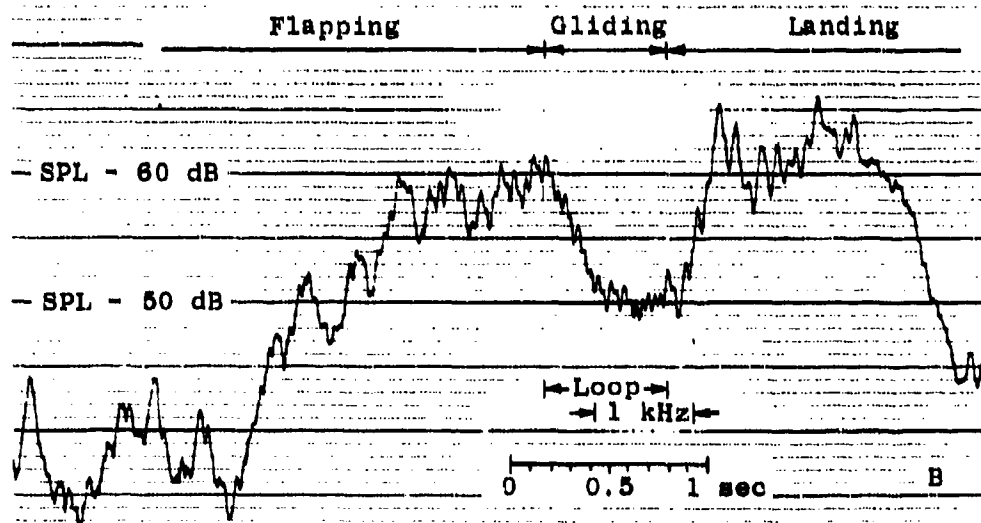
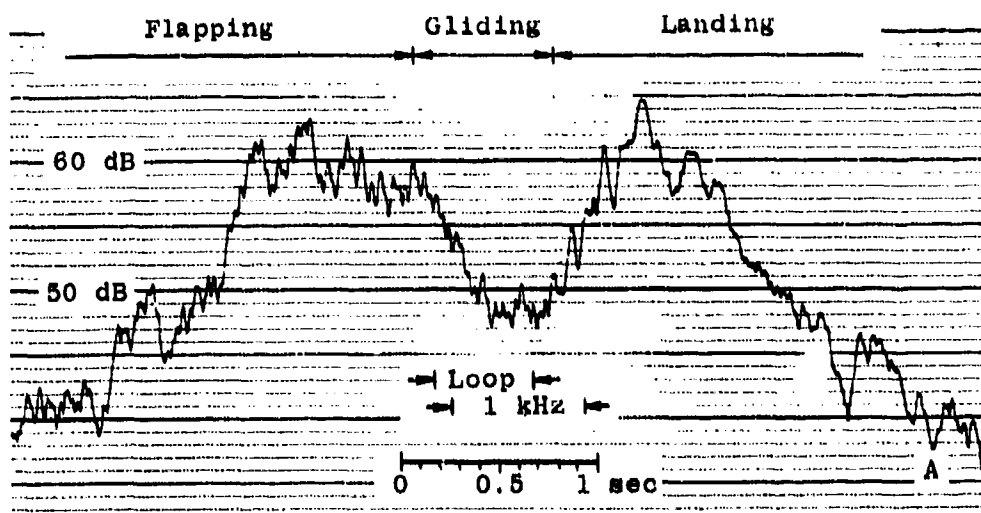


Figure 57. Typical Recordings of Overall Sound Pressure Level. (A, Flight No. 102; B, Flight No. 109)

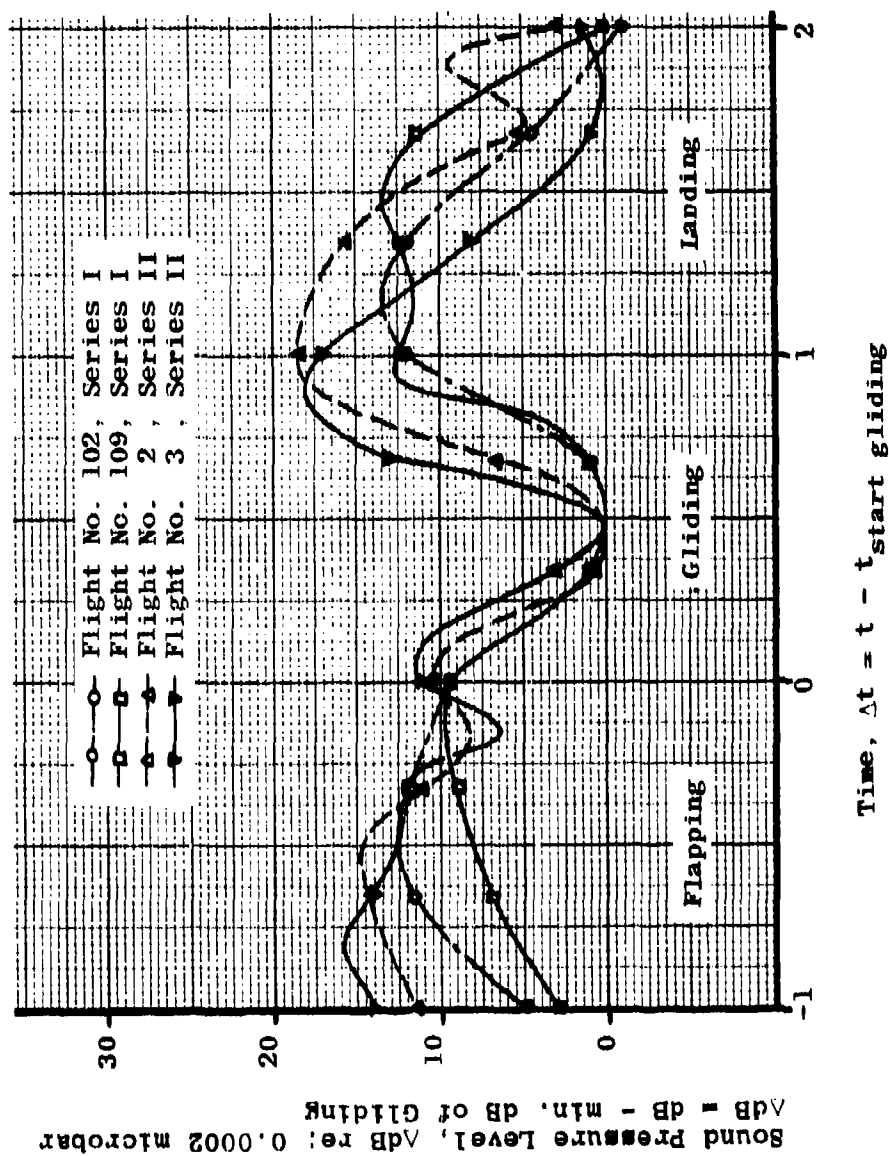


Figure 58. Sound Pressure Level of a Gliding Owl.

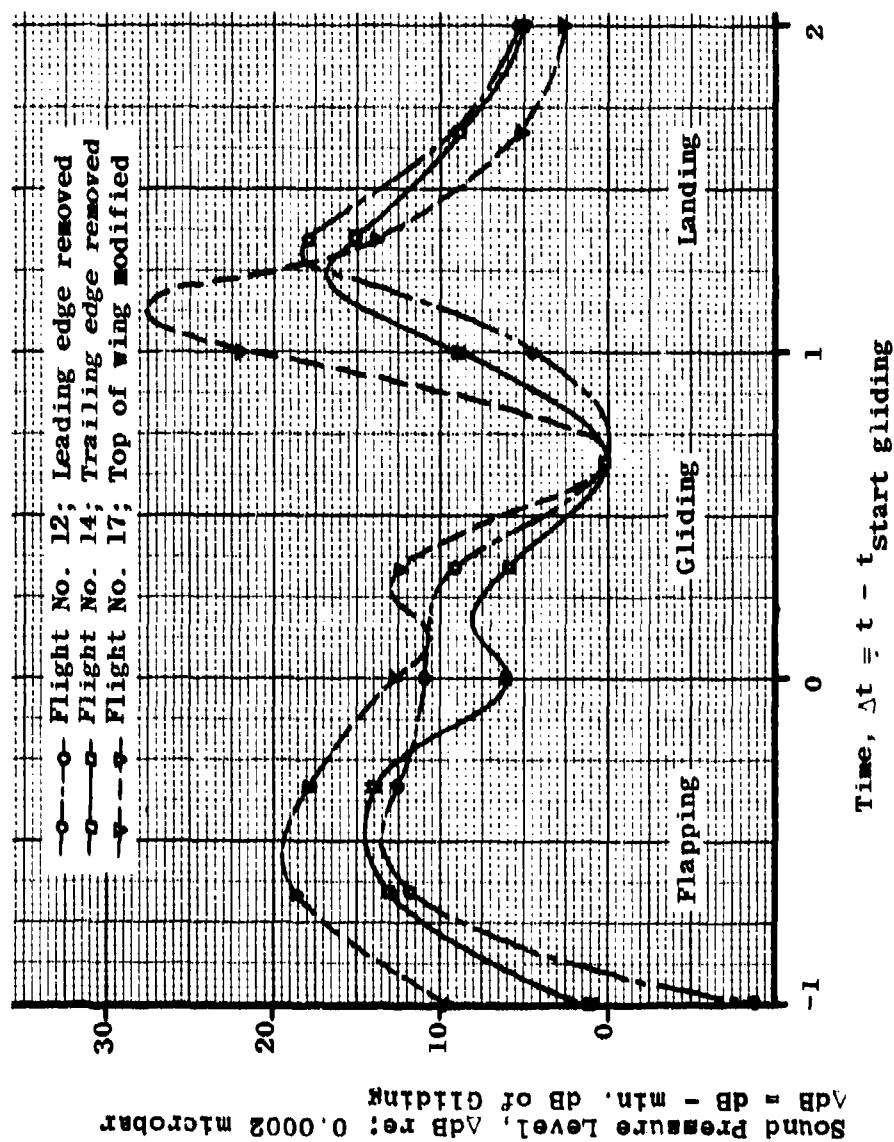


Figure 59. Sound Pressure Level of a Gliding Modified Owl

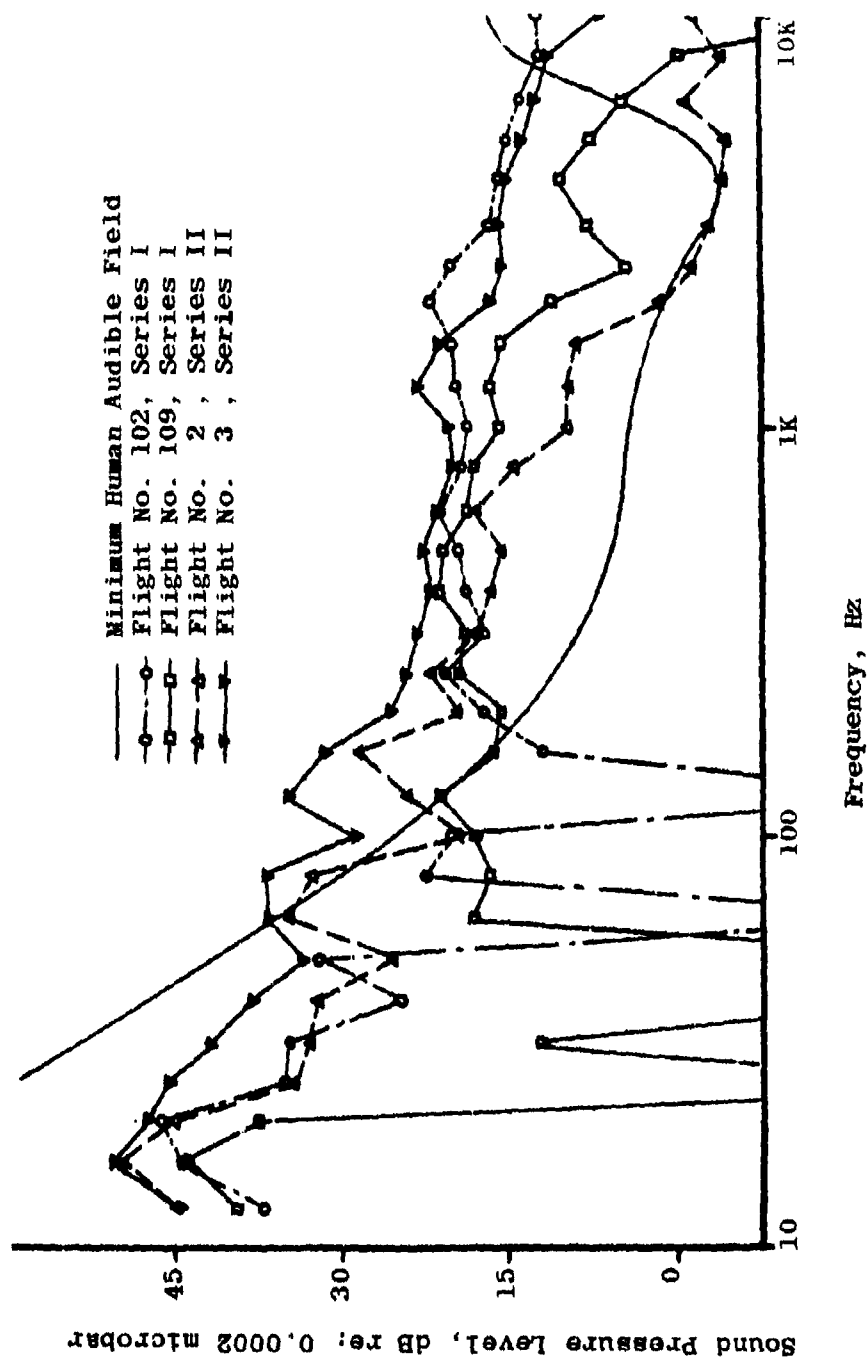


Figure 60. Frequency Analysis of the Sound Pressure Level of a Gliding Owl

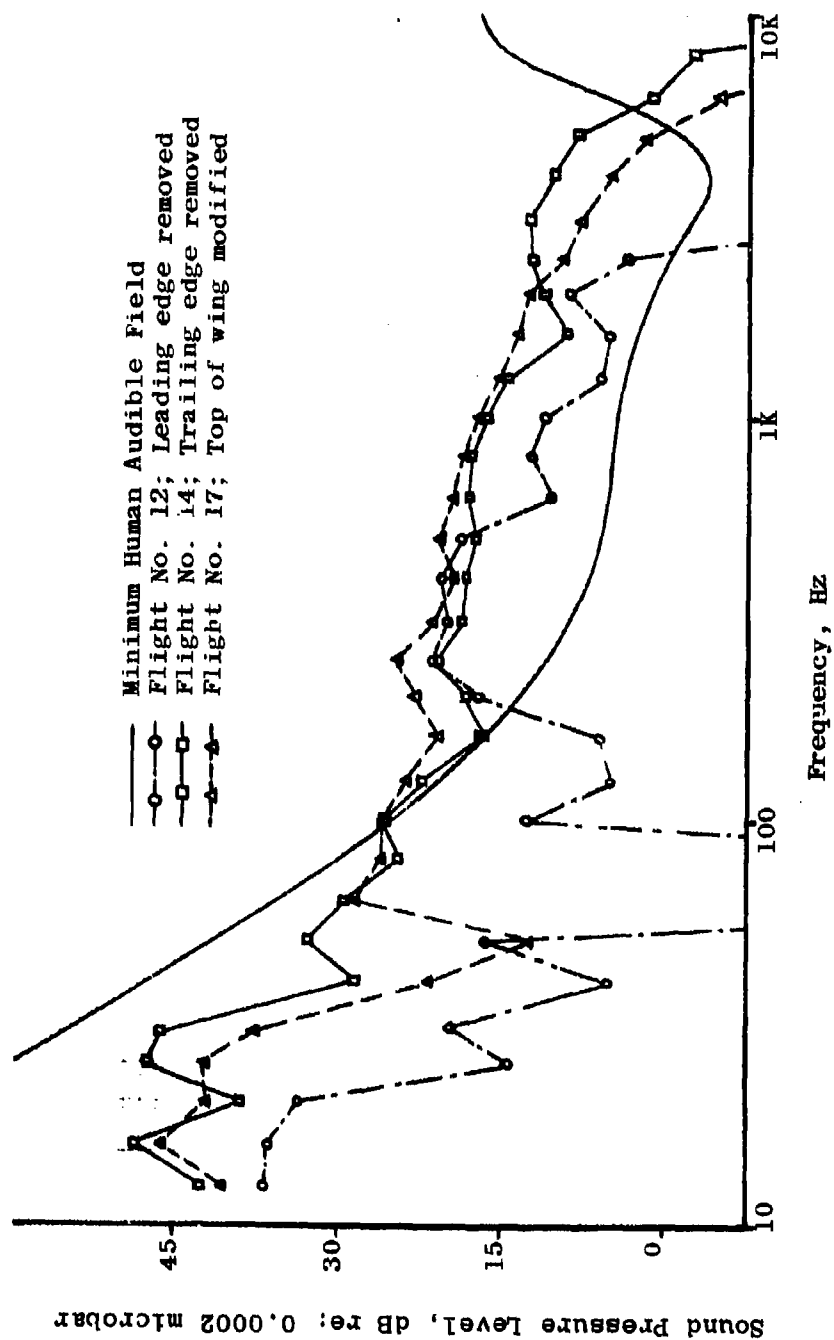


Figure 6L Frequency Analysis of the Sound Pressure Level of a Gliding Modified Owl

Frequency Analysis of Flight No. 7, Series II, for Several Distances of Observation;

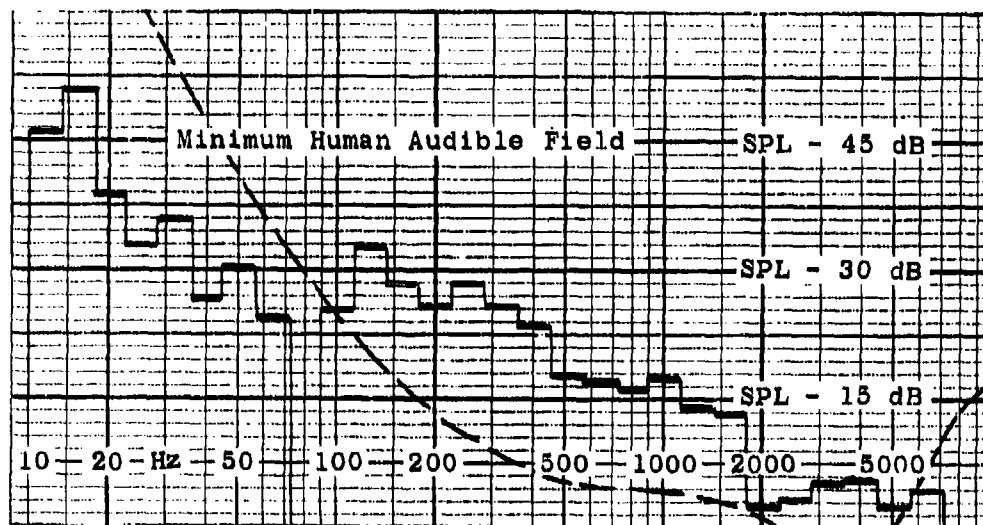


Figure 62. Distance of Observation; 1 meter.

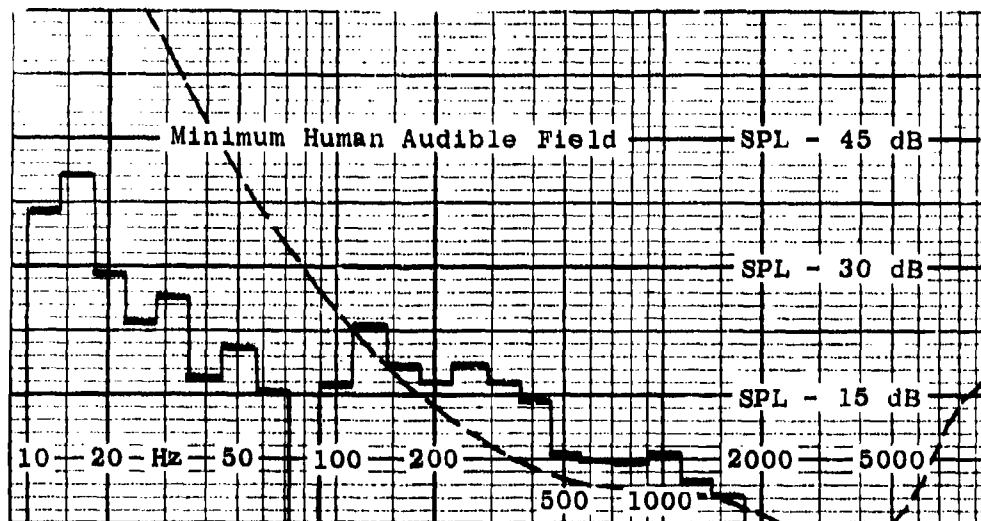


Figure 63. Distance of Observation; 3 meters.

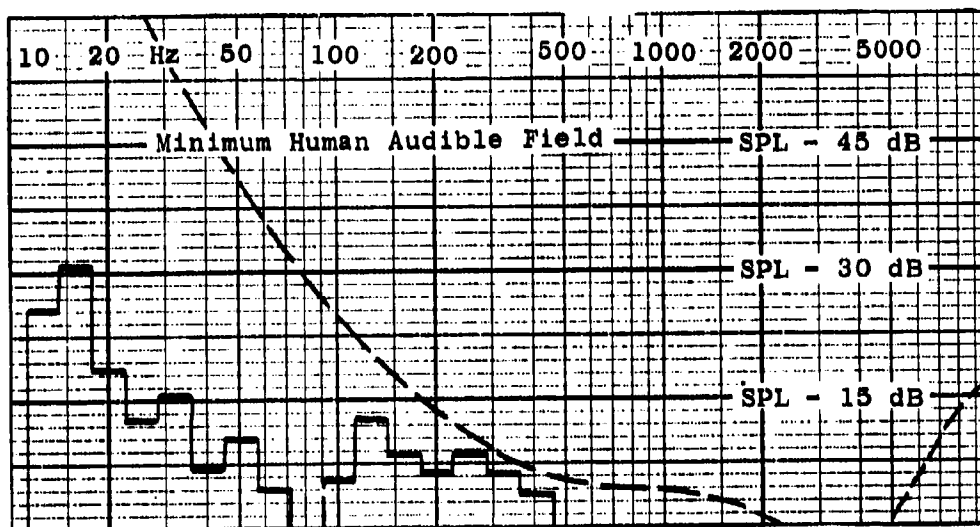


Figure 64. Distance of Observation: 10 meters.

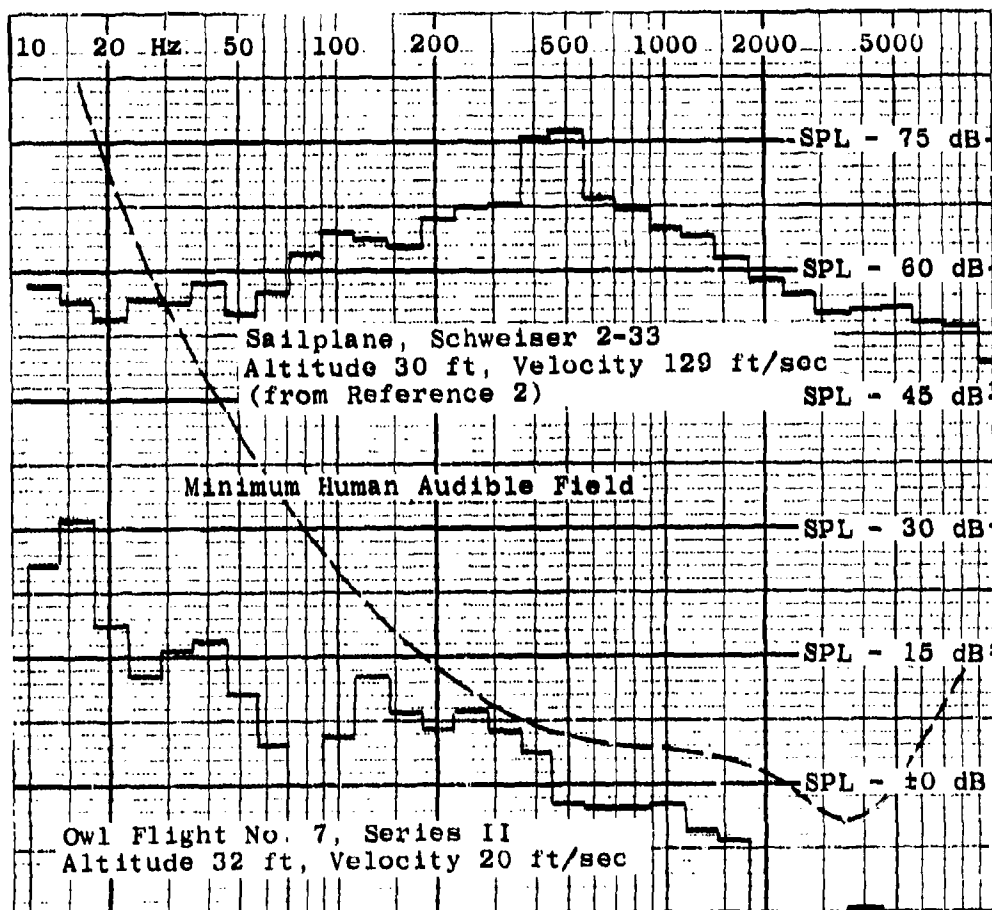


Figure 65. Comparison of Spectrum Shape of Aerodynamic Noise Produced by Owl and Sailplane

TABLE VII

TEST SERIES I: ACOUSTIC MEASUREMENTS OF OWLS
DECEMBER 13, 1970

Flight No.	Bird	Flight Quantity	Comments
100	Owl Rebel	no gliding phase	bird didn't land
101	Owl Rebel	good gliding phase	
102	Owl Rebel	good gliding phase	
103	both owls	no gliding phase	bird didn't land
104	Owl Rebel	good gliding phase	
105	Owl Rebel	good gliding phase	one flap during gliding phase
106	Owl Rebel	no gliding phase	bird didn't land
107	Owl Rebel	good gliding phase	
108	Owl Rebel	no gliding phase	bird didn't land
109	Owl Rebel	good gliding phase	
110	Owl Rebel	no gliding phase	bird didn't land
111	Owl Rebel	no gliding phase	bird didn't land
112	Owl Rebel	no gliding phase	bird didn't land
113	Owl Rebel	no gliding phase	bird didn't land
114	Owl Rebel	no gliding phase	bird didn't land
115	Owl Rebel	no gliding phase	bird didn't land

TABLE VIII

TEST SERIES II: ACOUSTIC MEASUREMENTS OF OWLS
JANUARY 10, 1971

Flight No.	Bird	Flight Quantity	Comments
1	Owl Rebel	good gliding phase	no sine-signal during gliding phase
2	Owl Rebel	good gliding phase	
3	Owl Rebel	good gliding phase	
4	Owl Rebel	good gliding phase	wing touched wall
5	Owl Rebel	good gliding phase	
6	Owl Rebel	good gliding phase	less gliding than before
7	Owl Rebel	good gliding phase	
8	Owl Rebel	no gliding phase	bird lands like a parachute
9	Owl Rebel	good gliding phase	wing touched wall
10	Owl Rebel	good gliding phase	sine-signal was too short
11	Owl Rebel	good gliding phase	wing touched wall
12	Owl Rebel	good gliding phase	wing touched wall
13	Owl Rebel	good gliding phase	sine-signal was too long
14	Owl Rebel	good gliding phase	
15	Owl Rebel	no gliding phase	bird lands like a parachute

TABLE IX

TEST SERIES III: ACOUSTIC MEASUREMENTS OF OWLS - MARCH 4, 1971

Flight No.	Bird	Flight Quantity	Status of Bird Modification	Comments
1	Rebel	no gliding phase	unmodified	bird lands like a parachute
2	Rebel	gliding	unmodified	low swoop
3	Rebel	good gliding phase	unmodified	
4	Rebel	gliding	unmodified	low swoop
5	Rebel	good gliding phase	unmodified	
6	Rebel	good gliding phase	unmodified	
7	Rebel	no gliding phase	leading edge removed	bird lands like a parachute
8	Rebel	good gliding phase	leading edge removed	
9	Rebel	good gliding phase	leading edge removed	
10	Rebel	bad gliding phase	leading edge removed	
11	Rebel	bad gliding phase	leading edge removed	
12	Rebel	good gliding phase	leading edge removed	
13	Rebel	good gliding phase	trailing edge removed	

Table IX continued

14	Rebel	good gliding phase	trailing edge removed	
15	Rebel	gliding	trailing edge removed	low swoop
16	Rebel	good gliding phase	trailing edge removed	
17	Rebel	good gliding phase	top of wing removed	
18	Rebel	gliding	top of wing removed	low swoop
19	Rebel	good gliding phase	top of wing removed	
20	Rebel	gliding	top of wing removed	low swoop
21	Rebel	good gliding	top of wing removed	

TABLE X
DATA OF THE TESTED OWL

Weight	1.52 lb
Wing area*)	344.8 in ²
Wing span	38.1 in
Wing sweep angle	32.7 deg. forward
Chord at half span	11.0 in
Wing loading	$4.41 \cdot 10^{-3} \text{ lb/in}^2 = .635 \text{ lb/ft}^2$
Wing aspect ratio	4.21

*)Wing area includes the body area intercepted by the wing.

APPENDIX V

BIONIC STUDY OF SILENT FLIGHT

1. INTRODUCTION

Owls hunt their prey during low levels of ambient light and location of their prey is by means of aural detection and penetrating vision. A frequent source of food for the owl is the wood mouse which has large ear lobes and responds quickly to any detectable noise, especially in higher frequencies. This information combined with the knowledge that the owl has a low attack speed implies that the owl must be capable of noiseless flight. This capability is needed not only to prevent his prey from becoming alarmed, but also, to hear the faint sounds of his prey. Upon these observations, ornithologists have reported the owl to be silent for many years.

R. R. Graham [1] was the first to draw attention to the owl's silent flight. He identified three peculiarities common to the owl's silent flight. Using a combination of these three features Graham proposed a hypothesis on the silent flight. However this hypothesis has not been verified nor proven invalid. Speculations by others as to the reason for quiet flight have followed Graham's early suggestions.

The main questions which arise are

1. Is the owl's flight unusually quiet?
2. If so, what can be profited by this information?
3. What characteristics allow this silent flying?
4. How can this information be translated into technology?

These and similar questions are investigated in the research described in this study.

2. THE BIONIC-CYBERNETIC APPROACH

The past half century has been characterized by scientific personnel becoming more and more specialized in their area of work. It is not clearly understood how such highly specialized knowledge by itself can be productive to human society. On the other hand a too superficial knowledge of many subjects can produce little or no practical applications. This indicates that true progress can be accomplished only with a composite approach.

Bionics is a new way of analyzing problems of living systems and machines by the pooling of the work of the biologist, the psychologist, the mathematician and the engineer. When Steele [31] introduced the word bionics in 1958 he gave it this definition:

It is the science of systems whose function is based on living systems, or which have characteristics of living systems, or which resemble these.

Gerardin [32] has expanded upon this definition to show the active role it must play in the future of mankind when he said,

Bionics is the result of bringing together the analytical activity of biologists and the synthetic activity of the engineers. It is a systematic study of the behaviour of living mechanisms so that the principles discovered may be adapted for use in manmade systems.

A well phrased illustration of the engineer's dependence upon his own knowledge and his concept of an innate ability to create is given by Hertel [33]

Since Nature has 'unlimited time and resources' and has been 'extravagant and wasteful' in building the present, it is not therefore, surprising that Nature has developed systems and components which are incomparably more advanced and superior to all that Homo sapiens has conceived and Homo Faber has devised and built. It appears to me as an overabundance of presumption and a lack of reverence for creation that we human beings neglect or even refuse to admit the inferiority of our methods to the ways of Nature.

This strong emphasis on the systems approach requires that cybernetics be applied whenever it contributes to comprehension. Where cybernetics is,

The science which studies the communication and the processes of control in living organisms and machines as defined by Wiener [34].

A more recent definition that has been given by Helvey [35] is simply,

Cybernetics is the science of interactions.

To emphasize the need for a systems approach to problem solving, the following is quoted from the Program of the Communist Party of the Soviet Union [36]

... cybernetics and electronic computers and control

instruments will receive wide employment in the production processes of industry, construction, and transportation, in scientific research, in planning and designing calculations, and in the sphere of metering and control.

In order to transfer bionic information from a living system to mechanical technology it is necessary to have as much knowledge of the living model as possible. Otherwise the model and the prototype will not be isomorph and the results of one could not be expected to follow from the other. Because of the desire to transfer those characteristics of the owl which contribute significantly to its silent flight into airplane technology it is necessary to be familiar with the flight dynamics of the owl as well as the "design characteristics" of its wings and body.

3. BIOLOGICAL STUDY OF THE OWL'S FLIGHT MECHANISMS

Every motion of the bird in flight, every change in shape and position of the feathers, is designed to extract energy from the air and use it to establish the desired flight. The wings and feathers of the bird in flight use the same principles and similar mechanism, such as: wings, propellers, steering and high-lift devices in much the same way as an airplane.

a. Biological Characteristics of Bird Locomotion

To appreciate the analogy between bird and airplane flight it is important to know the basic construction of the wing of a bird, Figure 66. From Figure 66 we can see that the wing is of the same basic construction as the human arm, the feathers being attached to the "forearm" and the "hand, with the small "alula," or "bastard wing" constructed as a "thumb." The feathers on the hand are known as "primaries," and those on the forearm are "secondaries." The "tertiary" feathers grow from the "elbow." The "scapulars" grow from the scapular membrane, which reaches from the "shoulder" out to the elbow. A strong elastic membrane of two layers of skin, the "patagium," stretches between the shoulder and the "wrist." The feathers along the front edge of the wing grow from this membrane, which holds them in position to give the wing a straight, streamlined leading edge, even when the elbow is partially bent.

The bird's wing acts not as a single piece of flying equipment but as a composite, each part having a different function or movement. The inner portion of the wing, from shoulder to wrist, corresponds to the wing of an airplane. It moves comparatively little during flight but, like the wing of an airplane, supplies the required lift. The outer section of a

bird's wing, starting at the wrist, constitutes the propeller and is also used for control surfaces.

Bird flight can be divided into two main sections, gliding flight and flapping flight. The later division covering normal "powered" flight, take-off and "aerobatics," which are usually special maneuvers used in catching prey or in combat. For comparison with airplane flight flapping flight can be disregarded.

With only slight muscular activity the bird can change the angle of attack of his wing in gliding flight. With equal ease it can vary the camber, the span and the sweep angle thus affecting the lifting surface, the lift-to-drag ratio and the control surfaces.

The shape of flight feathers (remiges) in action is the result of many different factors. The design of the "vane", Figure 67, and the way it responds to air pressure; the design of the "barbs" which make up the vane and affect its elasticity and shape; and the design of the "shaft." The vane, made up of parallel rows of barbs, stands out on each side of the "rachis" sloping toward the tip. From each side of the barbs rows of "barbules" slope out toward the feather edge.

Bird feathers have a remarkable number of quality design standards. They are lightweight which is in part due to the hollow or "foam" filled shaft and barbs. Through the use of an extremely thin-walled construction with the lightweight "foam" for support, the feathers show a high load-bearing capacity. Optimum shape, power cross-sectional dimensions and excellent materials results in a high degree of stiffness, elasticity and flexibility. They resist damage because of the many divisions of pliant parts. Each barb may completely separate from the one next to it and be joined back by merely making contact again.

It is especially interesting to note how Nature has handled, in the flight feathers, the aeroelastic problem of "induced airfoil oscillations." The following flight characteristics in birds combine to produce a "critical velocity" higher than the maximum flight velocity. The critical velocity is that velocity at which oscillations are generated which may rupture vibrating parts. The features which have been perfected in the bird to obviate flutter are: good resistance to feather torsion and bending due to the hollow cross section of the calamus; the ultra-light construction of the vanes to ensure minimum moment of mass about the rachis axis; the form of the remiges, with narrower anterior vane sections and broader posterior vane sections permits the resultant of the aerodynamic forces to lie behind the shaft. Consequently, the aerodynamic axis (the center-of-pressure locus) lies behind the centroidal axis which in turn falls behind the torsion axis.

b. Unique Features of the Owl's Flight Structure

With the above knowledge of the aerodynamic role of feathers and the wings it enables us to analyze the unusual characteristics of the owl which allow it to fly silently. Following is the list of the three unique characteristics of the owl's wing which were listed by Graham [1].

1. The Leading Edge Comb. There is a remarkably stiff, comb-like fringe on the front margin of every feather that functions as a leading edge of the wing. The teeth of this comb are extensions of the barbs of the anterior part of the vane.
2. The Downy Upper Surface. Both the anterior and the posterior parts of the upper surface of the feathers are covered with a thick, fluffy down-like covering.
3. The Trailing Edge Fringe. Along the trailing edge of the wing and of each primary feather, there is a fringe with ragged outline. The fibers of which it is formed are extensions of the barbs that make up the posterior part of the vane.

c. Suggested Biological Explanation of the Owl's Silent Flight

In all previous attempts to explain the silent flight of the owl it has been stressed that the "hooked comb" on the leading edge of the leading remegis functions somehow to suppress noise. This emphasis on the leading edge comb has resulted from the lack of same on the fishing owl of Asia (*Ketupa flovipex*). This owl differs from the others in being a fish preying bird and therefore not requiring any silencing mechanism because its prey is submerged and unable to hear the owl.

Graham [1] set the pace on emphasizing the assumed importance of the leading comb as the primary apparatus in reducing the radiated noise. His conclusion was that the leading edge comb served as a false leading edge of the wing and performed the task of gradually slowing down the velocity of the air which flowed through the comb and over the top of the wing. The benefit of this, he concluded, was to smooth out the pressure gradient and thereby reduce any associated sound generated. Concerning the trailing edge fringe Graham postulated that the fringe allowed a mixing of the upper and lower streamlines in such a way that the noise-producing vortices did not form. The down-like texture of the feathers allowed them to move relative to one another without generating mechanical noise, Graham concluded.

A. Rapset [37] who had done much research in experimental bird aerodynamics, formed an analogy between the leading edge comb and a swinging wire. He noted that two pieces of wire twisted together and swung through the air will generate noise at a much lower intensity and frequency than a single piece of wire. He suggested that the toothed leading edge acts in the same way, i.e., in a manner to reduce the vortex noise emitted by the flow over the wing.

4. EXPERIMENTAL AERODYNAMIC INVESTIGATION OF THE GLIDING OWL

Free-flying birds are capable of a variety of steady and unsteady modes of flight. Some birds have exceptional abilities in flapping flight during take-off, other birds are able to soar for long periods of time apparently with little effort yet others have outstanding maneuvering abilities.

a. Types of Gliding Flight

Knowing the practical limitations of tactical aircraft and being cognizant of the definition of bionics this project was limited to the investigation of gliding flight. Gliding flight is that steady state motion in which no propulsive forces are supplied by the birds muscles or the aircraft's propulsion unit. There are three ways [38] by which an air vehicle may fly in the gliding mode. First the vehicle may maintain or gain altitude by gliding in an air mass that has an upward velocity component equal to or greater than its sinking speed, V_g . The second condition of gliding flight is described by the air vehicle flying in an air mass that has a horizontal velocity. In this condition the vehicle maintains its altitude if the horizontal velocity is sufficient to make the following equation an equality

$$L = W = 1/2 \rho S V^2 C_L$$

where L is the lift force, W is the weight of the vehicle, ρ is the air density, S is the appropriate wing area, V is the gliding velocity and C_L is the nondimensional lift coefficient which is a function of the airfoil shape and the angle of the airfoil to the glide path.

The first and second cases of gliding flight are dependent upon the aforementioned dynamic atmospheric conditions. In the third case the gliding flight is restricted to flight in motionless, air masses, but is influenced by the initial glide conditions, gravitational forces and the vehicle's aerodynamic

characteristics. In this gliding mode the path of flight is inclined downward with the angle ϕ . The gliding velocity and the angle of inclination are the main factors for the determination of the aerodynamic characteristics of the gliding vehicle. In this respect the acceleration forces are negligible (see Reference 39).

This third type of gliding flight can be investigated by sailing the vehicle in the open atmosphere when vertical or horizontal air currents are negligible. This approach was used by Raspet [37] and Farrar and Farrel [40] in the early mornings or late afternoons to study the gliding characteristics of the buzzard. This condition can be simulated by investigating the gliding vehicle in a wind tunnel. This procedure has long been used to study mechanical vehicles but only recently living birds [39, 41] have been trained to glide free in a wind tunnel.

b. Bionic Need for Aerodynamic Characteristics

Several studies (42 through 44) have been executed to determine those aerodynamic properties, which, when changed, result in a different level of noise and its frequency produced by the flying aircraft. The apparent parameters include the general contour of the vehicle such as cavities, protrusions and similar variations in body geometry which may generate sound during flight. However, often the mechanism of sound generation is not well understood. The dependence of sound production on aircraft speed is recognized but the relationship describing the dependence is still being investigated. Researchers have suggested that the noise varies according in some function of the change in wing loading, aspect ratio, drag, and Reynolds number. Investigation of this function or scaling parameter was not included in the scope of this study therefore no conclusions are drawn. The aerodynamic parameters in this study were established to provide a foundation from which the acoustic data through a bionic approach can be translated in the correct scaling factors for sailplanes.

c. Experimental Aerodynamic Procedure and Data Reduction

In the gliding flight of the owl the necessary acoustic data were recorded in open atmospheric conditions instead of in a wind tunnel. This decision was influenced by the readily available room in which the owls could fly freely. This decision was also encouraged by the long training which would be required to attain successful flights in a wind tunnel. Also the necessary low turbulence wind tunnel was not available, which would be required to obtain valid acoustic data.

In order to utilize the living owls as instruments to

establish experimental aerodynamic and acoustic data extreme difficulties had to be overcome. The objective was to have the owls fly a repeatable course and have a maximum distance in a gliding mode. The measurements were made in the room illustrated in Figures 68 and 69. After prolonged training of the owls the flight was standardized by forcing the owls to fly from a high perch over a string barricade to a low perch. The altitude difference between the low and high perches was 5 feet and the horizontal distance was 38 feet.

It was not possible to train the owls to leave the high perch and glide the angle of 7.5 degrees to the low perch because the owls after leaving the high perch flapped their wings until they were very near the low perch and they took a variety of routes to the lower perch. Furthermore, they landed on every possible protrusion in the room. Therefore, every object was removed or covered in a manner to encourage the owls to land only on the two perches. The low perch was consistently used as a feeding place. Much experimentation was necessary to establish an environment which forced the owls to fly the same route every time with minimal deviation. To achieve this a barricade was erected over which the owls had to fly to reach the low perch (see Figures 68 and 69). It was necessary that the birds see the lower perch at the time of departure from the high perch in order to determine the flight direction. Therefore, no solid barrier like a sheet of cloth or even transparent plastic was satisfactory. Consequently, a loose white cotton string barricade was erected by hanging six feet long streamers approximately one foot apart from a horizontal string. It occurred very infrequently that the owls, whose wing span about three feet, tried to pass through the vertical strings. To achieve the maximum gliding distance the string barricade was systematically varied in position, both in the vertical and horizontal location.

In the dimly lit room the owls took off from the high perch in flapping flight to gain velocity, then passing over the barrier they went into the gliding mode toward the low perch. About three feet before arriving to the low perch they changed the angle of attack of their wings and further slowed down their flight by using their tail and wing tip feathers as flaps and high drag devices.

The feeding of the owls was done once a day approximately at the same time. The main food was chicken gizzards and small balls made of the bone dust accumulated from sawing up fresh beef bones so that it provided, besides the bone marrow, the necessary calcium for the owls. Regular attention had to be given to the water supply because the owls consumed much water. There were no difficulties during the nine months of working with the owls with parasites or diseases.

During the acoustic experimentation with the owls the room was well lighted, but during the rest periods the light was

subdued. The windows were covered with dark paper to prevent the birds from flying against the glass.

The two Florida Barred owls (*Strix varia alleni*) were purchased from an animal dealer as adult birds. The experimental tests were conducted with only one of the owls. The physical properties of this owl are listed in Table XI.

Although a cage was available for the owls it was determined to be advantageous to leave the owls free in the room where they could use the two perches. This had the disadvantage that other birds, especially if they were smaller than the Barred owls, could not be used for experimentation because the Barred owls, being birds of prey, killed them.

It was tried in a few cases to work also with hawks pre-trained by their owners. However, they would not fly a course from which repeatable and meaningful flight dynamic data could not be obtained.

The Barred owls never became fully domesticated although sometimes they took food from the trainer's hand.

Photographs of the gliding owl were taken in order to obtain the flight velocity, V , and the gliding angle, ϕ . One method was through the use of the grid pattern on the wall and floor of the experiment room, established by eighth inch wide black tape. Furthermore, the locations of the camera and lights relative to the floor and wall were known. The position of the flying owl at two times in each flight was established by sequential triggering two electronic light flash units mounted on the ceiling of the test room. They provided, through capacitor discharge, sufficient light, of $1/2000$ second duration, to illuminate the owl and the turntable which was used for timing (Figure 70). The strategic location of the flash units permitted shadows to be cast on the grid on the floor and wall. Difficulty was encountered in developing the photographic system since the location of the bird at the flash times was determined from the shadows cast on the wall and floor. The positioning of these shadows was controlled by the location of the electronic flash units, the position of the camera, flight path of the bird and time of flash triggering. The triggering of the two flash units was accomplished via individual remote switches operated by an observer. To use the entire glide time for determining the velocity the flash operator anticipated the beginning of the glide phase and triggered the first flash. The second flash unit was triggered just as the owl broke the glide mode, but before it began to flap its wings for landing. Many flights were made to adapt the observer to trigger the flash units at the proper times. The time interval (Δt) was determined by reading the percent of a revolution that the constant speed turntable made between dual flashes which were made visible by a dark line on the white turntable. The speed of rotation of the turntable was standardized prior to each test.

The vertical, longitudinal and lateral positions were then measured on the photograph (Figure 70) to finally establish by triangulation the distance traveled along the glide path. The numerical procedure for determining the total distance traversed in time Δt was obtained from the following relationships where the letters X, Y and Z define the apparent position as determined from the photographs, whereas, the starred letters denote the actual coordinates of the bird. The other alphanumericics refer to physical dimensions of the room and equipment locations; (see Figures 71 and 72).

$$\frac{X^*}{X} = \frac{R - Z^*}{R} \quad (1)$$

$$\frac{Y^* - C}{Y - C} = \frac{R - Z^*}{R} \quad (2)$$

$$\frac{3 - Z^*}{3 - Z} = \frac{H - Y^*}{H} \quad (3)$$

Solving from Z^* from Equation (3) we find

$$Z^* = 3 - \frac{(H - Y^*)(3 - Z)}{H} \quad (4)$$

where, from Equation (2)

$$Y^* = C + \frac{(R - Z^*)(Y - C)}{R} \quad (5)$$

substituting Equation (5) in Equation (4) and solving for Z^* gives

$$Z^* = \frac{R[HZ + Y(3 - Z)]}{RH + (3 - Z)(Y - C)}$$

thus knowing Z^* the expressions for X^* and Y^* can be obtained from Equations (1) and (2) respectively in terms of physical dimensions, measured apparent values and known actual coordinate values.

Conditions at the first and second flashes are denoted by

the subscripts (1) and (2) respectively. By taking the distance between X_1^* and X_2^* , defined as DX^* and similarly for DY^* and DZ^* the actual flight distance, Δt , in time Δt is:

$$\Delta D = (DX^*)^2 + (DY^*)^2 + (DZ^*)^2$$

Therefore knowing ΔD and Δt the flight velocity, V , which is assumed to be constant, is calculated as

$$V = \Delta D / \Delta t$$

The glide angle, ϕ , is obtained from the following relationship:

$$\phi = \arctan (DY^*/DX^*)$$

The glide angle and the gliding flight velocity are tabulated in Table XIII.

Another method of obtaining the flight velocity and the glide angle was through the use of a high speed movie camera (48 frames/sec). From this film the position of the owl relative to the wall grid, was recorded (see Figure 73) and plotted. For that portion of glide which was along a straight path the glide angle and the velocity were determined. Extracting data from the movie film was difficult because of inadequate lighting arrangements.

The velocity was calculated by multiplying the movie frame rate times the ratio of the distance traversed to the number of frames during the straight gliding region of the flight. The following velocity calculation example using data from Figure 73 illustrates the method:

$$(48 \text{ frames/sec}) (5.4 \text{ ft}/11 \text{ frames}) = 23.6 \text{ ft/sec}$$

The nominal location where the owl departed from straight gliding flight path was established from the movie data relative to the wall grid. It was noted that the second flash of the dual flash test was frequently made when the owl was past the end of the straight flight. From the flights where data were recorded simultaneously on dual flash photographs and on movie film it

was determined that the data from the dual flash photographs should be adjusted to account for the delayed second flash of the dual flash test. The velocity from the dual flash experiment has been increased by 49 percent to make it consistent with the movie data. The aerodynamic data from the movie film experiment is presented in Table XIV.

d. Discussion of Experimental Aerodynamic Results

Aerodynamic forces are described in the conventional manner as lift, L , and drag, D , which are respectively perpendicular and parallel to the bird's flight path through the air. The following assumptions are made relative to their gliding flight:

1. The gliding is, due to compensation by the bird, at a constant velocity, therefore no acceleration consideration is required.
2. The flight path is a straight line. At these conditions the lift and drag forces are balanced by weight, W , of the bird (see Figure 74.)

If ϕ is the angle of the flight path to the horizontal (the glide angle) then,

$$L = W \cos \phi$$

and

$$D = W \sin \phi$$

where

$$\phi = \tan^{-1} \frac{DY^*}{DX^*}$$

Lift and drag forces are related to non-dimensional coefficients by the equations

$$C_L = 2L/(\rho SV^2)$$

and

$$C_D = 2D/(\rho SV^2)$$

where C_L and C_D are the lift and drag coefficients respectively.

The basic performance of an aircraft during equilibrium gliding in still air is described by these parameters; air speed, glide angle, and sinking speed relative to the air. The sinking speed equation is:

$$\text{Sinking speed} = V/(L/D)$$

An important parameter in the description of gliding performance is Reynolds number, Re , because it is functionally related to the lift and drag coefficients.

The Reynolds number is defined as:

$$Re = \frac{Vc}{\nu}$$

where c is a characteristic length associated to the airfoil. The length of the wing chord at half span was chosen for c . The kinematic viscosity, ν , of air was calculated at ambient conditions.

The aerodynamic results are summarized and tabulated in Tables XIII and XIV. The mean value of the results from the data is the arithmetic mean, $\frac{1}{N} \sum_{i=1}^n x_i$ as listed in Table XII.

The standard deviation, σ , which is based on the arithmetic mean is defined in the following equation [45]

$$\sigma = \left[\frac{1}{N-1} \sum_{i=1}^n x_i^2 - \frac{1}{N(N-1)} \sum_{i=1}^n x_i^2 \right]^{1/2}$$

From these mean values the following parameters are calculated,

$$Re = 1.31 \times 10^5$$

$$L/D = 2.25$$

The mean value of the aerodynamic data may be used in any future scaling of the data but the large deviations in the measured parameters should be taken into consideration. These data show that the owl is certainly a "low performance" flyer. This is especially noted in the gliding flight when compared to a gliding black buzzard (Coragyps atratus) which has a lift-to-drag ratio range from 15.0 to 20.0 over its normal flight velocity range [37]. From the same reference the sinking speed of the buzzard in its normal flight velocity range is roughly 3.0 ft/sec whereas for the owl the mean sinking speed is

10.94 ft/sec. This comparison shows that the owl is not as well adapted to high performance gliding flight as in the black buzzard.

5. OWL MODIFICATIONS FOR ACOUSTIC TESTS

After studying the movie and still photographs and considering the potential quieting mechanisms of the gliding owl a methodology was developed for the purpose of determining the effect of various physical features of the owl which enhance or damp the radiated noise. Numerous acoustic tests of the gliding owl were made with the bird in an unmodified condition. These data were obtained on three different occasions and on the last test systematic modification of the owl's physical characteristics were made.

Figure 75 shows the owl wing in an unmodified condition. The first modification (Figure 76) was made to the wing by removing the leading edge comb as shown in Figure 77. Following this modification the noise produced during gliding flight was recorded. Next, a major portion of the trailing edge (approximately 3/4 inches) was removed to provide a conventional straight trailing edge (Figure 78). Finally, upon completion of the acoustic test following the trailing edge modification a large feather panel was removed (Figure 79) from the upper surface of each wing. It was suspected that these contour feathers gave the owl the ability to reduce the acoustic output by virtue of its compliance. Acoustic recordings were made following this adjustment completing the bionics experimental effort using live birds.

6. CONCLUSION OF BIONICS STUDY

- a. A great effort was required to train the owls to perform a desired program repeatedly. Only after acclimating to the experiment room and the associated equipment would they fly a reproduceable course. Short term attempts with hawks were unrewarding.
- b. Variations in the configuration characteristics of the owl from flight to flight resulted in significant variation of the aerodynamic flight performance factors.
- c. There are a variety of features associated with the owl feathers which indicate the importance of compliance in acoustic quieting of the wing.
- d. The physical modifications of the owl's wing did not

appreciably affect his performance characteristics.

- e. Application of information gained from the owl studies to airplanes can only be made when the results of all phases of this project are considered.

Only a brief discussion of the Bionics input to the total program were included in this Appendix. The Bionics approach is implicit throughout other sections of this report.

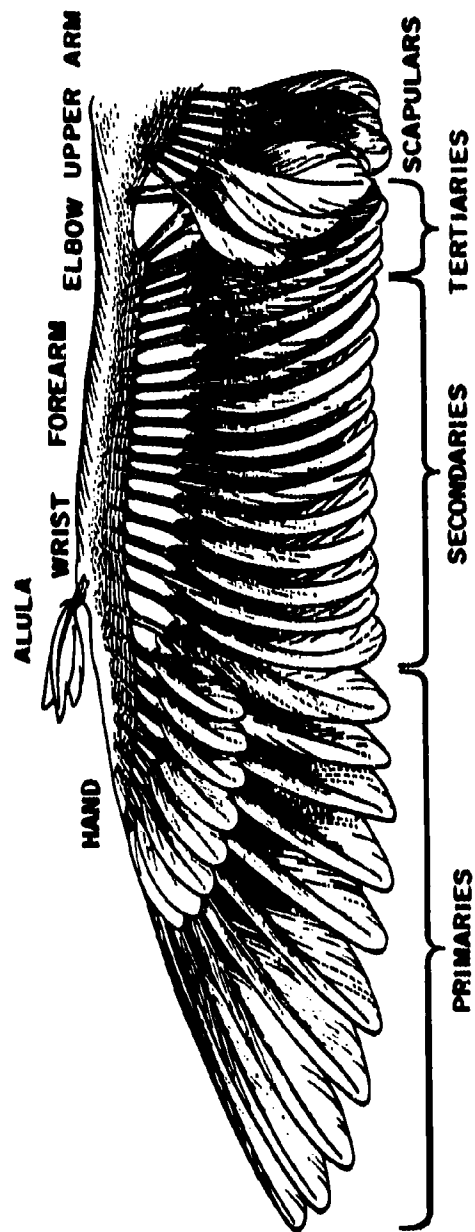


Figure 66. Basic Construction of a Bird Wing.

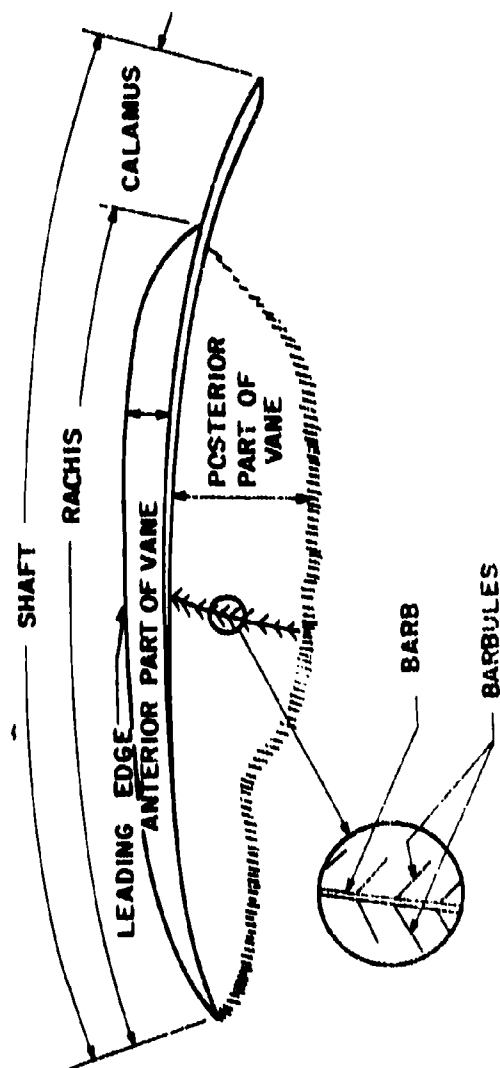


Figure 67. Basic Features of a Feather.

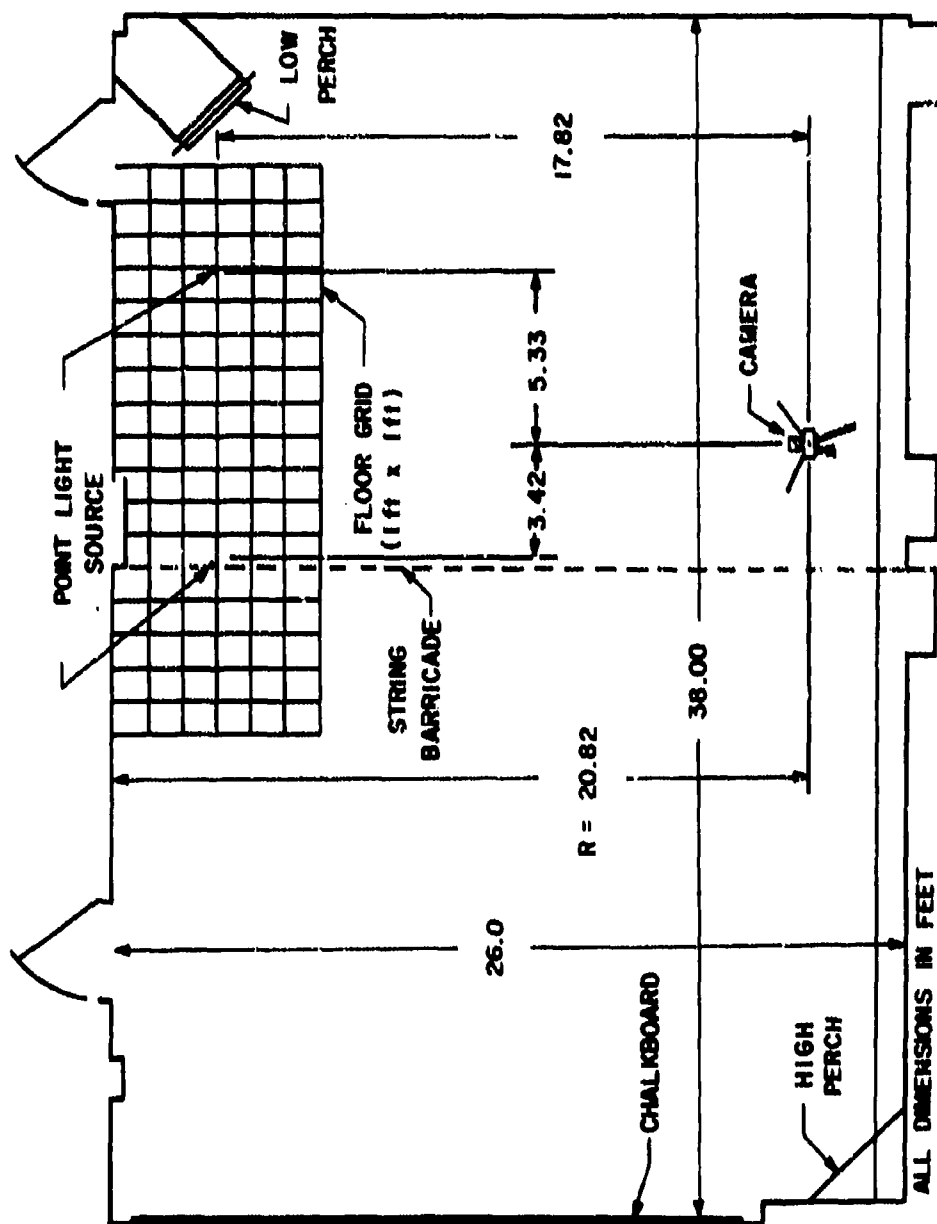


Figure 68. Floor Plan of Experiment Room.

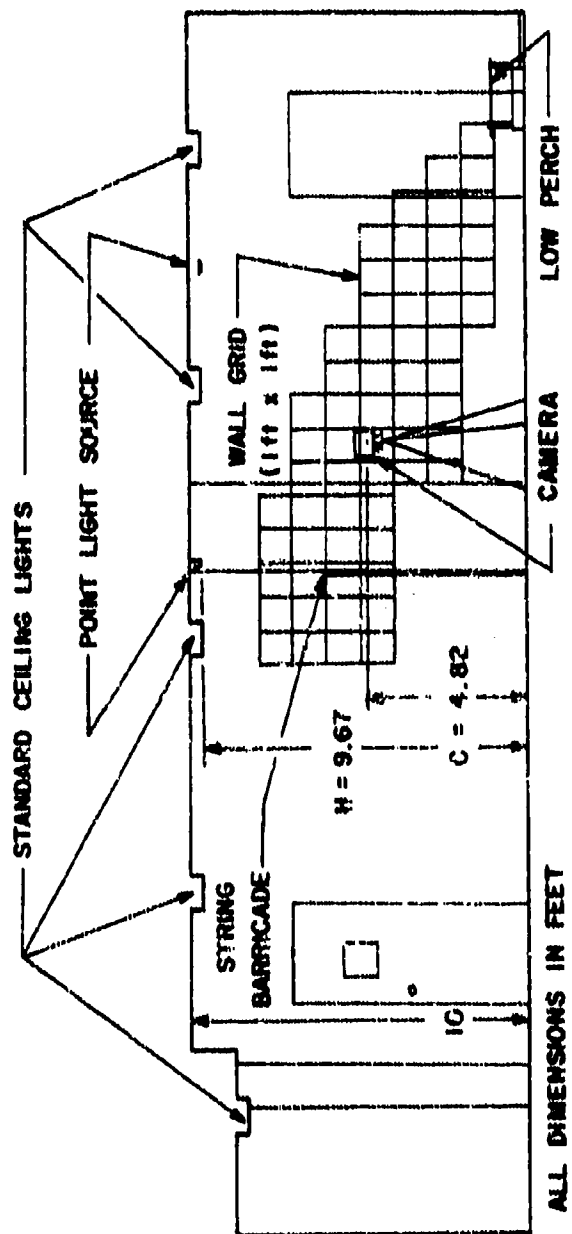


Figure 69. Profile View of Experiment Room.



Figure 70. Dual Flash Photograph of a Gliding Owl.

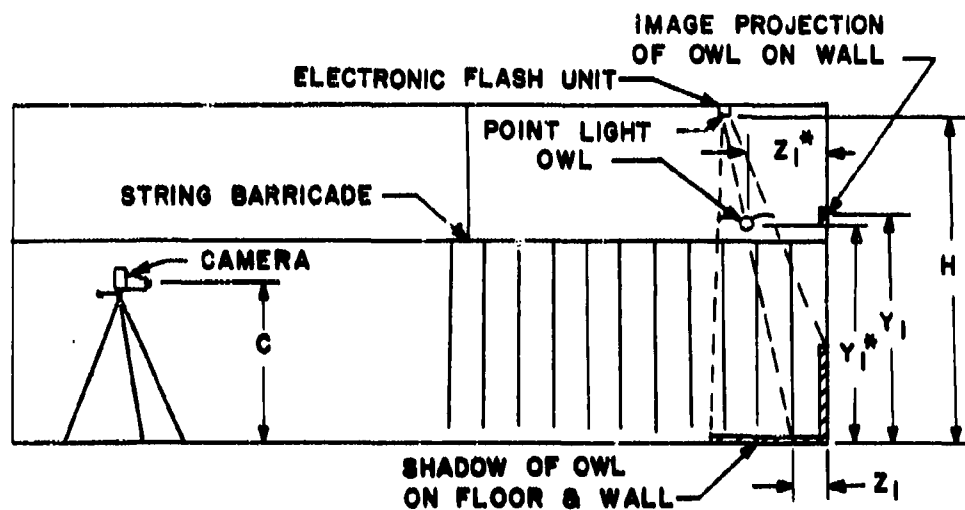


Figure 71. Sketch Looking Into Flight Path of Owl at Flash Number 1.

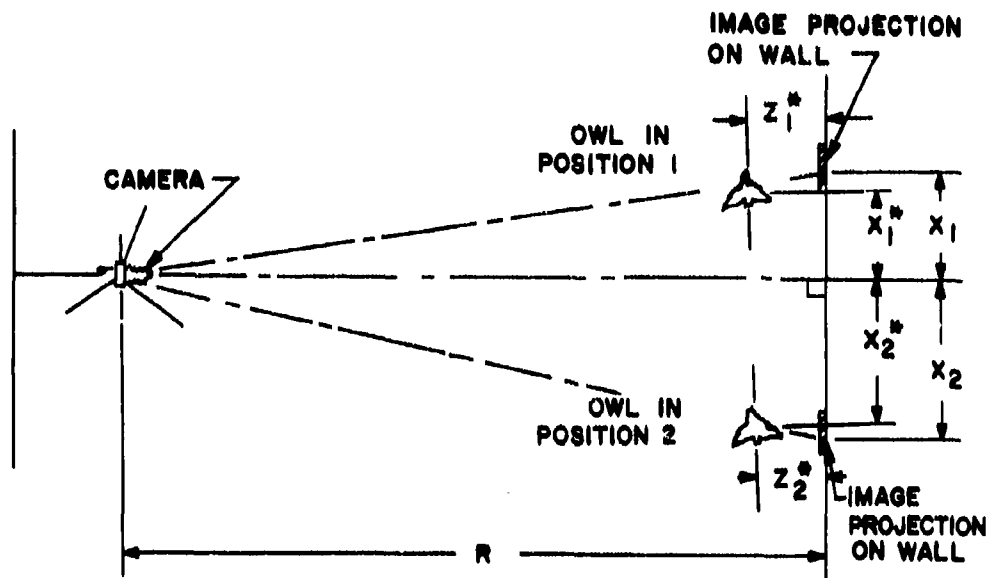


Figure 72. Sketch Looking Down on Flight Path of Owl.

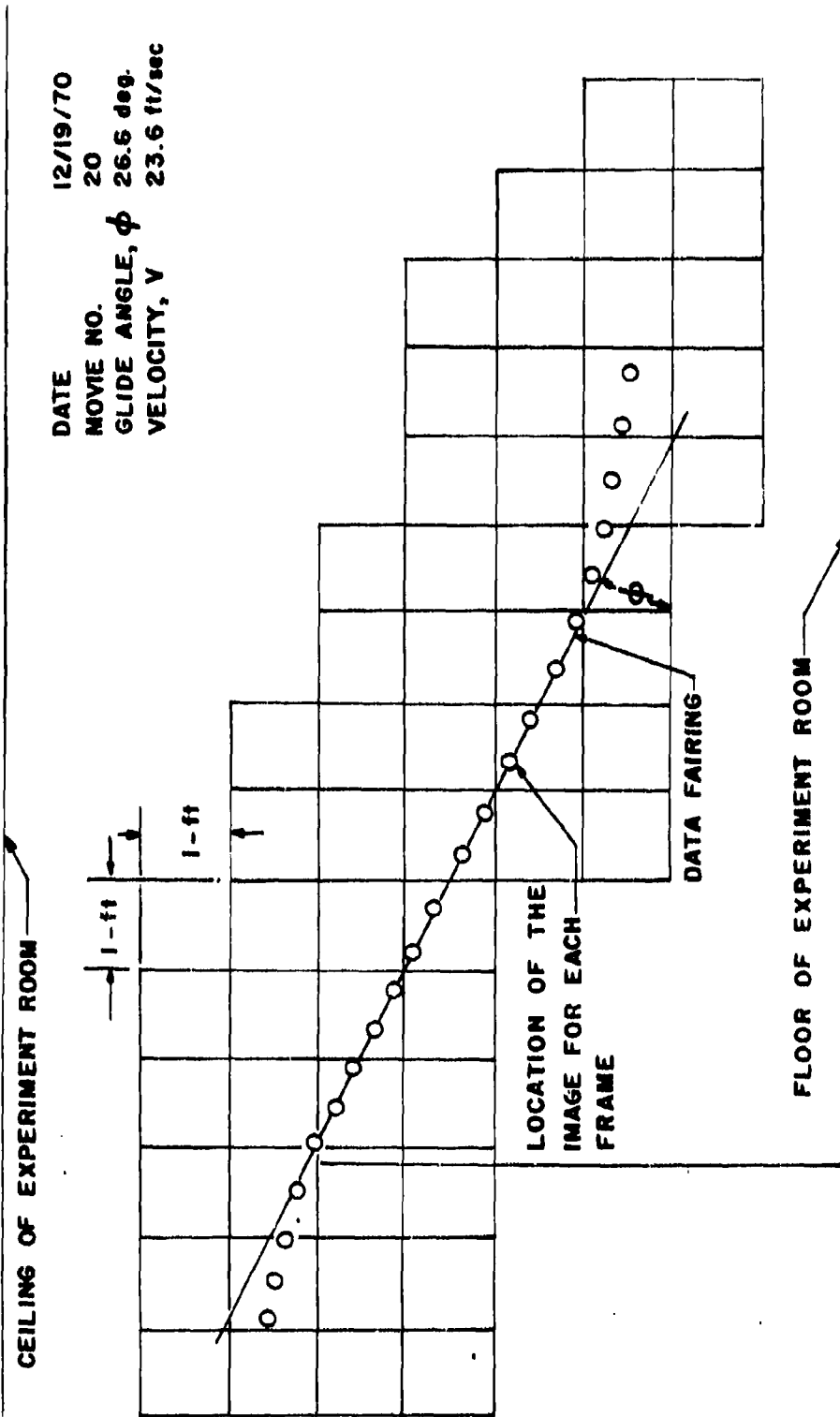


Figure 73. Typical Plot of the Movie Data Results.

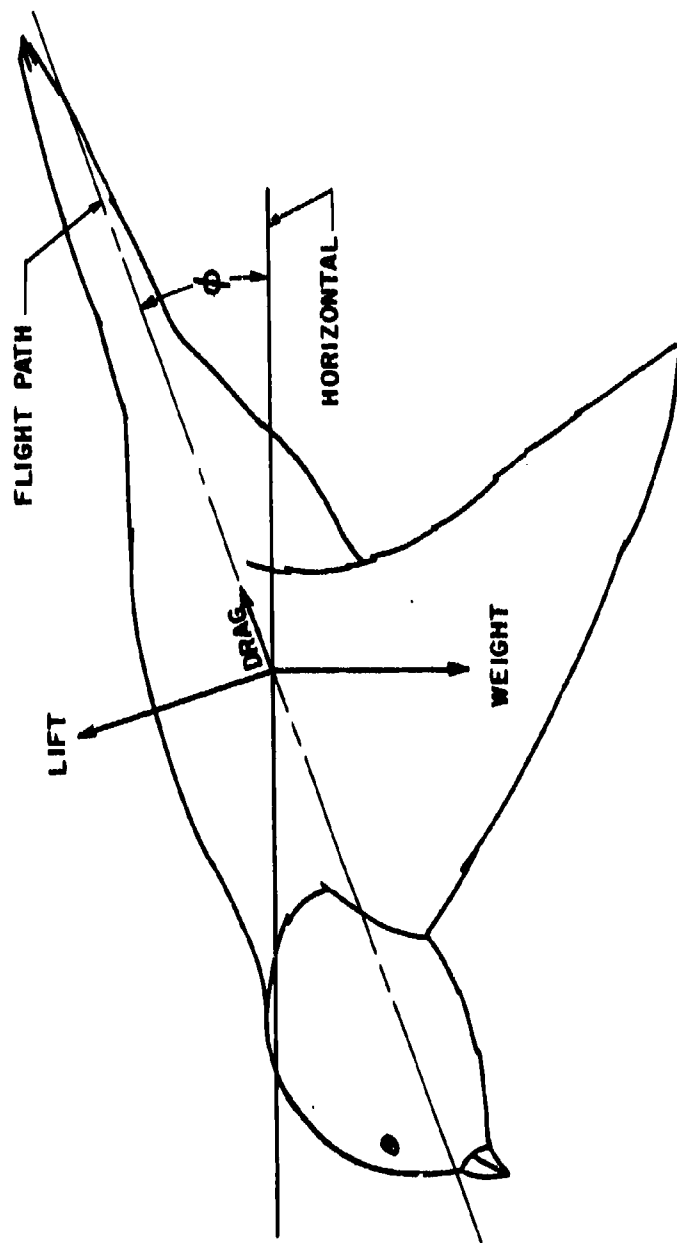


Figure 74. Forces on a Bird in Equilibrium Gliding.

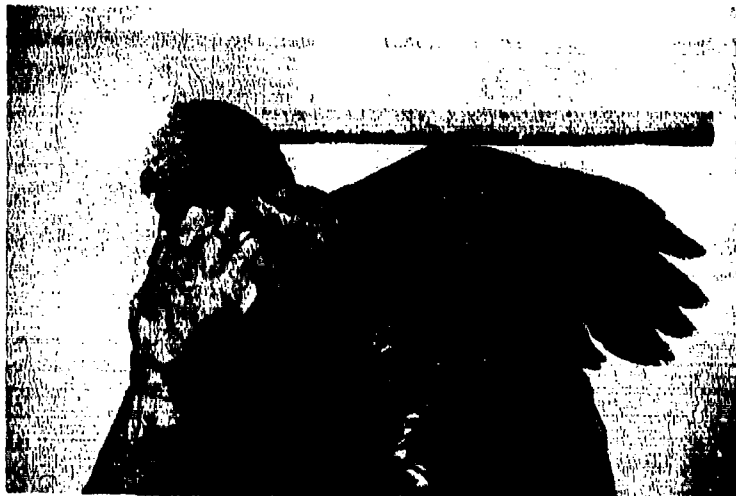


Figure 75. Photograph of an Unmodified Owl Wing.

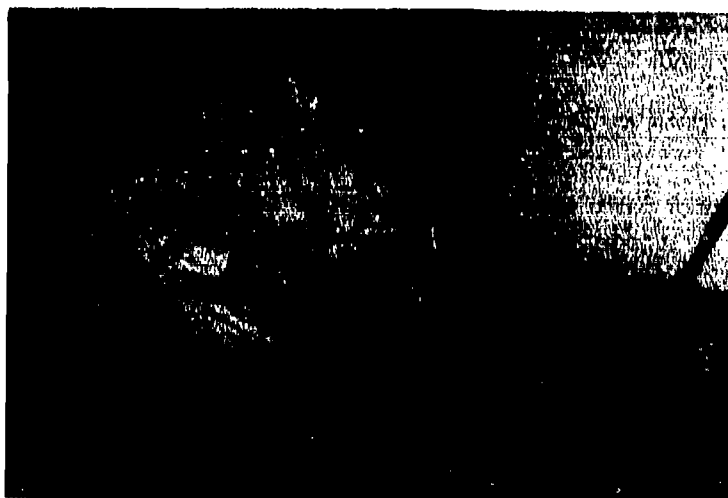


Figure 76. Photograph of the Removal of the Leading Edge Comb from an Owl Wing.



Figure 77. Photograph of an Owl Wing with the Leading Edge Comb Removed.



Figure 78. Photograph of an Owl Wing with the Trailing Edge Fringe Removed (Top View).



Figure 79. Photograph of an Owl Wing with the Upper Contour Feathers Removed.

TABLE XI
PHYSICAL PROPERTIES OF TESTED OWL

Parameter	Value
Weight, lb	1.52
Wing area*, in. ²	344.8
Wing span, in.	38.1
Wing sweep angle, deg	32.7 forward
Chord at half span, in.	11.0
Wing loading, lb/ft ²	0.635
Wing aspect ratio	4.21

*Wing area includes the body area intercepted by the wing

TABLE XII
MEAN VALUE AND STANDARD DEVIATION OF SEVERAL
AERODYNAMIC PARAMETERS OF THE OWL

Parameter	Mean Value	Standard Deviation
Velocity, ft/sec	24.04	± 4.26
Glide angle, deg	25.86	± 3.99
Lift coefficient	0.027	
Drag coefficient	0.012	
Sinking speed, ft/sec	10.94	

TABLE XIII
AERODYNAMIC DATA OF GLIDING OWL
FROM DUAL FLASH PHOTOGRAPHS

Date 1970	Flight Number	Velocity, ft/sec	Glide Angle, deg	Reynolds Number $\times 10^{-6}$	Lift-to- Drag Ratio	Lift Coef	Drag Coef	Sinking Speed, ft/sec
11/22	2	25.25	19.09	0.136	2.888	0.025	0.008	8.74
11/22	5	22.26	23.19	0.20	2.333	0.031	0.013	9.54
11/22	3	20.04	22.84	0.108	2.373	0.039	0.016	8.44
11/22	6	22.44	21.09	0.121	2.592	0.031	0.012	8.65
11/22	7	23.52	22.07	0.127	2.465	0.028	0.011	9.54
11/22	9	21.86	26.57	0.118	1.999	0.032	0.016	10.93
11/22	10	21.60	26.60	0.117	1.996	0.032	0.016	10.81
11/22	11	21.99	25.23	0.119	2.121	0.031	0.015	10.36
11/28	3	22.55	25.27	0.122	2.118	0.030	0.014	10.65
11/28	4	20.61	24.70	0.111	2.173	0.036	0.016	9.48
11/28	5	21.08	23.19	0.114	2.333	0.035	0.015	9.03

TABLE XIII (continued)

Date 1970	Flight Number	Velocity, ft./sec	Glide Angle, deg	Reynolds Number $\times 10^{-6}$	Lift-to- Drag Ratio	Lift Coef	Drag Coef	Sinking Speed ft./sec
11/28	6	22.24	22.71	0.120	2.388	0.031	0.013	9.31
11/28	7	21.83	25.40	0.118	2.105	0.032	0.015	10.36
11/28	13	21.96	25.20	0.119	2.124	0.032	0.015	10.33
11/28	14	20.55	24.37	0.111	2.206	0.036	0.016	9.31
11/28	15	19.86	23.74	0.107	2.273	0.039	0.017	8.73
11/28	16	21.12	22.93	0.114	2.363	0.035	0.014	8.93
11/28	17	21.27	23.95	0.115	2.250	0.034	0.015	9.45
12/5	2	21.58	25.34	0.117	2.110	0.033	0.015	10.22
12/5	3	24.27	24.17	0.131	2.228	0.026	0.011	10.89
12/5	4	25.27	26.17	0.137	2.034	0.023	0.011	12.42
12/5	6	26.74	26.15	0.144	2.036	0.021	0.010	13.13

TABLE XIII (continued)

Date 1970	Flight Number	Velocity, ft/sec	Glide Angle, deg	Reynolds Number $\times 10^{-6}$	Lift-to- Drag Ratio	Lift Coef	Drag Coef	Sinking Speed ft/sec
12/19	5	25.30	21.67	0.137	2.516	0.024	0.009	10.05
12/19	6	25.54	22.63	0.138	2.397	0.023	0.009	10.65
12/19	7	25.68	23.26	0.139	2.119	0.023	0.010	12.12
12/19	8	25.11	22.22	0.136	2.447	0.025	0.010	10.26
12/19	12	19.22	26.93	0.104	1.967	0.040	0.020	9.77
12/19	13	22.59	21.81	0.122	2.498	0.031	0.012	9.04
12/19	15	24.22	22.52	0.131	2.411	0.026	0.011	10.04
12/19	17	23.63	22.29	0.128	2.439	0.028	0.011	9.68
12/19	14	24.94	23.42	0.135	2.307	0.024	0.010	10.81

TABLE XIV
AERODYNAMIC DATA OF GLIDING OWL
FROM MOVIE FILM

Date 1970	Flight Number	Velocity, ft/sec	Glide Angle, deg	Reynolds Number $\times 10^{-6}$	Lift-to- Drag Ratio	Lift Coef	Drag Coef	Sinking Speed ft/sec
12/19	7	25.85	25.00	0.140	2.144	0.023	0.010	12.05
12/19	10	22.15	26.09	0.120	2.041	0.031	0.015	10.85
12/19	11	22.70	23.50	0.123	2.299	0.030	0.013	9.87
12/19	12	21.82	28.29	0.118	1.857	0.031	0.017	11.74
12/19	13	21.62	29.39	0.117	1.774	0.031	0.017	12.18
12/19	14	24.00	26.00	0.130	2.050	0.026	0.013	11.70
12/19	15	24.00	27.69	0.130	1.904	0.026	0.013	12.60
12/19	17	23.41	27.79	0.126	1.896	0.027	0.014	12.34
12/19	18	23.53	26.50	0.127	2.005	0.027	0.013	11.73
12/19	20	23.61	26.59	0.127	1.996	0.027	0.013	11.82
12/19	21	24.00	24.50	0.130	2.194	0.027	0.012	10.93

TABLE XIV (continued)

Date 1970	Flight Number	Velocity, ft./sec	Glide Angle, deg	Reynolds Number $\times 10^{-6}$	Lift-to- Drag Ratio	Lift Coef	Drag Coef	Sinking Speed ft./sec
12/19	22	25.45	23.39	0.137	2.310	0.024	0.010	11.01
12/19	23	21.82	28.19	0.118	1.865	0.031	0.016	11.69
12/19	24	24.20	25.00	0.131	2.144	0.026	0.012	11.28
12/19	25	23.66	24.39	0.128	2.204	0.027	0.012	10.73
12/19	26	23.66	24.29	0.128	2.214	0.027	0.012	10.68
12/19	31	25.04	27.29	0.135	1.937	0.024	0.012	12.92
12/19	34	23.66	23.79	0.128	2.267	0.027	0.012	10.43
12/19	37	24.53	23.29	0.132	2.322	0.026	0.011	10.56
12/19	39	23.04	23.29	0.124	2.322	0.029	0.012	9.92
12/20	2	22.68	25.19	0.122	2.125	0.030	0.014	10.67
12/20	4	24.00	22.00	0.130	2.475	0.027	0.011	9.69

TABLE XIV (continued)

Date 1970	Flight Number	Velocity, ft/sec	Glide Angle, deg	Reynolds Number $\times 10^{-6}$	Lift-to- Drag Ratio	Lift Coef	Drag Coef	Sinking Speed ft/sec
12/20	6	24.41	26.50	0.132	2.005	0.025	0.012	12.17
12/20	7	23.23	26.89	0.125	1.971	0.028	0.014	11.78
12/20	8	26.67	25.39	0.144	2.106	0.021	0.010	12.66
12/20	9	21.82	25.59	0.118	2.087	0.032	0.015	10.45
12/20	10	24.49	26.09	0.132	2.041	0.025	0.012	11.99
12/20	15	24.71	20.59	0.133	2.660	0.026	0.009	9.28
12/20	21	24.89	23.89	0.134	2.256	0.025	0.011	11.02

REFERENCES

1. Graham, R. R., "The Silent Flight of Owls," Journal of Royal Aeronautical Society, Vol. 38, 1939.
2. Smith, D. L. and Paxson, Lt. R. P., "The Aural Detection of Aircraft," Air Force Flight Dynamics Laboratory, TM-69-1-FDDA, September 1969.
3. International Standards Organization, Document ISO, R 226, 1961.
4. Smith, D. L., Paxson, Lt. R. P., Talmadge, R. D., and Hotz, E. R., "Measurement of the Radiated Noise from Sailplanes," Air Force Flight Dynamics Laboratory, TM-70-3-FDDA, July 1970.
5. Fletcher, H., "Auditory Patterns," Reviews of Modern Physics, Vol. 12, January, 1940, pp. 47-65.
6. Hoehne, Vernon O. and Luce, Ross G., "Evaluation of the Feasibility of Developing an Airplane Having a Silent Mode of Operation," ARPA project AGILE, Batelle Memorial Institute Report No. BAT - 171-49, July 22, 1966.
7. Burdrall, E. A. and Urban, R. H., "Fan Compressor Noise: Prediction, Research, and Reduction Studies." Final Contract Report to FAA, January 1971.
8. Swan, Walter R., Lecture at University of Aachen, Germany, "Short Course on Aircraft Noise Abatement Co-sponsored by The University of Tennessee Space Institute, March, April, 1971.
9. Hubbard, H. H., et.al., "A Reveiw of Rotating Blade Noise Technology," Aerodynamic Noise Symposium, Paper No. B1, Leicestershire, England, Sept, 1970.
10. Marshall, Douglas W., "On the Relative Strength of the Major Aerodynamic Noise Sources of the Eppler 266 Airfoil in the Low Subsonic Mach Number Regime," Masters of Science Thesis at The University of Tennessee Space Institute, December 1970.
11. Short Course Proceedings, "Aircraft Noise Abatement," Co-Sponsored by The University of Tennessee Space Institute and the Technical University of Aachen. March, April, 1971.
12. Blick, E. F., Private Conversation. The University of Oklahoma, Norman, Oklahoma, December, 1970.

13. Walters, R. R. , "Turbulent Boundary Layer Characteristics of Flow Over a Compliant Surface," A Dissertation Submitted to The Graduate College, University of Oklahoma, 1969.
14. Nisewanger, C. R. , "Flow Noise and Drag Measurements of Vehicle with Compliant Coating," U.S. Naval Ordinance Test Station, China Lake, California, July 1964.
15. Strouhal, V. , "Über eine besondere Art der Tonerregung," Ann. Phys. und Chem., 5:216, October, 1878.
16. Gruschka, H. , Private Communication. The University of Tennessee Space Institute, Tullahoma, Tennessee, November, 1970.
17. Doak, P. E. , "Acoustic Radiation from a Turbulent Fluid Containing Foreign Bodies," Proceedings of the Royal Society of London, 254 (Series A):129-145, March, 1960.
18. Curle, N. , "The Influence of Solid Boundaries on Aerodynamic Sound," Proceedings of the Royal Society of London, 231 (Series A):505-514, September, 1955.
19. Lighthill, M. J. , "On Sound Generated Aerodynamically," Proceedings of the Royal Society of London, 222 (Series A):1-32, March, 1954.
20. Sharland, I. J. , "Sources of Broadband and Discrete Frequency Noise in Axial Flow Fans Due to Vortex Shedding and Aerodynamic Interactions," Journal of Sound and Vibration, 1:302-322, July, 1964.
21. Harrison, M. , "Pressure Fluctuations on the Wall Adjacent to a Turbulent Boundary Layer," Second Symposium-Naval Hydrodynamics, R. Cooper, editor. Washington, D. C.: Department of the Navy, 1958. Pp. 107-136.
22. Willmarth, W. , "Wall Pressure Fluctuations in a Turbulent Boundary Layer," National Advisory Committee for Aeronautics TN 4139, Washington, D. C. , March, 1958.
23. Bull, M. K. , and J. L. Willis, "Some Results of Experimental Investigations of the Surface Pressure Field Due to a Turbulent Boundary Layer," University of Southampton AASU Report No. 199, Hampshire, England, November, 1961.
24. Franken, Peter A. , "Methods of Space Vehicle Noise Prediction," Wright Air Development Division WADC Technical Report 58-343 Vol. II, Wright Patterson Air Force Base, Ohio, September, 1960.

25. Skurdzyk, E., and G. Haddle, "Noise Production in a Turbulent Boundary Layer by Smooth and Rough Surfaces," Second Symposium-Naval Hydrodynamics, R. Cooper, editor. Washington, D. C.: Department of the Navy, 1958. pp 75-105.
26. Etkin, B., G. K. Korbacher, and R. T. Keefe, "Acoustic Radiation from a Stationary Cylinder in a Fluid Stream," The Journal of the Acoustical Society of America, 29:30-36, January, 1957.
27. Schlichting, Hermann, Boundary Layer Theory. Sixth edition. New York: McGraw-Hill Book Company, Inc., 1968.
28. Perkins, C. D., and R. E. Hage, Airplane Performance and Stability. New York: John Wiley and Sons, Inc., 1967.
29. Abbott, I. H., and A. E. Von Doenhoff, Theory of Wing Sections. New York: Dover Publications, Inc., 1959.
30. Glauert, H., The Elements of Airfoil and Airscrew Theory. Second edition. London: Cambridge University Press, 1969.
31. Bernard, E. E., and M. R. Kare, (editors), "Bionics Symposium-Living Prototypes - The Key to New Technology," Wright Air Development Division Technical Report 60-600, Wright-Patterson Air Force Base, Ohio, September, 1960.
32. Gerardin, Lucien, Bionics. New York: McGraw-Hill Book Company, Inc., 1968.
33. Hertel, Heinrich. Structure-Form-Movement: Biology and Technology. Translation from the German edited by Milton S. Katz. New York: Reinhold Publishing Corporation, 1966.
34. Wiener, N., Cybernetics. Cambridge: The M.I.T. Press, 1948.
35. Helvey, T. C., The Age of Information - An Interdisciplinary Survey of Cybernetics. Englewood Cliffs: Educational Technology Publications, 1971.
36. Krayzmer, Leonid Pavlovich, Bionics. Translation from the Russian by the Joint Publication Research Service. Washington: U.S. Department of Commerce, 1962.
37. Raspet, August, "Biophysics of Bird Flight," Science, 32: 191-200, July 22, 1960.
38. Cone, C. D., Jr., "The Soaring Flight of Birds," Scientific American, 206:130-140, April 1962.
39. Tucker, Vance A., and Christian G. Parrott, "Aerodynamics of Gliding Flight in a Falcon and Other Birds," Journal of Exploratory Biology, 52:354-367, 1970.

40. Farrar, F. D., Jr., and C. E. Farrell, Unpublished report. Vanderbilt University, Nashville, Tennessee, June, 1960.
41. Pennycuick, C. F., "Wind-Tunnel Study of Gliding Flight in the Pigeon (*Columba livra*)," Journal of Exploratory Biology, 49:509-526, 1968.
42. Hoehne, Vernon O., and Ross G. Luce, "The Quited Aircraft as a Military Tool." American Institute of Aeronautics and Astronautics Paper No. 69-792, presented at AIAA Aircraft Design and Operations Meeting, Los Angeles, California, July, 1969.
43. von Gierke, H. E., "Physical Characteristics of Aircraft Noise Sources," The Journal of the Acoustical Society of America, 25:367-378, May, 1953.
44. Beranek, L. L., et al. "Experiments in External Noise Reduction of Light Airplanes," National Advisory Committee for Aeronautics TN-2C79, Washington, D. C., May, 1950.
45. Hald, Anders, Statistical Theory with Engineering Applications. New York: John Wiley and Sons, Inc., 1952.
46. Eyring, Carl F., "Jungle Acoustics," The Journal of the Acoustical Society of America, 18:257-270, October, 1946.
47. Ingram, J. D., "A Summary of Aerodynamic Noise," Flight Dynamics Laboratory FDL-TDR-64-132, Wright-Patterson Air Force Base, Ohio, December, 1964.
48. Smith, D. L., et al. "Measurements of the Radiated Noise from Sailplanes," Flight Dynamics Laboratory TM-70-3-FDDA, Wright-Patterson Air Force Base, Ohio, July, 1970.

UNCLASSIFIED

Security Classification

DOCUMENT CONTROL DATA - R & D		
(Security classification of title, body of abstract and indexing annotation must be entered when the overall report is classified)		
1. ORIGINATING ACTIVITY (Corporate author)		2a. REPORT SECURITY CLASSIFICATION
University of Tennessee Space Institute Tullahoma, Tennessee		UNCLASSIFIED
		2b. GROUP
3. REPORT TITLE		
Low Speed Aerodynamics for Ultra-Quiet Flight		
4. DESCRIPTIVE NOTES (Type of report and inclusive dates)		
Final Technical Report July 1970 - May 1971		
5. AUTHOR(S) (First name, middle initial, last name)		
Kroeger, Richard A. Grushka, Heinz D. Helvey, Tibor C.		
6. REPORT DATE	7a. TOTAL NO. OF PAGES	7b. NO. OF REFS
MARCH 1972	155	48
8a. CONTRACT OR GRANT NO.	8b. ORIGINATOR'S REPORT NUMBER(S)	
F33615-70-C-1762	AFFDL-TR-71-75	
9. PROJECT NO.	9b. OTHER REPORT NO(S) (Any other numbers that may be assigned this report)	
1471		
10. DISTRIBUTION STATEMENT		
Distribution limited to U. S. Government agencies only; test and evaluation; statement applied December 1971. Other requests for this document must be referred to AFFDL/FY, WPAFB, Ohio 45433		
11. SUPPLEMENTARY NOTES		12. SPONSORING MILITARY ACTIVITY
		Air Force Flight Dynamics Laboratory Wright-Patterson AFB, Ohio
13. ABSTRACT		
<p>A combined aerodynamics, acoustics and bionics study was conducted in an attempt to discover novel mechanisms to reduce the noise associated with aircraft flight. The strigiformes order of birds, selected in the bionics effort as possessing characteristics of silent flight, was studied extensively. Three mechanisms producing the potential for acoustic quieting were discovered as a result of this study. These are: (1) vortex sheet generators, (2) compliant surfaces, and (3) distributed wing porosity.</p> <p>An experimental program aimed at initiating full scale flight evaluation of these concepts was outlined. The detailed results of these studies are included.</p> <p>This report develops design concepts which may be applied to obtain ultra quiet flight for covert/reconnaissance/surveillance aircraft such as the YO-3.</p>		

DD FORM 1 NOV 65 1473

UNCLASSIFIED

Security Classification

